A numerical analysis of liquefaction mitigation using Stone Column

Thesis submitted in partial fulfilment of the requirements for the degree of

Master of Engineering in Civil Engineering

Submitted By

Shaifur Rahaman

Examination Roll No. – M4CIV23022
Registration No. -160026 of 2021-2022

Under guidance of

DR. RAMENDU BIKAS SAHU
Professor
Department of Civil Engineering, Jadavpur University

And

DR. NARAYAN ROY
Assistant Professor
Department of Civil Engineering, Jadavpur University

Civil Engineering Department

Jadavpur University, Kolkata 700032

(2023)

JADAVPUR UNIVERSITY

FACULTY OF ENGINEERING AND TECHNOLOGY

DEPARTMENT OF CIVIL ENGINEERING

CERTIFICATE OF RECOMMENDATION

I hereby recommend that the thesis entitled "**A numerical analysis of liquefaction mitigation using Stone Column"** submitted by **Shaifur Rahaman** carried out under our supervision and guidance be accepted in the partial fulfilment of the requirements for the degree of "**Master of Engineering in Civil Engineering**" in Jadavpur University.

Thesis Supervisor **Thesis Supervisor**

Dr. Ramendu Bikas Sahu
Professor
Dept. of Civil Engineering,
JADAVPUR UNIVERSITY
Kolkata-700032

Dr. Narayan Roy
Assistant Professor,
Dept. of Civil Engineering
JADAVPUR UNIVERSITY
Kolkata-700032

Countersigned by

DEAN,
Faculty of Engineering and Technology
JADAVPUR UNIVERSITY
Kolkata-700032

H.O.D,
Dept. of Civil Engineering,
JADAVPUR UNIVERSITY
Kolkata-700032

JADAVPUR UNIVERSITY

FACULTY OF ENGINEERING AND TECHNOLOGY

DEPARTMENT OF CIVIL ENGINEERING

CERTIFICATE OF APPROVAL

The foregoing thesis is hereby approved as a creditable study of an engineering subject carried out and presented in a manner of satisfactory to warrant its acceptance as a pre- requisite to the degree for which it has been submitted. It is understood that by this approval, the undersigned do not necessarily endorse or approve any statement made, opinion expressed and conclusion drawn therein but approve the thesis only for the purpose for which it has been submitted.

COMMITTEE OF FINAL EXAMINATION FOR
EVALUATION OF THE THESIS WORK

1. **_____ (Signature of Examiner)**

2. **_____ (Signature of Examiner)**

3. **_____ (Signature of Examiner)**

DECLARATION

I, Shaifur Rahaman, a student of Master of Engineering in Civil Engineering, Civil Engineering Department, Jadavpur University, Faculty of Engineering and Technology, hereby declare that the work being presented in this thesis work entitled "**A numerical analysis of liquefaction mitigation using Stone Column**" is authentic record of work that has been carried out at the Department of Civil Engineering, Jadavpur University, under the guidance of Dr. Ramendu Bikas Sahu, Professor, Civil Engineering Dept. Jadavpur University. And Dr. Narayan Roy, Assistant Professor, Civil Engineering Dept., Jadavpur University.

Date: ----------

Place: Jadavpur

SHAIFUR RAHAMAN

Examination Roll No. – M4CIV23022

Registration No: 160026 of 2021-2022

Class Roll No: 002110402002

Civil Engineering Department

Jadavpur University

ACKNOWLEDGEMENT

It is my greatest fortune to perform the thesis work in the Civil Engineering Department, Jadavpur University. I express my heart-felt gratitude to my esteemed guides Dr. Ramendu Bikas Sahu, Professor, Dept. of Civil Engineering, Jadavpur University and Dr. Narayan Roy, Assistant Professor, Dept. of Civil Engineering, Jadavpur University. It is because of their noble and continuous guidance, encouragement as well as valuable advices at every aspect and strata of the problem from the embryonic to the development stage that my thesis has been in the light of the day. My special thanks to Head of Civil Engineering Department for allowing me to carry out the research investigation with various facilities of the department. I am also grateful to all research scholars and appreciate the support of librarian, technicians and other staffs of our department for their cordial assistance throughout my thesis work. I express my appreciation to my friends for their understanding, patience and active co-operation throughout my course. I feel pleased and privileged to fulfill my ambition of my parents and I am greatly indebted to them for their scarification in nurturing me and bearing the inconvenience throughout my academic course. Any omission in this brief acknowledgement does not mean lack of gratitude.

Date: ----------

Place: Jadavpur

SHAIFUR RAHAMAN

Examination Roll No. – M4CIV23022

Registration No: 160026 of 2021-2022

Class Roll No: 002110402002

MCE Student Specialization:

Soil Mechanics & Foundation Engineering

Civil Engineering Department

Jadavpur University

ABSTRACT

In this study, a numerical analysis is carried out for mitigation of liquefaction using stone column. The generation of excess pore pressure and also dissipation of excess pore pressure in both cases, without stone column and with stone column cases are analysed in detailed. FLAC 2D software based upon finite difference method are used here to simulate the real earthquake situation. A parametric variation was done by varying the three different stone column length with two different natural earthquake having same PGA but different time record, different dominant frequency. Loose saturated sand and medium dense saturated sand layer are considered here as liquefiable layer. A single stone column of diameter of 0.8m is installed at the centre of the liquefiable layer. Then pore pressure generation and dissipation with stone column are checked along the depth on stratified soil layer. And also, from the centre of the stone column in lateral distances various points are considered like soil-column interface, 1.5d, 3d, 4.5d (d = diameter of stone column = 0.8m) where excess pore pressure parameters are calculated. And finally comparing these results. Liquefaction potential is measure here in terms of excess pore water ratio, r_u which is the ratio of excess pore water pressure to the effective stress at that depth. When r_u value reached to 1, the soil is termed as liquefied. The result got from these studies when the stone column is installed in liquefiable saturated sandy layer the excesses pore pressure ratio, r_u is drastically reduced up to 1.5d distances from centre of the column in either left or right side. So, the stone column is safely reduced liquefaction about a total 3d length around the stone column. And stone column having length of 10m is sufficiently mitigate moderate to high PGA earthquake.

TABLE OF CONTENTS

LIST OF FIGURES

LIST OF TABLES

CHAPTER – 1
INTRODUCTION

1.1 Introduction:

Liquefaction is the serious problem in geotechnical engineering. It is a phenomenon that can result in devastating damage during seismic events like Settlement and Ground Deformation, Tilting of Structures, Lateral Spreading etc. So, the evaluation of the liquefaction potential of a soil deposit and its reduction has become one of the significant aspects. During earthquake loose saturated soil got liquified under cyclic loading condition. The soil and pore fluid interaction under cyclic loading condition develops of pore pressure. The increases in the excess pressure which may reduction of effective stress and the loss of shear strength occurs. At a point the excess pore pressure is equal to the effective stress, then shear stress of soil becomes zero and soil got liquefied as a result various superstructure sink under the loose saturated soil (i.e. like liquid).

Mitigation using stone columns is the very popular technique employed to address the risk of soil liquefaction. Stone columns, also known as stone piles or vibro-stone columns, are a popular method among the various ground improvement technique for minimize liquefaction risks. These columns consist of compacted stone or gravel that is inserted into the liquefiable soil to improve its load-bearing capacity and reduce the likelihood of liquefaction-induced damage. Stone column installation technique can help to mitigate the liquefaction as it provides a drainage path because of their high permeability and reducing the seismic shear stress experience by soil under cyclic/earthquake loading. During earthquake excess pore water pressure generates in the soil, dissipates as the water flows towards the stone column having infinite permeability, hence the pore water pressure cannot reach its limiting value and finally safe by it. Considering various positive and negative effects in stone column such as reconsolidation settlement, encased with geotextiles, well resistance, smear, clogging and stiffness of the stone column can be analyzed properly to improve its effectiveness. Considering all these effects we can estimates how the excess pore water pressure generation, dissipates and ground acceleration develop by using mathematical model and also generating a stone column model using software models (like finite elements based or finite difference based) to observe the reduction of soil liquefaction by reducing excess pore water pressure.

The fundamental concept of liquefaction mitigation is to replace the susceptible soil to liquefaction with gravel in vibratory manner, in order to reduce the liquefaction hazard and improve soil in four main ways. (1) Reducing the build up excess pore water pressure by increasing the drainage of soil surrounding the column. (2) Densification of soil surrounding the column while installing the stone column which prevent the cyclic deformation during the

earthquake. (3) Reinforcing the treated soil area science, the column has stiffer than the surrounding soil. (4) Increasing the lateral stresses in the soil surrounding the column.

Priebe (1989) investigated that stone column can mitigate liquefaction by seismic shear stress redistribution. The reinforcement can mitigate the risk of liquefaction through several mechanism, including (1) increasing the soil density during installation of granular stone column. (2) Increasing the lateral effective confining stress in the soil. (3) provided drainage by induced excess pore pressure gets dissipated almost as fast as it is generated (Baez 1995; Adalier and Elagamal 2004; Green et al. 2008). Boulanger et al.(1998) evaluated that the drainage capacity of stone column for reducing liquefaction with different hydraulic conductivity have the secondary benefit and the primary benefit is the densification. Installation of stone column can densify the ground, and densification effects decrease with the distance increase from the point of densification (A. Murali Krishna et al. 2006).

Various studies gave very much importance on permeability and larger elastic modulus of stone column. Ounce (1987) concluded that well resistance (limited permeability) cannot be ignored even permeability of stone column is more than 400 times of the surrounding soil. And the elastic modulus of stone column to sandy soil has a range from 4-20.

Rollins et.al (2015) concluded that stone column can worked with greater efficiency's when it is incorporated with pre-fabricated vertical drain. Meshkinghalam et al. (2017) proposed a study and investigated that stone column drainage performance is effective at depths of about 3–3.5 m from ground surface. Moreover, stone column causes drainage at zone with distance of about 2.5 m from its center. The effect of column drainage is vanished at distance more than 2.5 m.

1.2 History of liquefaction studies

The study of liquefaction, particularly in the context of soil mechanics and geotechnical engineering, has a rich history dating back to the early 20th century. Liquefaction refers to the phenomenon where saturated soil temporarily loses its strength and behaves like a liquid during seismic events or other sudden loading conditions. Here is a brief overview of the history of liquefaction studies:

In 1920s-1930s of Early Observations, The study of liquefaction began with observations of earthquake-induced ground failures, primarily in Japan and California. Engineers and scientists noted that during strong earthquakes, sandy and silty soils could lose their shear strength and exhibit behaviors to liquid.

In 1940s-1950s, Austrian-American civil engineer Karl Terzaghi made significant contributions to the understanding of soil liquefaction. He developed the concept of effective stress and conducted laboratory experiments to investigate the liquefaction phenomenon. Terzaghi's work laid the foundation for modern geotechnical engineering.

With the increasing awareness of seismic hazards, research into liquefaction intensified during the 1960s and 1970s. Researchers conducted laboratory tests to better understand the factors influencing liquefaction susceptibility, such as soil type, saturation, and earthquake magnitude.

During 1980s-1990s period, researchers developed empirical methods to predict liquefaction potential and assess the vulnerability of structures to liquefaction-induced ground shaking. These methods relied on field data from past earthquakes and allowed engineers to make informed decisions regarding construction and land use in seismically active areas.

Software for simulating liquefaction using finite difference and finite element techniques first became available in the early 21st century. For simulation research, several constitutive models dealing with materials as well as coupled solid-fluid models were employed. Availability of high-performance computational facilities enabled the researchers to develop programs which can simulate earthquakes and predict the stresses and pore water pressure development to a good relative degree of accuracy. Some prominent examples of commercial software are Plaxis (with a particular license), OpenSees, (Open System for Earthquake Engineering), FLAC (Itasca, 2000), Abacus (Abaqus, 2010), and Being free and open source makes the program accessible to researchers, making it a very effective substitute for proprietary software.

1.3 Objective and Scope of the study

1.3.1 Objective of the study

The objective of the present investigation is to study the feasibility of using stone column for liquefaction mitigation in a sandy deposit during an earthquake excitation.

1.3.2 Scope of the study

i. Liquefaction analysis has been conducted numerically using FLAC2D to determine the pore water pressure characteristics of typical stratified sandy soil deposit with and without stone column.

ii. A parametric study has been performed to determine the generation and dissipation of excess pore water pressure (EPWP) for two natural earthquakes, namely Lomaprieta and Mammoth-Lake Earthquake having same PGA but different time duration and different dominant frequencies.

iii. A parametric study has been conducted by varying the length of the stone column (5m, 10m and 15m) within the loose to medium dense sand deposit.

iv. Pore-water pressure dissipation characteristic at different lateral distances (1.5d, 3.0d, 4.5d from center) from stone column are studied.

CHAPTER – 2

LITERATURE REVIEW

2.1 What is liquefaction?

A more precise definition as given by Sladen et al (1985) states that "Liquefaction is a phenomena wherein a mass of soil loses a large percentage of its shear resistance, when subjected to monotonic, cyclic, or shocking loading, and flows in a manner resembling a liquid until the shear stresses acting on the mass are as low as the reduced shear resistance".

2.2 Soil Liquefaction Mechanism

Loose cohesionless soils, such as fine sands, are more susceptible to liquefaction during a seismic activity because of their tendency to densify under cyclic loading. During the rapid cyclic loading of an earthquake, saturated soils typically do not drain rapidly enough to relieve excess pore water pressures. As a cohesionless soil undergoes earthquake loading, the soil tends to densify which in turn increases the pressure applied to any water present in the soil. Once the excess pore water pressure reaches the vertical effective stress, the load begins to be carried by the water instead of the soil. In this situation, the soil loses its strength and begins to act more like a liquid than a soil, termed as "liquefaction". In soils with poor drainage, the same problem is encountered as the excess water is unable to escape the soil and the soil is then susceptible to liquefaction. Poor drainage is a problem in soils with high fines contents. Higher fines content tends to increase the strength of the soil structure but significantly limits drainage since the fines fill in the void spaces that previously acted as a drainage path for excess water. Soils with high fines content also densify less due to the reduction of voids as the fines fill in the available void spaces. Thus saturated, loose, cohesionless soils as well as cohesionless soils with high fines content are susceptible to liquefaction due to the effects of densification and poor drainage during the rapid cyclic loading of an earthquake.

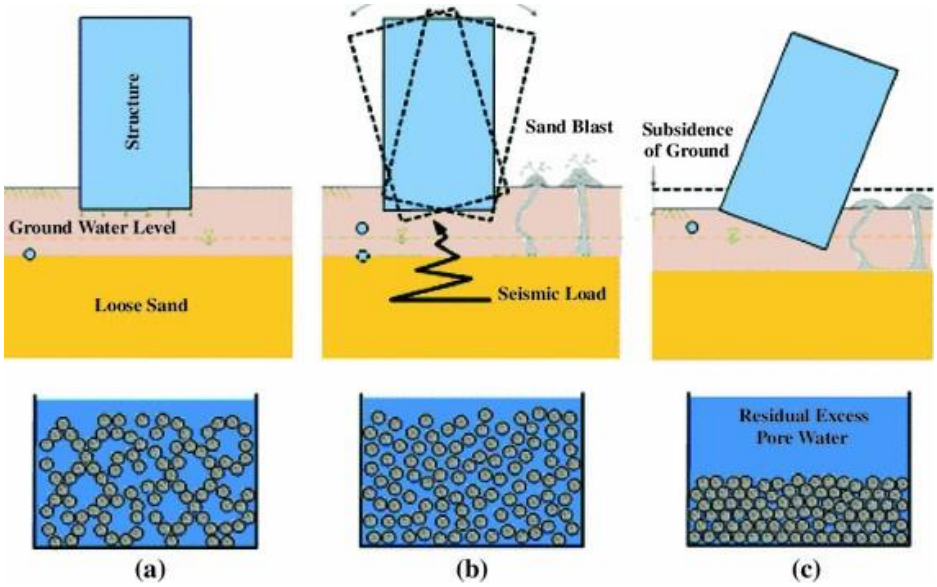

Figure 2.1: Liquefaction phenomena (source: google.com)

2.3 FACTORS AFFECTING LIQUEFACTION

Lee and Seed (1967) have extended this work for studying the various factors affecting liquefaction and identified the followings:

- Relative density of soil
- Earthquake intensity and duration
- Soil type
- Soil relative density
- Particle size distribution
- Presence and absence of plastic fines
- Ground water table location
- Permeability
- Overburden session
- Structure load

2.4.1 Stone Column Liquefaction Mitigation Technique

There are several different liquefaction techniques currently used in practice. These techniques include vibro-compaction, drainage, explosive compaction, deep soil mixing, deep dynamic compaction, permeation grouting, jet grouting, and stone (gravel) columns. The research done for this project focused on the stone column method only with the emphasis being on the effectiveness of the stone column method in sandy soils, thus only the stone column method is addressed here.

2.4.2 Vibro Stone Column

The Vibro-Stone Column technique is one of the most widely-used ground improvement processes to densify loose granular soils. In this method inserting a vibrating poker into the ground, and includes Vibro-Compaction and Vibro-Replacement. The latter process is often referred to as (Vibro-) Stone Columns.

Stone columns are installed using either top- or bottom-feed systems, either with or without jetted water.

2.4.2.1 Dry bottom-feed method

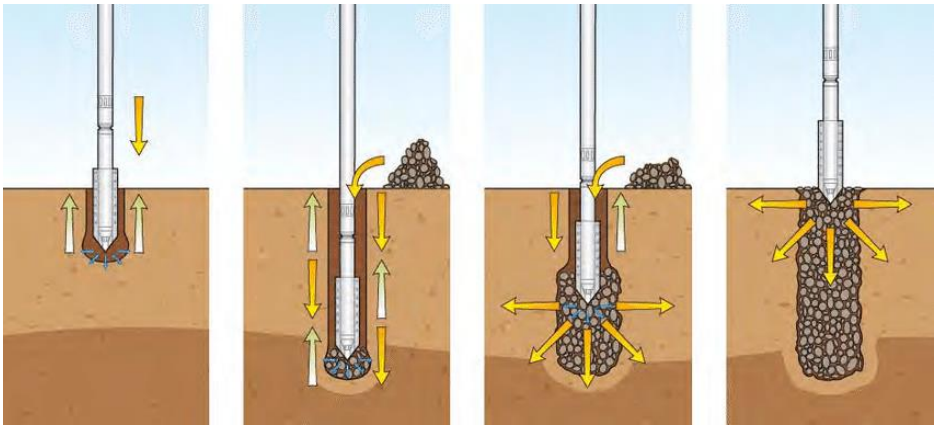

Fig-2.2: Vibro stone column installation by bottom feed method (source: google.com)

The dry bottom-feed process feeds stone to the vibrator tip through an attached feed pipe. Pre-drilling of dense strata at the column location may be required for the vibrator to penetrate to the design depth. This method of construction creates a high modulus stone column that reinforces the treatment zone and densifies surrounding granular soils.

2.4.2.2 Wet top-feed method

In the wet top-feed process, the vibrator penetrates to the design depth using the vibrator's weight and vibrations, as well as water jets located in the tip. The stone (crushed stone or recycled concrete) is then added at the ground surface to the annular space around the vibrator created by the jetting water. The stone falls through the space to the vibrator tip and fills the void created as the vibrator is lifted several feet. The vibrator is lowered, densifying and displacing the underlying stone. The vibro replacement process is repeated in lifts until a dense stone column is constructed to the ground surface.

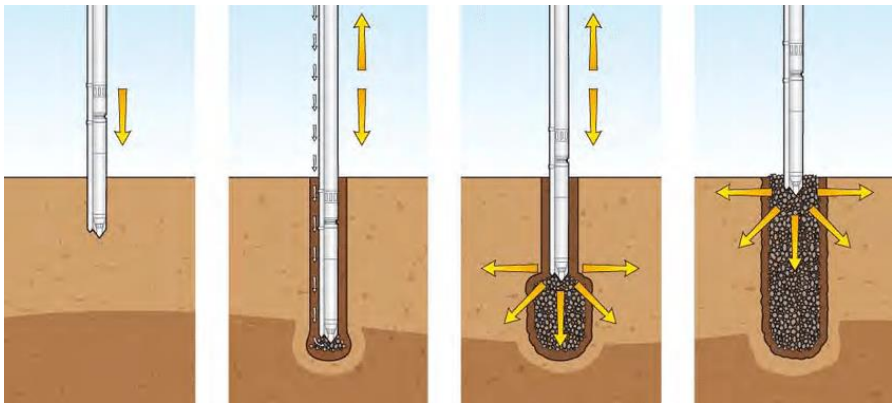

Fig-2.3: Vibro stone column installation by top feed method (source: google.com)

2.5 Evaluation of Liquefaction potential

The Seed and Idriss (1971) simplified procedure has been considered using the following expression to compute the cyclic shear stress ratios (*CSR*) caused by earthquake ground motions at a depth *z* beneath the ground surface

$$\mathrm{CSR} = 0.65\left(\frac{\sigma_{vo}a_{maxo}}{\sigma_{vo'}}\right) * \frac{rd}{MSF} \ldots\ldots\ldots\ldots\ldots\ldots\ldots (1)$$

For the correction of penetration resistances in sand, Seed et al. (1975) included the normalization of penetration resistances in sand to an equivalent σ_{vo} of one atmosphere (P_a = 101 kPa) as part of the semi-empirical procedure takes the form:

$$N_{160} = C_N * N_{60} \ldots\ldots\ldots\ldots\ldots\ldots\ldots (2)$$

where $(N_1)_{60}$ = Corrected value of standard penetration resistance
C_N = Correction factor

Liao and Whitman (1986) has proposed one of the most commonly used expressions for the overburden correction factor (or normalization), which is given by-

$$\mathrm{C_N} = \left(\frac{Pa}{\sigma_{vo'}}\right)^{0.5} \ldots\ldots\ldots\ldots\ldots\ldots\ldots (3)$$

i) Stress reduction coefficient (r_d)

The coefficient of stress reduction factor r_d could be expressed appropriately as a function of depth (z) and earthquake magnitude (*M*). The following relationship has been established using those results:

$$Ln(rd) = \alpha(z) + \beta(z)M \ldots\ldots\ldots\ldots\ldots\ldots (4)$$

Where, $\alpha(z) = -1.012 - 1.126\sin\left(\frac{z}{11.73} + 5.133\right)$

$$\beta(z) = 0.106 + 0.118\sin(z + 5.142)$$

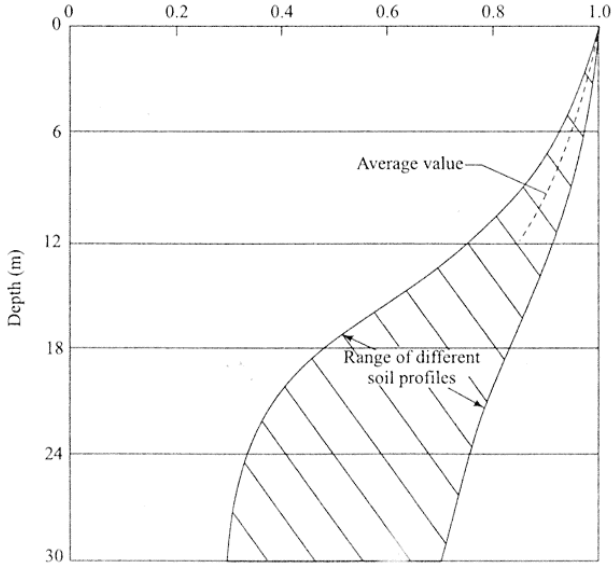

Fig. 2.4 Reduction factor versus depth (Seed and Idriss, 1971)

Where, z is the depth in meters beneath the ground and r_d is the stress reduction coefficient parameter.

ii) Magnitude scaling factor (MSF)

For the adjustment of induced CSR during earthquake magnitude *M* to an equivalent CSR at an earthquake magnitude (*M* =7.5), the magnitude scaling factor (*MSF*) has been applied.

The *MSF* is thus given as: $MSF = \frac{CSR_M}{MSF_{M=7.5}} \ldots\ldots\ldots\ldots\ldots (5)$

By this re-evaluation, the MSF relation is formed and was then expressed by (Idriss 1999) as: $MSF = 6.9 \exp\left(\frac{M}{4}\right) - 0.058 \ldots\ldots\ldots\ldots\ldots (6)$ Where, $MSF \leq 1.8$

The re-evaluated relationship between the number of equivalent uniform stress cycles and the magnitude of the earthquake shown in Fig. 2.5:

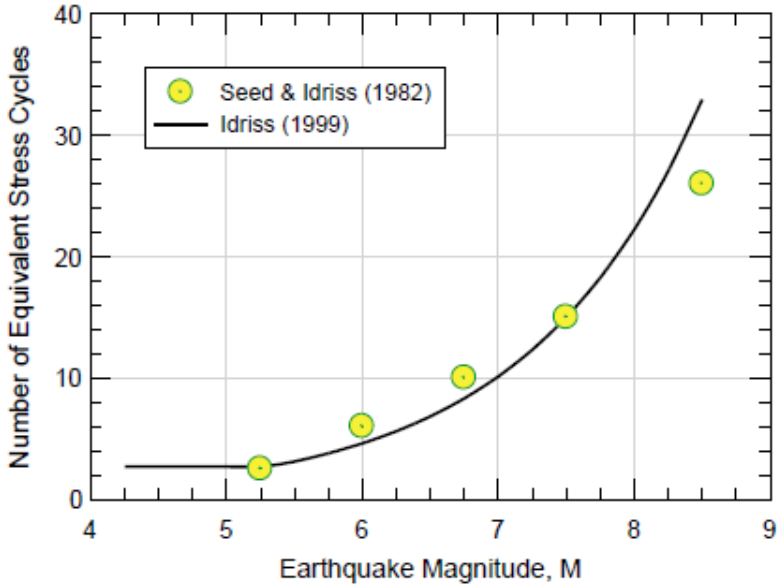

Fig. 2.5 Number of equivalent stress cycles versus earthquake magnitude (Idriss and Boulanger, 2006)

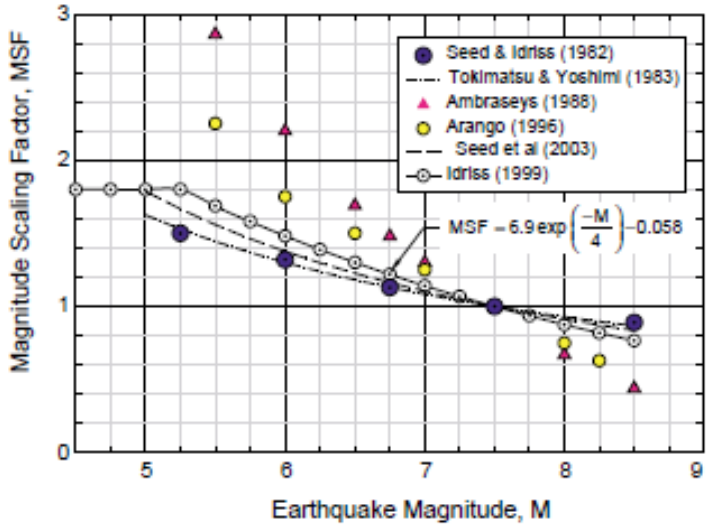

Fig. 2.6 Magnitude scaling factor values suggested by several investigators (Idriss and Boulanger, 2006)

MSF values obtained through Eq. (6) are presented in Fig 6, together with those suggested by others. The re-evaluated MSF values are slightly higher than those initially proposed by Seed and Idriss (1982).

$$K_\sigma = 1 - C_\sigma Ln\left(\frac{\sigma'_{vo}}{P_a}\right) \leq 1$$

$$C_\sigma = \frac{1}{18.9 - 17.3(D_R)^{0.5}} \leq 0.3$$

The correlation between $(N_1)_{60}$ and D_R for the purpose of liquefaction evaluations, the following expression is given:

$$D_R = \left(\frac{N_{160}}{46}\right)^{0.5}$$

***ii)* Factor of Safety against Liquefaction**

Finally factor of safety for liquefaction is defines as: $FOS = \frac{CSR}{CRR}$ ... ... (7)

The factor of safety against liquefaction for each layer of soil deposits are evaluated by using Eq 7

Where, *CSR* = cyclic stress ratio generated by the earthquake shaking
and *CRR* = cyclic resistance ratio for earthquakes magnitude of 7.5

The factor of safety against liquefaction for each layer of soil deposits are evaluated by using Eq.7.

If *FOS* is less than 1, liquefaction will be occurred.

whereas if *FOS* is greater than 1, chances of liquefaction occurring is rare.

2.6 Relevant Works in Past

Now, we are going cover an extension review of the existing literature related to this study. The literature review is going to cover analytical, empirical, numerical, experimental works

---

Seed and Idriss (1971) gave two parameters to determine the liquefaction resistance of the soil, (i) CSR or earthquake induced stress in the soil and (ii) CRR, which is the resistance against liquefaction.

$$\text{CSR} = \left(\frac{\text{amax}}{\text{g}}\right) * \left(\frac{\sigma_0}{\sigma_{0'}}\right) * \text{rd}$$

This CSR value should be reduced by 35% to represent the most significant cycles over the full period of loading.

$$\text{R}_\text{d} = 1.0 - 0.00765\text{z} \quad \text{for z<9.15m}$$

$$\text{R}_\text{d} = 1.174 - 0.0267\text{z} \quad \text{for 9.15m<z<23m}$$

Where, a max= maximum acceleration during earthquake and Z= depth of concern

Rayhani et al. in 2007 conducted a ground response study of the Bam Earthquake (2003) by using subsurface geotechnical and geophysical data from two distinct sites. They estimated the local site condition on earthquake ground motion on that location. Finite difference code (FLAC) was used in this work to implement both non-linear methods and compare them to equivalent-linear alternatives. Both nonlinear and equivalent liner approaches display a peak in the response spectra with a period between 0.3 and 1.5 seconds. Non-linear analysis had lower levels of amplification than the corresponding liner approach, especially over lengthy durations. When utilizing the equivalent liner approach, the amplification factor was around 1.4, however when employing the complete nonlinear method, it was about 1.35. The corresponding liner method's maximum spectral acceleration was 15% more than the non-linear methods. According to the research's findings, the equivalent liner technique demonstrated more amplification and additional response than the complete non-linear analysis.

Madhav and Krishna et al. in 2008 gave an overview on the mitigation of the earthquake liquefaction by granular piles. The construction of gravel drains and granular piles is the most extensively used remedial solution for liquefaction mitigation. Granular piles offer a means of drainage, compact the soil around them, and strengthen the earth already there. The operation of the stone columns is affected by many processes throughout the liquefaction mitigation procedure. Drainage is a key basic process that allows produced surplus pore water pressures to be released almost as quickly as they are created. The other processes include reinforcement, storage, dilatation, and densification. All mechanisms and their mechanics must be taken into account while analyzing the gavel drain system's performance.

Bouckovalas et al. (2009) has been reviewed the Seed & Booker's (1977) work on liquefaction mitigation using infinitely permeable gravel drains In order to better understand the rate at which extra pore pressure builds up in the unimproved ground (expressed as $\frac{\delta u_g}{\delta N}$). In the first investigation, it was considered that the excess pore pressure ratio (r_u) at a specific time was the only factor affecting this rate. But then it was understood that there are actually two conflicting variables at play in this rate. The excess pore pressure ratio (r_u), which affects the first factor, causes the rate at which excess pore pressure builds up to progressively grow. Second, another component is the development of sand fabric toward a more stable state. This evolution is affected by either the number of cycles ratio (N_{eq}) or the amount of time that has passed since the shaking began, and it results in steadily declining rates of excess pore pressure buildup.

In summary, the following were the major changes to the original solution to the problem that emerged from the aforementioned revision:

i. Excess pore pressures peak reached early in seismic shaking and then start to fall while shaking continues, unless the improved ground liquefies. But in the original paper, excess pore pressure reached at the end of the seismic loading.

ii. The updated estimates of the improved ground's peak excess pore pressure $r_{u_{max}}$ are consistently lower than the earlier estimates. The greatest difference for mild seismic shakings with $\frac{N_{eq}}{N_1} = 1$ somewhat larger than 20% and occurs at the low range of excess pore pressure ratio, that is $r_{u_{max}}$ 0.3. The highest difference for greater shakings with $\frac{N_{eq}}{N_1} = 2$ is on the order of 50% and occurs at intermediate excess pore pressure ratio values (i.e., $r_{u_{max}}$ = 0.3-0.7).

iii. The difference in the volume of gravel drains needed for a typical value of the maximum excess pore pressure ratio in the improved ground, such as $r_{u_{max}}$=0.4, is about equivalent to 15% for mild shakings ($\frac{N_{eq}}{N_1} = 1$) and 15 to 25% for heavier events ($\frac{N_{eq}}{N_1} = 2\ to\ 4$). Beyond the value of $r_{u_{max}}$ = 0.4 larger difference were observed.

Weber et al. in 2010, on the basis of centrifuge testing observation confirm that smear and disturbance occur owing to stone column installation and the region influenced can be divided into three sections:
(1) a penetration zone, where the sand particles are squeezed through the clay;
(2) a smear zone where the soil particles have experienced a significant reorientation; and a
(3) densification zone, where the structure of the clay does not appear to change, but compaction of the clay is measurable. The extremes of the disturbed zone around model stone columns are determined to extend to about 2.5 times the column radius.

Vargas et al. (2014) in their paper on this work has performed a liquefaction analysis for a site using two dimensional numerical models that take into account the irregular ground and the constitutive models that involve the dynamic pore-pressure generation from volumetric strain induced by seismic excitation. This paper highlights the means considerations of numeric model, as such as, input parameters, model calibration, steps calculations, among other. Moreover, model results are compared with simplified empirical methods and field measurements.
They have considered Hotel Sapanca site during the 1999 Kocaeli (Izmit) Turkey earthquake for their study. The site is located on the southern coast of Lake Sapanca, approximately 20 km of the Izmit Bay southwest of the city of Adapazary. Following earthquake parameter was used. The Kocaeli (Izmit) earthquake (Mw 7.4). The Sakarya strong motion had a peak ground acceleration of 0.37 g (Fig 9). Permanent lateral displacement of 1.50 m according to the measurements of ground fissures occurred.

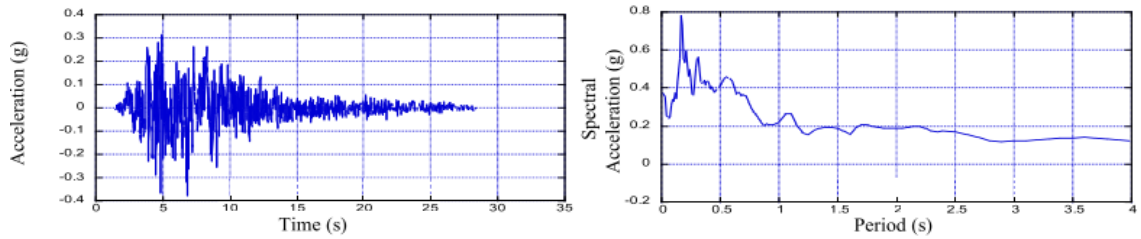

Figure 2.7 Acceleration record and response spectra from Sakarya strong motion record. (vargas et al.)

The strength parameters were derived from the in-situ tests (SPT and CPT), which were carried out by researchers from different Universities. The dynamic soil properties such as shear wave velocity and shear modulus were estimated using the empirical relation based on direct measurements of in-situ tests depending on cone tip resistance. Then the model was developed considering horizontal layers as derived from bore hole data and the dynamic simulation was carried out using a Finite Difference Method with FLAC-2D software. The programme includes such process to calculate pore pressure generation under cyclic loading. The response of the soil during earthquake, in terms of effective stress, excess pore pressure and excess pore pressure ratio as a function of the time, at a corresponding point is generated through FLAC.

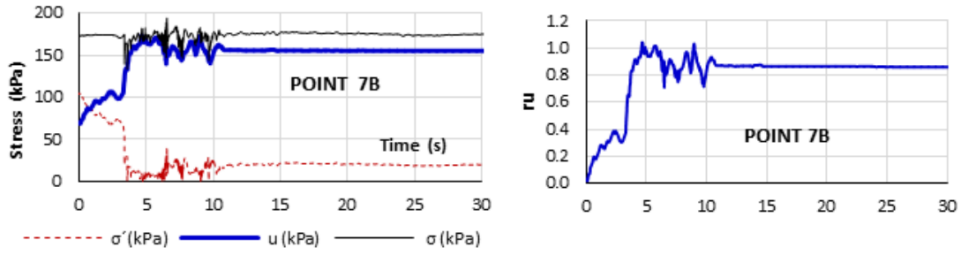

Figure. 2.8: Excess pore-pressure ratio (ru), pore pressure and effective stress. (vargas et al.)

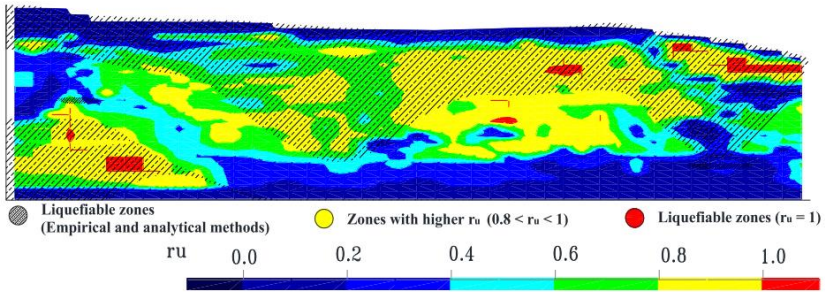

Figure 2.9: Excess pore-pressure ratio contours. (vargas et al.)

then compared the data from the FLAC to the actual result and arrived at the conclusion that the modelling should include three steps: 1) Model calibration (Free Field), 2) Static equilibrium calculation for the site including the steady-state groundwater conditions and 3) Seismic calculation and dynamic pore pressure generation. From the above data the author concluded that more case studies should be analyses, in order to generalize the model results.

Tang et al. in 2015 conducted a numerical analysis to check the improvement of liquefaction in a sand stratum with the help of stone column. They first simulate a centrifugal test data using a 3D finite elements base software so predicted stone column and silty sand ground response on 50 g gravitational acceleration field. Then a parametric study was conducted to analyzed the effect of stone column by varying permeability of stone column and surface load with a sinusoidal type loading. The major outcome of this study was listed below .....

i. The shear stress reduction co-efficient ratio of the reinforced or unreinforced ground depends on the vertical as well as horizontal locations

ii. When compared to the unimproved stratum, Stone Column remediated silty stratum generally showed stiffer responses. Nevertheless, complete liquefaction in the upper-half silt stratum was not prevented.
iii. Permeability of stone column played a very important role in liquefaction prevention. When Stone column permeability has higher than a critical value, there was a rapid dissipation of excess pore water pressure built up. And also, significantly reduce the soil acceleration attenuations. Similarly, the SC with low permeability failed to achieve the benefits of reducing liquefaction hazard because it was unsuccessful in preventing the excess pore water pressure generation in silty sand, particularly nearby the ground surface.
iv. Although the stiffening advantage from the higher load applied at the SC zone was minimal, it did result in acceleration of the attenuation type after the stratum was completely liquefied. However, as depth increased, the accumulation of pore water pressure somewhat decreased.

Asaadi et al. conducted study in 2015 to assess the possibility of instability for the safe and earthquake-resistant construction of deep foundation. The liquefaction susceptibility of saturated sand interacting with a single concrete pile was simulated in this work using the FLAC 2D finite difference approach. Soil liquefaction was assessed using a nonlinear effective stress analysis, and the interaction between the soil and the pile was taken into account utilizing interface elements. In order to analyze liquefaction in the soil mass over a period of time, Ru was chosen as the pore water pressure ratio. A parametric study was done on three different types of soil masses (loose, semi-dense, and dense) under three different ground motions (Kocaeli, Kobe, Bam) with varying main frequencies and peak accelerations were subjected to a series of numerical simulations. Excess pore pressure, lateral movement, and settlement time histories were used to analyze the impact of these characteristics. The finding from these studies was__

i. In every case, liquefaction susceptibility at low depth exceeds liquefaction potential at high depth. It was found that chance of liquefaction decreases with depth as the relative density of soil increases with depth.
ii. The highest amount of Ru near the pile was always less than 0.95, showing that theoretically, soil liquefaction does not occur. The pile also produced a smoother pore pressure diagram, suggesting that the pile avoids excessive shear deformation by reinforcing the soil.
iii. When liquefaction start was taken into account, it was shown that liquefaction happens more quickly the greater the peak ground acceleration. And also horizontal displacement of the pile head and the surrounding soil settlement both increased as the earthquake's maximum amplitude reached.
iv. When the earthquake predominant frequency value increased, the rate of dissipation increased, and the soil's response to liquefaction reduced for both near pile and free-field locations.

This study was not gave any important relationship between the earthquake predominant frequency and the objective deformations.

Salem ben et al. in 2015 shows the generation and dissipation of excess pore pressure are analyzed by considering the granular-column installation effect. This effect is described by a decrease in horizontal permeability within a disturbed zone around the stone column, which is describe by constant, linear, and parabolic variations.

The main findings of this parametric study are following …

1. With increase of granular-column spacing, the generation of excess pore pressure increases, and a slower rate of dissipation is predicted.

2. Reduced soil permeability, and a larger disturbed zone around the granular column increases the peak value of the maximum pore pressure ratio $r_{u_{max}}$ during the cyclic loading and decreases the dissipation rate after cyclic loading.

Rollins et al. in 2015, present a case history in which the project (Utah department of transportation) had a liquefiable site is to be improved by stone column with pre-fabricated (wick) vertical drain.
The soil profile at the Shepard Lane contained a liquefiable layer between 3.3 and 4.3 m thick consisting of interbedded layer of silty sand (SM) and sandy silt (ML). The fines content in the liquefiable layer varied between 22 and 88% with a median value 53%. The plasticity index typically ranged from non-plastic to about 4%. The $(N_1)_{cs}$ value generally ranged from 7 to 25 with an average value 17. Liquefaction analyses established the penetration resistance acceptance criteria as a minimum $(N_1)_{cs}$ of 24 with an average $(N_1)_{cs}$ of 30 in order to provide an adequate factor of safety against liquefaction.
Due to the high fines content in the liquefiable soil layer the potential for mitigating the layer using stone column alone was considered to be very low. To evaluate the effectiveness of wick drains concert with stone column for producing the desired improvement a test program was undertaken at the site.

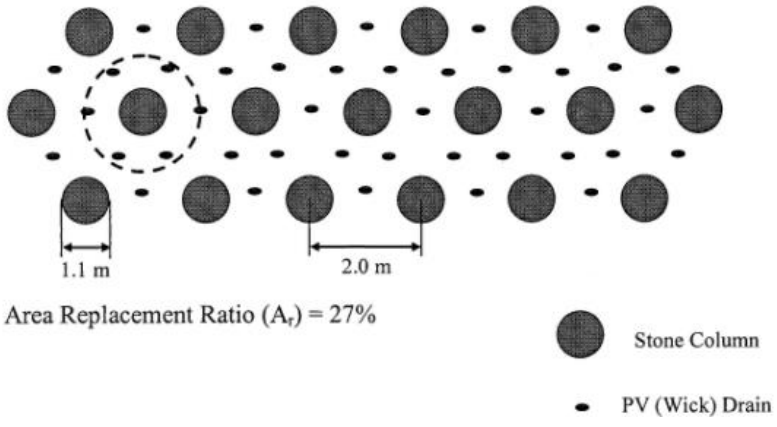

Fig 2.10: Arrangement of stone columns and prefabricated vertical drains for mitigating liquefaction hazard in silty silt/silty sand at Shepard Lane site in Farmington, Utah **(Rollins et.al.)**

Wick drain are place at the mid-point of each stone column as shown in Fig: 2.10. Tests were perform for stone column spacings of 2.0 m and 1.8 m on centers in a triangular pattern which, for the 1.1 m diameter of stone columns, corresponds to area replacement ratios of 27.4% and

33.9% . Decreasing the spacing did increases the $(N_1)_{cs\ values}$ as much as 60% . Continuous SPT sampling was performed before and after the treatment and result plotted in Fig 8. However for 2.0 m spacing was sufficient for getting $(N_1)_{cs}$ value. For this spacing, six wick drains are located at a radius of 1 m around each stone column as shown in Fig 2.10.

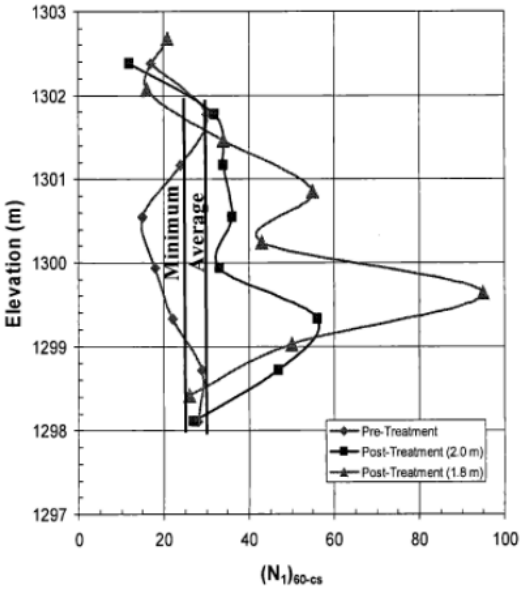

Fig. 2.11: Effects of decreasing stone column spacing from 2.0m to 1.8m on $(N_1)_{cs}$ value vs depth **(Rollins et.al.)**

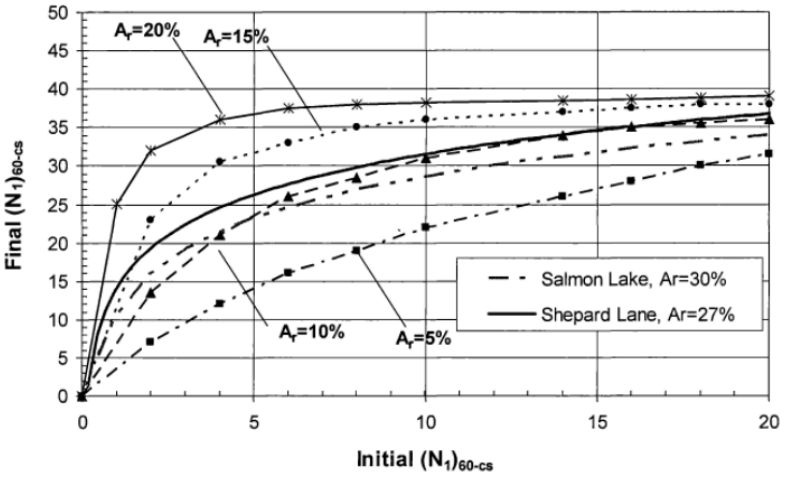

Fig. 2.12: Relationship between final and initial $(N_1)_{cs}$ value for low fines content sands(<15%) relative to observed trends for high fines content test sites with and PV drains. **(Rollins et.al.)**

The treatment plan was employed over an area of about 614 m^2. Prior to the stone column installation 698 wick drains were installed. Subsequently, 304 stone columns were installed to a depth of approximately 7.5 m using dry bottom-feed method. Typical treatment time for each stone column as was between 30 and 40 minutes.

After this experiment following result come with comparison with salmon lake site project….

….

1. Use of pre-fabricated vertical (wick) drains in concert with stone column treatment led to increase (90%) in the average SPT $(N_1)_{cs}$ value.
2. The effectiveness of stone column treatment increased as much as 60% as the column spacing and wick drain spacing decreased from 2.0 to 1.8 m.
3. The increased in penetration resistance is similar with the result from the Salmon Lake Dam where similar soil were encountered and wick drains also used.
4. The stone column treatment in silty sand/sandy silt with a replacement ratio of 27% was about as effective as stone column treatment in cleaner sand(<15% fines) with a replacement ratio between 10 and 15%

Huang et al. conducted a shaking table test in 2015 to analyze the effects of stone columns using four models, including two that contained saturated sand and two that contained composite stone column foundations. They measured the pore pressure generation, dissipation, and acceleration response during earthquake loading. According to the test results, the surrounding soils' ability to resist liquefaction during an earthquake depends on three factors: a) soil densification; b) drainage along the stone column; and c) a decrease in the soil's overall cyclic shear stress. After the experiments the following results presented in this study, the following conclusions were reached.

i. Enhanced Liquefaction Resistance: The study found that the liquefaction resistance of saturated sand deposits was significantly improved when stone columns were used during vibration. Stone columns reduced the excess pore water pressure (EPWP) buildup (in composite stone columns), increased overall ground stiffness, and notably reduced settlement.

ii. Interdependence of Factors: The effectiveness of densification, drainage, and redistribution of earthquake shear stress were interconnected. Densification played the most crucial role among these factors. Drainage and earthquake shear stress redistribution were more effective when the sand ground had a high density.

iii. Preliminary Findings: The results of this study are considered a preliminary attempt to quantify the effects of stone columns in mitigating liquefaction in sand deposits. Further tests are recommended to cover a broader range of conditions, including area replacement ratio, input motion parameters, stone column permeability, initial stiffness, diameter, and slenderness ratio. These additional tests are needed to fully understand the cyclic behaviors of sand deposits in the presence of stone columns.

These findings highlight the potential of stone columns as a liquefaction mitigation measure in sand deposits while emphasizing the need for further research to comprehensively explore their effectiveness under various conditions.

Meshkinghalam et al. 2017 proposed a study to investigation of application of stone columns in decreasing liquefaction potential. Liquefaction potential of sand bed was studied by FLAC3D and validated by the results of VELACS international project. The effect of stone column was studied on decreasing excess pore pressure and soil settlement individually at the center of the model with different diameters. The effects of columns group were also studied on decreasing excess pore water pressure and soil settlement in a triangle arrangement. Finally, an average vertical contact pressure of 100 kPa, which is approximately equal to the vertical pressure transmitted by a 10-story reinforced concrete building, was applied in the model.

1. It seems that stone column drainage performance is effective at depths of about 3–3.5 m from ground surface. Moreover, stone column causes drainage at zone with distance of about 2.5 m from its center. The effect of column drainage is vanished at distance more than 2.5 m. With increase of depth, the range of soil drained by stone column increases.
2. The columns group function will be better in settlement reduction, for centre to centre distance which is equal to 2.5–3.5 times of column’s diameter.

Banerjee et al. in 2017 numerically investigated the liquefaction potential of Kasai River sand using finite difference method base FLAC 2D software. In this study behavior of Kasai River sand checked on a shake table and numerically by applying a sinusoidal motions of amplitude 0.35 g at a frequency of 2 Hz. Then the surface settlement, lateral spreading, predominant frequency, amplification of the ground motion and pore water pressure development in both dry states and liquified states were analyzed separately. The finding from this research were _____

i. The numerical studies, shake table tests, and cyclic triaxial data all clearly indicate the sand from the Kasai River liquefies in about 8 cycles of 0.35 g sinusoidal motion at 2 Hz. When the dry sand deposit is shaken, it is discovered that the maximum settlement is around 10 mm. Under the same loading conditions, after liquefaction the maximum settlement to go up to 26 mm.
ii. Under liquefied state volume change take place about 4% , whereas the same sand in dry state changed volume 1.5% which is considerably smaller.
iii. The amplification of PGA at the ground level is substantially larger (about 1.9 times) in the liquefied sand than in the dry sand because dry sand provides more rigidity than liquefied sand does.
iv. When compared to dry sand, the maximum value of lateral spreading at the surface for liquefied sand is likewise much larger (approximately 2.50 times).

This suggests that if the sand from the Kasai River liquefies, superstructures may sustain damage to a considerably higher degree.

Salem et al. (2018) investigated the liquefaction susceptibility using FLAC2D software on a silty sand reinforced with stone column. The liquefaction potential of silty sand layer is calculated in terms of maximum pore water pressure ratio r_u . maximum pore water pressure ratio r_u is indicated by ratio of pore water pressure generation to initial effective stress. When this ratio r_u is reached the value 1.0 then that state considered as liquefaction occurrences. Previously this silty sand layer soil model was prepared to simulate the shaking table test and validate with various published experimental result. In this study, a parametric study was done by varying frequency and amplitude of a sinusoidal wave as a dynamic shaking and the effects of installation of stone column with the model. The results obtained, as the frequency of the shaking decreased, the liquefaction susceptibility decreased. And also decreased with amplitude of the motion. In the other part of this study result found that when the model is reinforced with stone column, the generation of excess pore pressure ratio is reduced significantly and the model was safe against liquefaction.

Pal and Deb et. al. in 2018 present a study to evaluate the performance of stone column for dissipation of pore water pressure during soil liquefaction. This study shows considering stiffness and limited permeability of the stone column, the maximum pore water pressure ratio reduced by 20-60% during soil liquefaction.

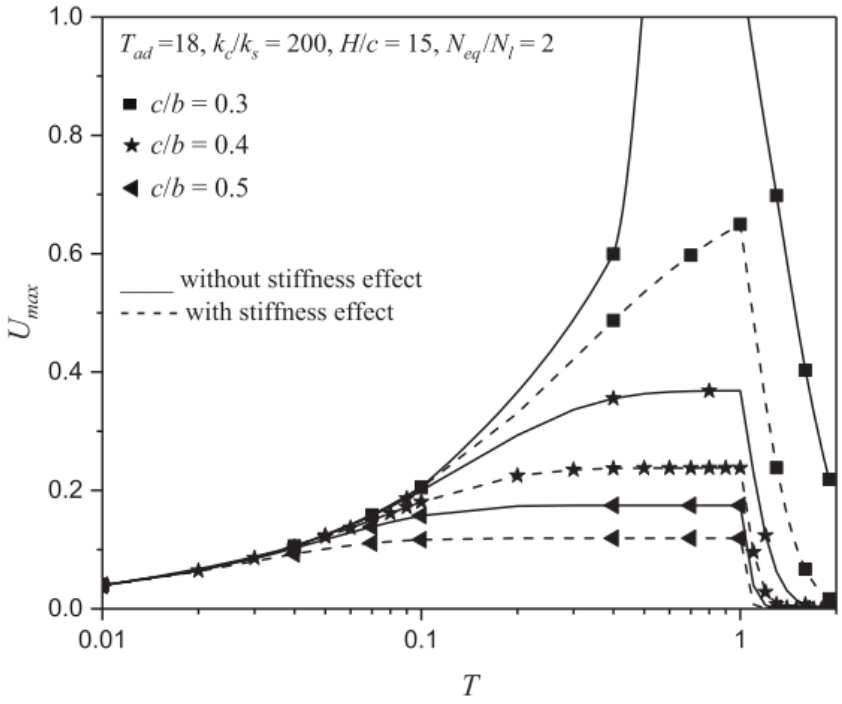

Fig. 2.13: Effects of area on Umax with and without considering the stiffness effect of the column (**Pal and Deb et. al.)**

Pal and Deb et. al. in 2019a, proposed a mathematical model to find out the generation and dissipation of excess pore water pressure considering smear effect, well resistance and stiffness of stone column for mitigation of liquefaction. Due to considering the limiting permeability and higher stiffness of stone columns, the following results were found ….

a) For Kc/Ks = 500, $\frac{m_{vs}}{m_{vc}} = 3$, the maximum excess pore pressure ratio increases by 20% due to smear effect.

b) Consideration of the limited permeability of stone column, further increase the pore pressure ratio by 28% to 71%.

c)Due to considering smear effects, increase in the stiffness of stone column decrease the pore pressure ratio up-to 66%.

Thus, smear effect, well resistance and stiffness effect of stone column should be considered to minimizing the liquefaction of soil.

Pal and Deb et. al. in 2019b, further considering clogging effect of stone column and shows how it affect the permeability of stone column to influencing the liquefaction potential measures.
In this paper, a mathematical model is proposed based on unit cell approach considering clogging of stone columns on performance of these columns during liquefaction under seismic conditions. The proposed model reveals that the clogging of stone columns significantly reduces the drainage capacity of these columns. A parametric study performs to investigate the influence of model factors such as permeability ratio, area ratio, compressibility ratio and hydraulic gradient on the drainage capacity of columns. From the parametric study, it can be concluded that hydraulic gradient is the most influencing parameter whereas the stiffness of columns not so important.
The difference between the peak values of the maximum excess pore pressure ratio obtained from the clogged and unclogged curve increases by 20% corresponding to an increase when the hydraulic gradient is between 0.3 and 0.9.

During the first earthquake, the clogging of the stone column starts towards the end of earthquake loading or when the excess pore water pressure starts to dissipate. However, during a second earthquake the variation of the excess pore water pressure can start at the beginning of the earthquake due to the clogging which occurred during the first earthquake. More time is required to dissipate the excess pore water pressure after a seismic event due to clogging.

The peak value of the excess pore water pressure ratio can increase up to around 50% due to clogging during the first earthquake and a greater difference between the peak values of the excess pore water pressure ratio obtained for clogged and unclogged case is observed due to successive earthquakes until the clogging reaches an optimum value. It has been observed that under the selected conditions, the difference between the peak values of the excess pore pressure ratio between the first and second earthquake is around 65%.

BABAEI and DABIRI et. al. (2019) conducted a numerical analysis to check the stone column effectiveness using FLAC 2D program. A group of stone column placed on a single layer of sand deposit, varying the diameter i.e. 0.6m, 1.2m and 1.8m at spacing 60 to 120 cm center to center of stone column while keeping length of the stone column constant of 9m. A harmonic loading used in this study as per Tang et al. (2015). Result obtained from this study that while keeping the diameter of 1.2m at a spacing of 1.2m under a surcharge load of 5 and 15 storied building, the excess pore water pressure reduced and performed better in soil liquefaction.

Kumar et.al. in 2020 This paper deals with how the granular columns perform as a mitigates the potential risk of liquefaction. The governing equation for evaluating ground subsidence with associated variation in the excess pore pressure (EPP) is based on Biot's consolidation equations with the implication under a cyclic load. A couple of equations are composed of the continuity equation and mass moment balance equation, which are further transformed into finite element form using a variational approach. A computer program was developed in FORTRAN 90 to carry out coupled analysis. The EPP dissipation and settlement results are analyzed by considering the granular column installation effect with variations in the length and number of columns.

The main outcomes are summarized as follows:

1. The outcome of the numerical mitigation model is very simple to use and is a time-saving and cost-effective approach. The generated EPP and settlement were evaluated at all depths and widths of assumed soil domains simultaneously. The coupled approach can model the gradual loss of soil strength due to the build-up of pore pressures during the dynamic loading, which predicts the real behavior with better precision.

2. Without a stone column, the liquefaction phenomena were observed along all the depths at an acceleration of 0.15 m/s^2 and the installation of the stone column stiffened the soil deposits and decreased the drainage path. Therefore, less settlement and EPP were observed. It was revealed that as the depth of penetration of the stone column increased, settlement decreased. The maximum percentage reduction in horizontal displacement and settlement were 24.4% and 30.66% respectively for a percent area ratio of 22.2%.

3. With the increase of granular columns, the chance of liquefaction at greater depth was minimized. As the percent area ratio increased from 2.78% to 5.55%, the generated EPP reduced by 16.97% and when this value increased from 2.78% to 8.33%, the generated EPP reduced by 35.48%. In addition, the effect of the side stone column below the foundation was insignificant in terms of EPP and settlement.

4. With the increase of granular column spacing, the generation of EPP increased, and a slower rate of dissipation was predicted.

Hleibieh and Herle et. al. (2020) analyzed the performance of stone column numerically to reduce the potential of soil liquefaction. This study is based on a hypoplastic model using a program TOCHNOG PROFESSIONAL. Here it showed how the drainage and stiffening effects of stone column is affects to reduce the risk of soil liquefaction. Column drainage and stiffening effects were analyzed separately and found that drainage of column does not show any major effect but stiffening of column makes a greater substantial effect. Due greater stiffening of stone column less excess pore water pressure generated. Also, this study analyzed the effect of various intensity of earthquake loading. Liquefaction due small medium earthquake is mitigated easily. But in case large or very large earthquake liquefaction delayed. Require more load cycles or require more time to generate excess pore water pressure to reach liquefaction state.

CHAPTER –3
METHODOLOGY

To study the behaviour of stone column for the analysis of Liquefaction and also mitigation in a stratified soil deposit under dynamic loading is performed using finite difference method implemented in FLAC2D version 8.1.447 by forming full-scale modelling of a stone column, subsequent without stone column in a subsoil strata and load conditions. In this study, basically, a parametric study has been performed considering the variation of stone column length, variation of different PGA, variation of different dominant frequency etc. and consequent effects on the behaviour of the stone column are analysed. A full-scale model of the stone column and without stone column on a 13.5 m depth liquefiable sandy layer is modelled in the FLAC2D. After that, the static stability analysis is done to ensure the static stability of the model. Then the dynamic loading is applied on bottom of a bedrock in the form of a shear stress wave derived from the acceleration time history of the Loma Prieta earthquake (1989) in California. High to moderate level of shaking has been applied at the base of the bedrock by the original and scaling of the PGA of the original input motion to the intended PGA values.

The steps of modelling are discussed below.

i. At first a full-scale model of stratified soil deposit without stone column and another stone column of different length placed on the same stratified soil deposit is developed.
ii. Then the initial boundary conditions are applied and meshing has done according the smooth wave propagation.
iii. After that material properties of Mohr-Coulomb are applied to the stone column and subsequent subsoil strata. And then Ground water property are assigned same way.
iv. Then the level of GWT is specified, in this case it is at ground level.
v. At the initial stage, the static stability analysis is done to ensure the static stability of the model in both cases one is without stone column and another is with stone column.
vi. Before going to the dynamic analysis, first, the Mohr-Coulomb model was changed to Finn-Byrne model for liquefaction analysis but considering high ff latency as per Finn/Byrne model
vii. then the model is run to ensure dynamic stable condition state before liquefaction analysis
viii. After that, dynamic mode is turned on. And large strain mode calculation also turned on.
ix. To run the dynamic step, various corrections have been made, such as velocity and displacement correction. The applied velocity time history is corrected as the same.
x. To check the mesh size the dominant frequency of the power spectrum was determined.
xi. Then the boundary condition suitable for dynamic analysis was applied, Quiet boundary condition at the base and Free-Field boundary condition at the vertical sides of the model to get better results.
xii. At last the dynamic step was run with couple flow mode considering ground water flow time step and dynamic time step must be same.
xiii. And then various parameters were determined afterward.

3.1. Brief Description of FLAC 2D and its salient features:

FLAC2D is a finite difference program used for engineering mechanics problems. This program simulates the behaviour of soil, rock etc under static and dynamic loading. The materials are represented by zones/elements which forms the grid that is fit to shape of the modelled geometry. Every element behaves according to the properties assigned to them in accordance with the boundary condition of the model. The plastic flow and plastic collapse can be calculated very accurately with FLAC as it uses Lagrangian calculation and mixes discretization zoning technique. This software is primarily developed for geotechnical and mining engineering problems FLAC offers several in-built constitutive models that allow the simulation of non-linear irreversible response that is the representative of geologic or similar materials. It offers several special features like:

i) interface elements for the separation

ii) plane-strain, plane-stress and axisymmetric geometry models.

iii) groundwater and consolidation calculation with the automatic phreatic surface generation

iv) graphical interface to facilitate for model construction

v) Dynamic analysis capability

vi) Optional viscoelastic and visco-plastic models for creep analysis.

vii) Optional thermal modelling capacity

viii) Optional two-phase model

ix) Facility to add user-defined constitutive models in C++, and compiled as DLL and can be loaded whenever needed.

FLAC also has inbuilt programming language FISH to extend its usefulness. In FISH, the user can write their function and own constitutive models if needed. It can be operated as either a menu-driven or command-driven program. A menu-driven command is useful for new users, but a command-driven program requires much more knowledge of the FISH language.

The plastic collapse and plastic flow are modelled with the mixed-discretization scheme. This is more accurate than the reduced integration method that is usually used by the finite element techniques. The FLAC uses an explicit solution scheme that follows arbitrary nonlinearity in stress/strain laws in almost same computing time as in case of linear laws, unlike implicit solution techniques that take quite large time for solving non-linear problems. FLAC tracks its elements in row-column numbering fashion rather than sequential fashion. It is easier to identify elements when interpreting outputs and assigning properties.

But there is a few disadvantages of the FLAC software. The linear simulations run slower in case of FLAC than with equivalent finite element programs. Actually, FLAC is most suitable for large-strain or non-linear problems. The time to solve a problem containing a composite material system depends upon the ratio of the longest natural period to the shortest natural period. This causes trouble to solve certain problems and solution time is very large.

The basic mode of FLAC is a two-dimensional plane strain model analysis. This condition is well conformed to the long structures, excavation with constant sectional features along the

length and subjected to the loading in the plane of its cross-section. This software also offers a plane-stress mode for analysis of plate-like structures. Now, in our study, the plane strain mode of analysis is used because the stone column is work in reality as a three-dimensional shape but here, we considered the unit cell of stone column as a two-dimensional strip. The out of plane stress-components are taken into account the plastic yield calculations in the plane strain analysis. Five Optional Features are available i.e. Dynamic analysis, thermal analysis, Creep analysis, thermal analysis and adding new constitutive models as DLLs in FLAC. With the incorporation of dynamic analysis option in FLAC, analyses can be performed in earthquake engineering like the stability of embankments, dams, liquefaction, soil-structure interaction easily. Problems like an underground explosion, blasting can also be calculated. In summary, it is safe to say that FLAC2D version 8.1.447 is a suitable choice for modelling and analysis of stone column on a loose saturated sand under seismic condition.

3.2 Conversion of Stone Column model 3D to model 2D

Consider a group of stone column of diameters 0.8m at a spacing of 2m centre to centre considered in three-dimensional model. Then the following way we can convert the 3D model to 2D model_____

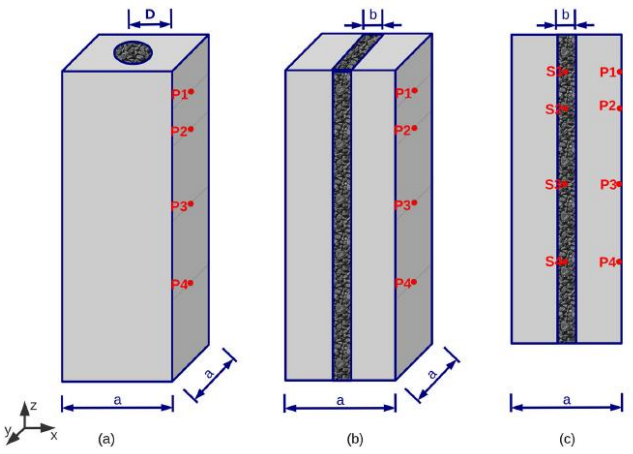

Fig. 3.1: 3D (a, b) and 2D (c) models of a stone column (Hleibieh and Herle et al.)

As per **Hleibieh and Herle et al. (2020),** In order for the area ratio (area of the surrounding soil/area of the columns) in the 2D model to match that in the 3D scenario, the width of the stone slice in the 2D model was modified.

So, supposed the diameter of the 2D slice is b=0.8m and the spacing is a=2m. So, by back calculation we can obtained the actual stone column diameter 'D', which is in 3D cases.

Influence dia in 2D cases = Influence dia in 3D cases = spacing of stone column = a = 2m

The influence area in 3D cases = $A_1 = 2^2 = 4\ sq.unit$

The stone column area in 3D cases = $A_1 = \frac{\pi}{4}D^2\ sq.unit$

So, area of the surrounding soil area in 3D cases = $A_s = \left(4 - \frac{\pi}{4}D^2\right) sq.unit$

From the above recommendation,

$\frac{4-\frac{\pi}{4}D^2}{\frac{\pi}{4}*D^2} = \frac{2}{0.8}$ or, D = 1.2 m

So, we can conclude that, the stone column of 1.2m diameter at spacing 2m in 3D case can be converted as a 2D slice of 0.8m diameter at same spacing 2m.

But in the case of this study, there is not required any such type of conversion as we considered a single two-dimensional slice of stone column install on stratified sandy soil deposit.

3.3 Description of the Stone Column model and Stratified Soil deposit:

To study the stone column effects on liquefiable soil, at first it is required to model the stone column.

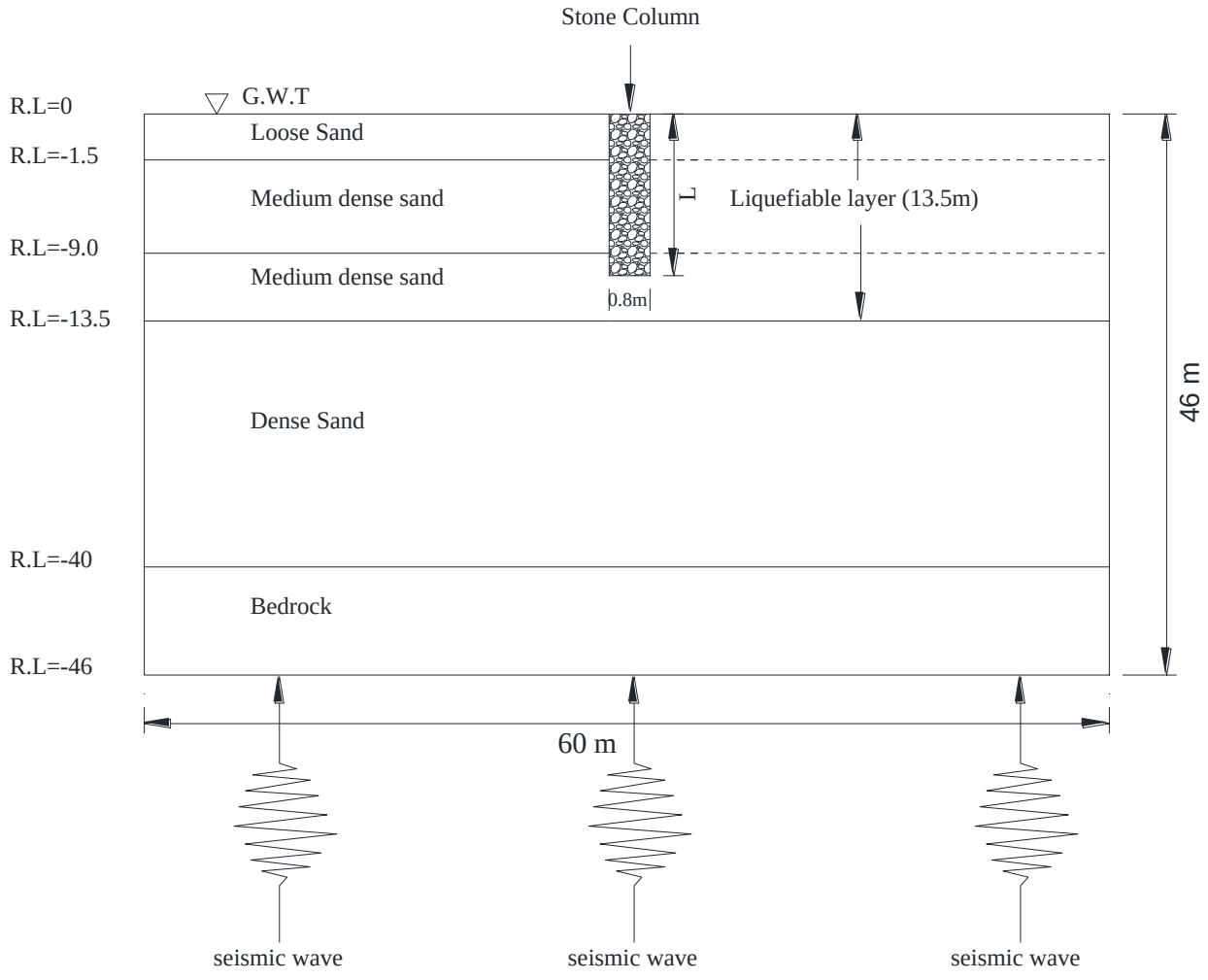

Figure 3.2: Schematic Diagram of the stone column on stratified soil deposit (not to scale)

In figure 3.2, a schematic diagram of the stone column model where a single stone column install on a loose saturated sand to medium dense fine sand. The geometrical description shown in the above figure. In this study three different length of stone column are considered i.e 5m, 10m, 15m. Bedrock is considered at the bottom most layer where the earthquake is applied on the simulations stage.

Table 3.1: Geometric variation of Stone Column model used in this parametric study

Model Name	Earthquake Motion	Length of Stone Column	Diameter of Stone Column	Liquefiable layer thickness
MOD1	Lomaprieta (0.3g)	Without	0.8	13.5
MOD2	Lomaprieta (0.3g)	5	0.8	13.5
MOD3	Lomaprieta (0.3g)	10	0.8	13.5
MOD4	Lomaprieta (0.3g)	15	0.8	13.5
MOD5	Mammoth-Lake (0.3g)	Without	0.8	13.5
MOD6	Mammoth-Lake (0.3g)	5	0.8	13.5
MOD7	Mammoth-Lake (0.3g)	10	0.8	13.5
MOD8	Mammoth-Lake (0.3g)	15	0.8	13.5

A parametric study is to be cover by varying different stone column length by using two different natural earthquake having both same 0.3g PGA and different time record and different dominant frequency. The details variation is showing in table 3.1

3.4 Material Properties of the stone column and the stratified soil layer:

The whole stratification of soil are divide into five layers and constructed with four different type materials.

i. Bottom most layer is the bedrock , moderate weahther rock having shear wave velocity of 1609 m/s.

ii. Above the bedrock there is dense to very dense fine sand layer of 16.5 m layer have friction angle 36^0 and zero cohesion. Shear wave velocity is 298 m/s.

iii. Then above the dese fine sandy layer, there is a medium dense fine sand layer of 11 m thick having friction angle 32° and shear wave velocity is 201 to 247 m/s.

iv. Top 1.5 m is loose sand layer of angle of friction is 30° and shear wave velocity is 192m/s.

v. Stone column having diameter of 0.8 m (2d colum slice) and length are varying in this study 5m, 10m, 15m. Stone column have very high stiffness, shear wave velocity is 1080 m/s and made of high permeable gravel, permeability is 100 cm/s. Modulus of elastisity for stone column is taken 10 to 40 times of the sourounding soil (Mehkinghalam et. al. 2017).

Table 1 represents the detailed properties of soil layer and stone column used for parametric analysis.

Density of soil material = ρ and Vs =Shear Velocity

Shear Modulus = Gmax = ρVs^2 ----------(3.1)

The shear modulus of different materials in different layers is calculated by the equation.3.1. We have adopted the Mohr-Coulomb constitutive model for the analysis in case of all the materials. Now for the dynamic analysis part, we have linked up this constitutive model with the hysteresis damping properties with 0.2% ralleigh damping parameter of the material to enable a realistic analysis.

Table 3.2: Properties of soil material used in the modelling and analysis

Properties	Unit	Loose sand	Medium dense fine sand (I)	Medium dense fine sand (II)	dense to very dense fine sand with mica	Bed rock	Stone Column
Depth	m	*0 - 1.5*	*1.5 - 9*	*9 - 13.5*	*13.5 - 40*	*40 - 46*	-
Dry Density (γ_{dry})	kg/m^3	1500	1650	1650	1700	2700	1850
Saturated Density (γ_{sat})	kg/m^3	1785	1931	1931	1955	2916	2000
Cohesion (c)	kPa	0	0	0	0	27200	0
Tension	kPa	0	0	0	0	1170	0
Friction angle (ϕ^0)	degree	30	32	32	36	27.8	45
Corrected SPT values (N_{160})	-	11	12	18	26	-	-
Shear wave velocity (Vs)	m/s	192	201	247	298	1609	1080
Shear modulus (G)	Mpa	55.42	66.63	100.8	151.3	6990	2160
Elastic modulus (E)	Mpa	144.1	173.2	262.2	393.4	19290	5616
Poisson's ratio (n)	-	0.3	0.3	0.3	0.3	0.38	0.3
porosity (n)	-	0.133	0.315	0.315	0.286	-	0.36
Permeability (k)	cm/s	0.0748	0.0748	0.0748	0.00624	-	100

3.5 Ground Water Flow Condition for this study:

Calculation of excess pore water pressure in the soil mass due to dynamic loading is main factor for modeling process of liquefaction phenomenon. There are different numerical approaches to model the behavior of two-phase medium. Generally, they can be classified as uncoupled and coupled analyses. In the uncouple analysis, the response of saturated soil is modelled without considering the effects of soil-water interaction, and then pore water pressure is included separately by means of a pore pressure generation model. In the coupled analysis a formulation is used where all unknowns are computed simultaneously at each time step. Although very little dissipation of pore pressure is likely during seismic excitation in most structure, FLAC able to carry out the groundwater flow calculation in parallel with the dynamic calculations. When both dynamic and ground water options are selected together (flow on and dyn on), the two-time step (ground water and dynamic) are forced to equal.

From various researchers proved that the finn model is best used in FLAC to model properly liquefaction.

For this study, in addition to the dynamic analysis, we carried out fluid flow analysis simultaneously, it means the dynamic simulation is done on flow or coupled flow condition.

3.6 Boundary Of Fluid Flow Analysis:

Upper boundary of the model along with the environmental boundary of stone column is kept fixed pore pressure condition. Its means upper boundary kept permeable, Fluid flows to and from the outside-world. Its mean the flow can permeate from internal and external environment.

3.7 Mesh Generation

After choosing materials and its properties of each layer of soil and stone column, next step is the generation of mesh. First create a 60m wide and 46m deep block of soil then divide into five zone. Then each zone is divided into small rectangular element and generate grid points. Now, for accurate results, mesh size should be as fine as possible. The mesh size finer more time will be required for cycling the model. If the mesh size is coarser then there will be error while wave propagation. So, a balance should be maintained in choosing the mesh size. The elements of mesh size is depends on the frequency content of the input acceleration history. The first acceleration history used is Lomaprieta earthquake. The original earthquake has 0.357g PGA but we converted the 0.357g PGA to 0.3g PGA using seismo-signal software. Note that significant frequency range for all scaled input motion would be the same.

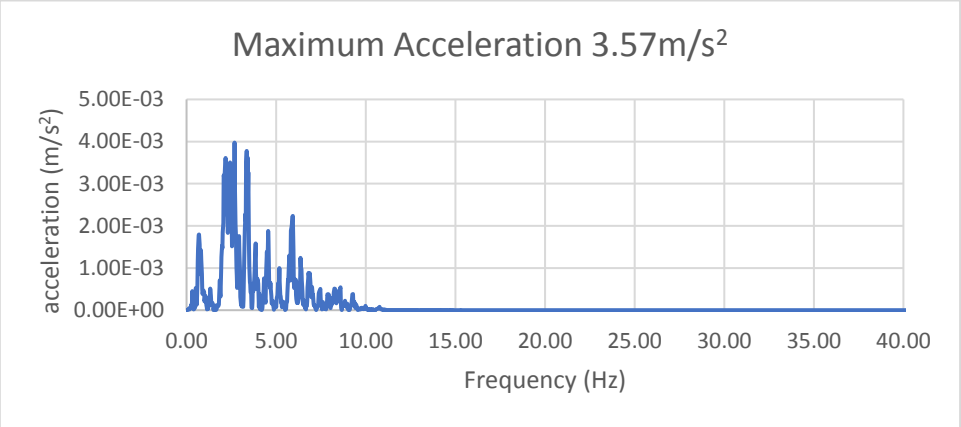

Fig. 3.3: Power spectrum of PGA 0.357g

From the plot of the power spectrum of the acceleration time history for maximum acceleration 0.357g, shown in the below figure, it is evident that a significant amount of power dissipation lies within the frequency of 10 Hz. Now, the maximum acceleration is scaled down for this analysis without changing the frequency content. So, 10 Hz can be taken as the guiding frequency for fixing the maximum mesh element size. Kuhlemeyer and Lysmer (1973) showed that for an accurate representation of the wave transmission through the soil model, the spatial element size, Δl, must be smaller than approximately one-tenth to one-eighth of the wavelength associated with the highest significant frequency. The mesh size is decided based on maximum frequency content and least shear velocity of the material. Now, the minimum shear velocity belongs to the top sand layer and the velocity is 192m/sec.

$$\text{Wave length } (\lambda)=\frac{Shear\ wave\ velocity\left(\frac{m}{\sec}\right)}{Significant\ maximum\ frequency(Hz)}=\frac{192}{10}=19.2\text{m}$$

Maximum element side length (Δl) is taken as one-eighth of the wavelength i.e.19.2m/8 =2.4m. Maximum grid size is taken 1.2m which is less than 2.4m, hence okay.

3.8 Boundary conditions of the model

In the static phase, the normal boundary condition for soil structures is applied to the model. Along the base, the fixed boundary and the roller boundary is subjected in the sides of the model and top surface of the model is kept free. The base of the model is not subjected to the roller boundary to avoid the free sideways motion which will lead to the unrealistic failure mode. Before the application of dynamic loading, the proper boundaries are to be applied to the model. The choices of boundaries depend on the mode of application of the input motion. In this study, the input motion is given at the model base (RL -46.0m) in the form of velocity shear stress waveform. There are other modes of application of input motion (like acceleration-time history, velocity-time history) that will be discussed later in detail. For the shear stress form of input motion, we can apply the most suitable boundary for seismic analysis that is available in FLAC2D. The "quiet" boundary criteria are applied along the base of the model (along RL 46.0m) and the "free field boundary" criteria are applied along both the vertical sides of the model (from RL -46.0 to RL 0.0 both sides). The top surface is kept pore pressure fixed boundary because the model will be cycling with flow on condition and water can interact with outer environment. The "quiet boundary" and "free field boundary" are discussed below in a few words.

3.8.1 Quiet boundary condition

The soil mechanics problem is modeled best when represented resting on an unbound medium extends to infinite. But for numerical modeling purpose, it is quite unrealistic because to model an unnecessary large extent of the medium on which the main structure rests as it will take a very large solution time. The near-surface earth structures are assumed to rest on half-space. This is similar to the problem that is to be addressed in this study. Numerical methods relying on the discretization of a finite region of space require that appropriate conditions be enforced at the artificial numerical boundaries. In the case of static analysis, the fixed or elastic boundaries can be placed at some distance from the main structures. But in case of dynamic analysis, this type of boundary condition the wave can be reflected back in the model instead of radiating out of the zone of interest. By using large strain mode it can be solved as material damping will nullify most of the reflected energy but it would not be computationally viable. The viscous boundary developed by Lysmer and Kuhlemeyer (1969) is used in FLAC2D. This boundary can be used in the time domain. The consistent boundary is most suitable for dynamic analysis but it works in frequency domain analysis. As this is an analysis done in the time domain, the quiet boundary is used in this analysis. The quiet-boundary scheme proposed by Lysmer and Kuhlemeyer (1969) involves dashpots attached independently to the boundary in the normal and shear directions. The dashpots provide viscous normal and shear tractions given by

$$t_n = -\rho . C_p . v_n \dots\dots\dots\dots\dots\dots . (3.2)$$

$$t_n = -\rho . C_s . v_s \dots\dots\dots\dots\dots\dots . (3.3)$$

where, v_n= normal component of the velocity at the boundary,

v_s =shear component of the velocity at the boundary

ρ= mass density of the soil layer

Cp= p-wave velocities

Cs =s-wave velocities

In this model, the quiet boundary is applied in both x and y direction at the base of the model. This prevents the reflection of the wave back to the embankment that minimizes unrealistic amplification at the free surface.

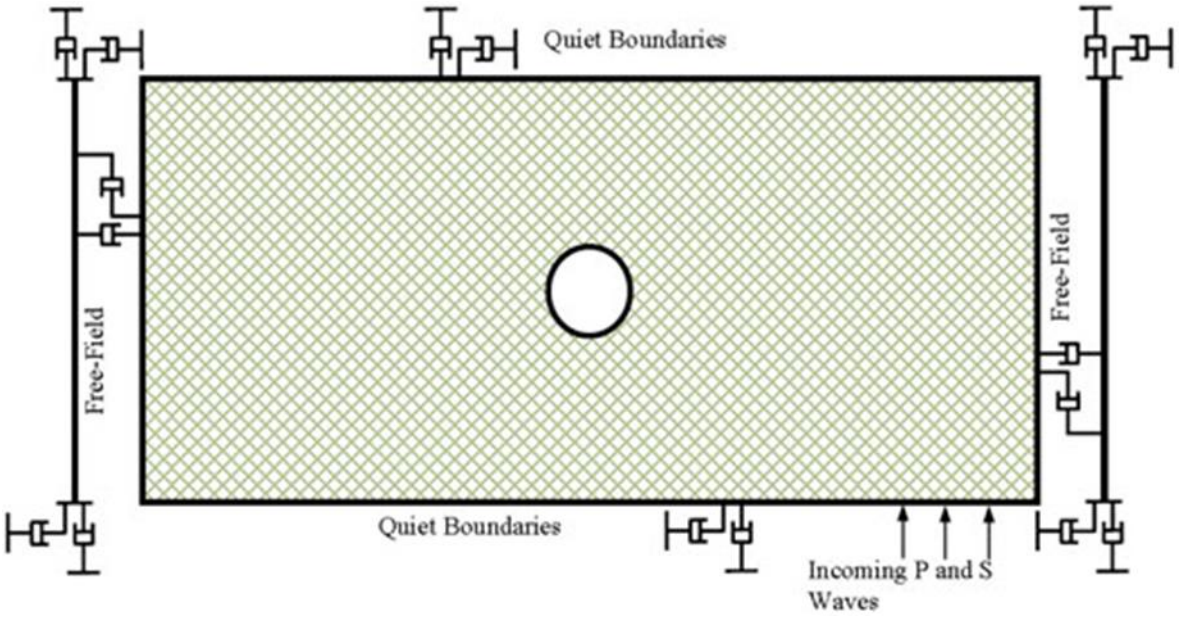

Fig. 3.4: Quiet boundary condition
(FLAC 2D 8.1, Dynamic Analysis manual)

3.8.2 Free-Field boundary condition

The seismic input is normally represented by plane waves propagating upward through the underlying material. The boundary conditions at the sides of the model must account for the free-field motion that would exist in the absence of the structure. The vertical boundaries should be placed at a significant distance from the zone of interest to minimize the wave reflections and to achieve free field condition. Sometimes this leads to the modeling of a significantly large model that in turn causes tedious calculations. An alternative procedure is to enforce the free-field motion in such a way that boundaries retain their non-reflecting properties (i.e., outward waves originating from the structure are properly absorbed).

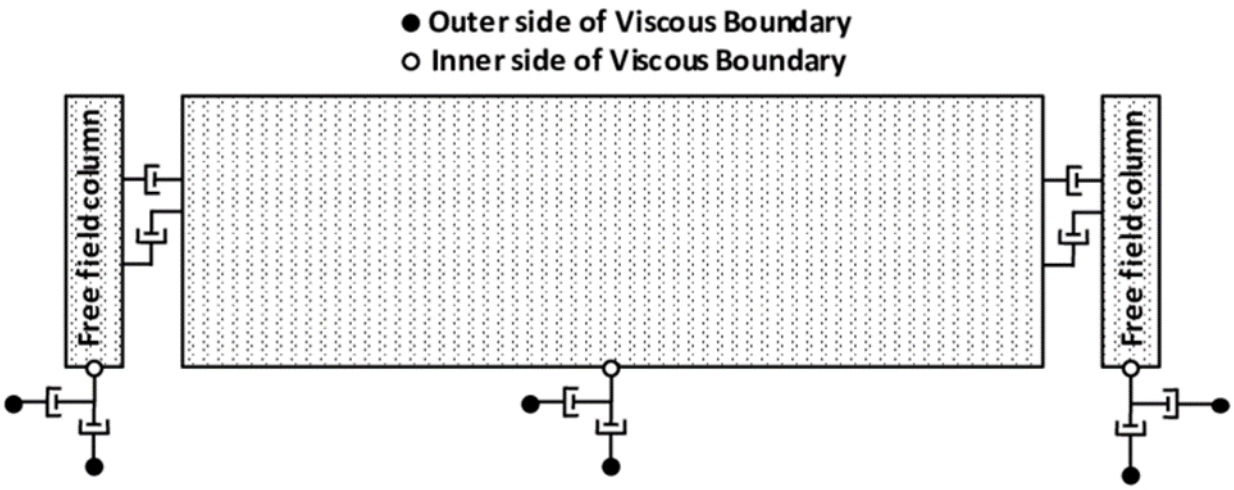

Fig. 3.5: Free-field boundary condition (FLAC 2D 8.1, Dynamic Analysis manual)

The lateral boundary of the model coupled with viscous dashpots create the condition of the quiet boundary that simulates the condition for infinite medium in the sideways and the unbalanced force is applied from free field to the main grid boundary. The plane waves that propagate upward is not distorted at the boundaries due to the free field condition that holds similar like an infinite model. The model is kept in static equilibrium before applying the free field condition.

3.9 Input motion details

3.9.1 Loma-Prieta earthquake (1987)

The stone column model is subjected to seismic loading representative of the 1987 Loma-Prieta earthquake in California and the original acceleration 0.357g but the record acceleration magnitude is scaled down to maximum accelerations of 0.3g. The dominant frequency of this earthquake is 0.325Hz .The original acceleration time history and scaled down time histories are shown in below figures.

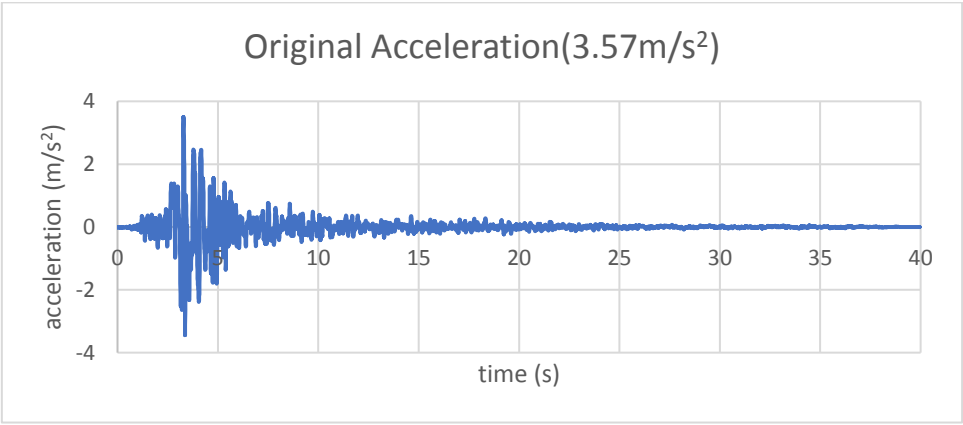

Fig 3.6: Lomaprieta earthquake acceleration-time history (original-0.357g)

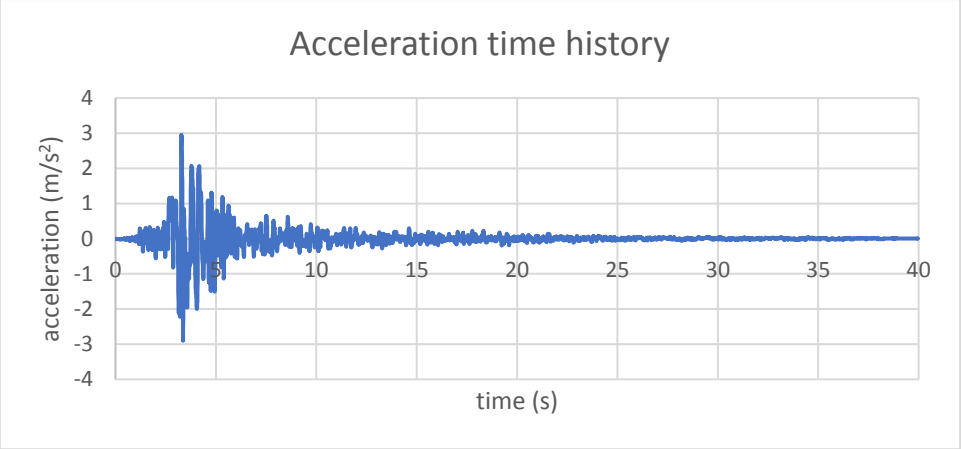

Fig 3.7: Lomaprieta Scaled down acceleration-time history (0.3g)

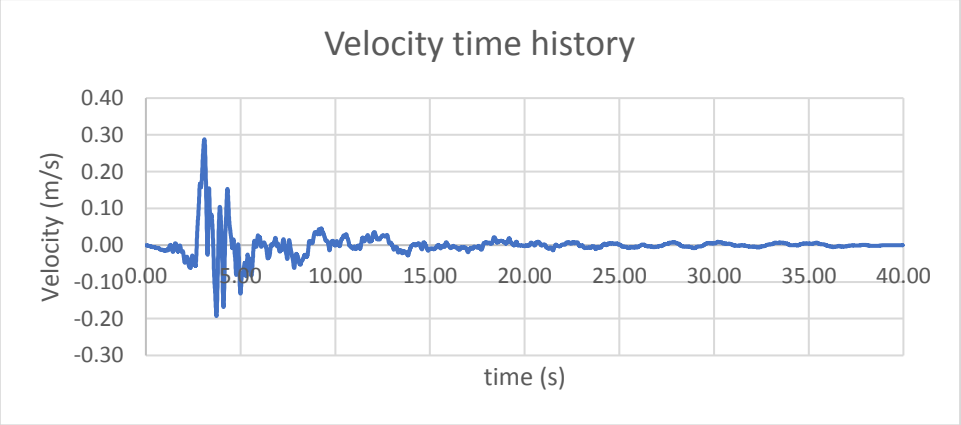

Fig 3.8: Lomaprieta earthquake velocity-time history (original-0.357g)

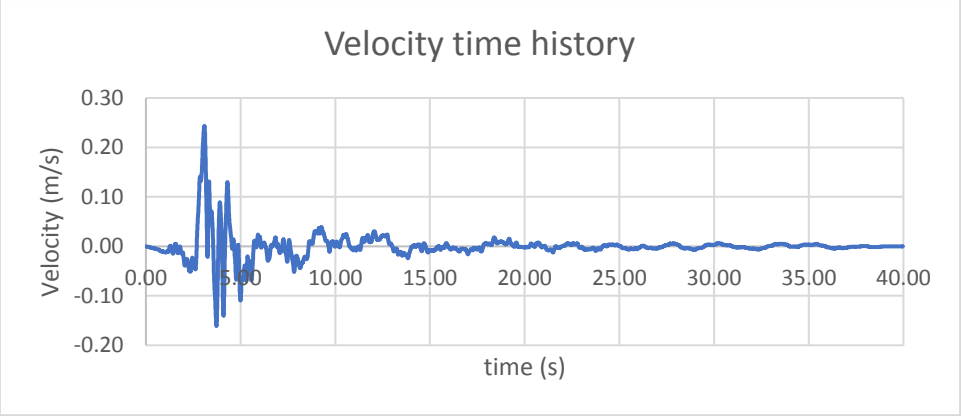

Fig 3.9: Lomaprieta earthquake velocity-time history (0.3g)

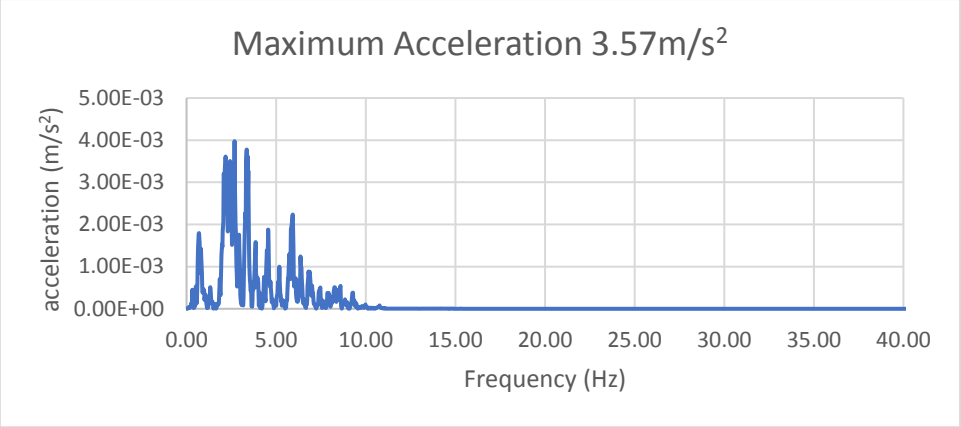

Fig 3.10: Power spectrum of Lomaprieta (PGA 0.357g)

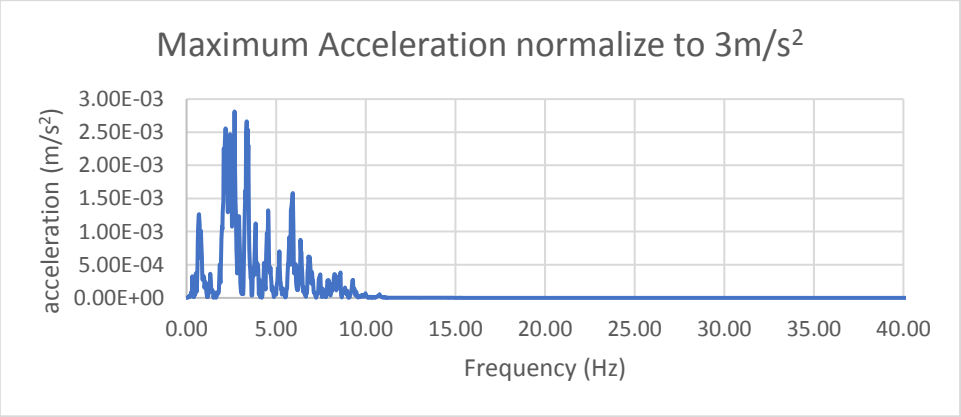

Fig 3.11: Power spectrum of Lomaprieta (PGA 0.3g)

3.9.2 Mammoth-lake earthquake (1980)

The second wave considered for the simulation is a seismic loading representative of the 1980 Mammoth-lake earthquake in California and the original acceleration 0.43g but the record acceleration magnitude is scaled down to maximum accelerations of 0.3g. The dominant frequency of this earthquake is 0.27Hz. The original acceleration time history and scaled down time histories are shown in below figures.

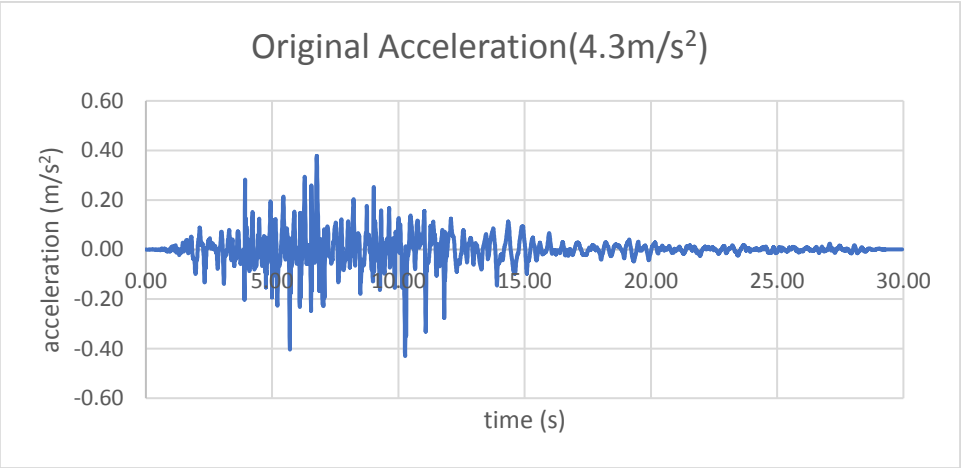

Fig 3.12: Mammoth-lake earthquake acceleration-time history (original-0.43g)

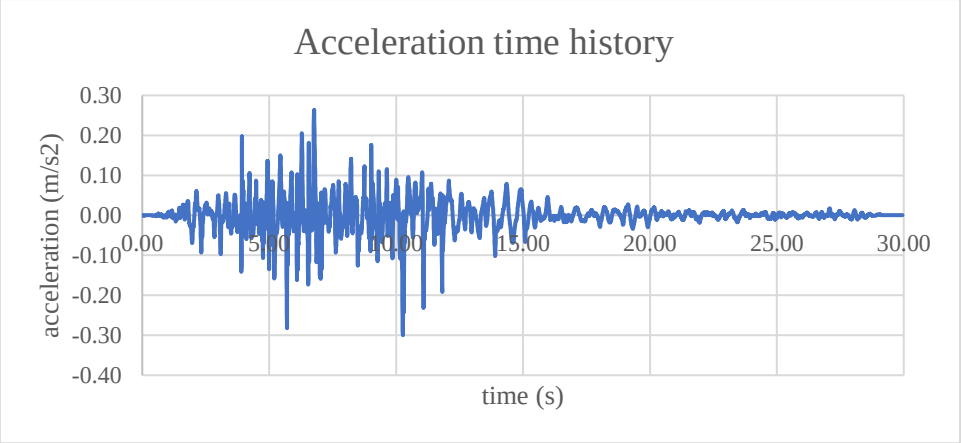

Fig 3.13: Mammoth-lake scaled down acceleration-time history (0.3g)

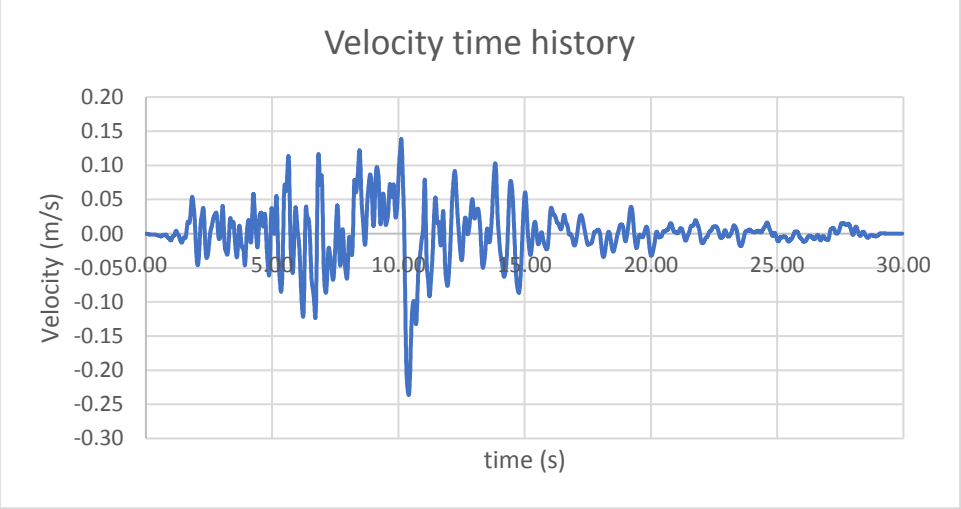

Fig 3.14: Mammoth-lake earthquake velocity-time history (0.43g)

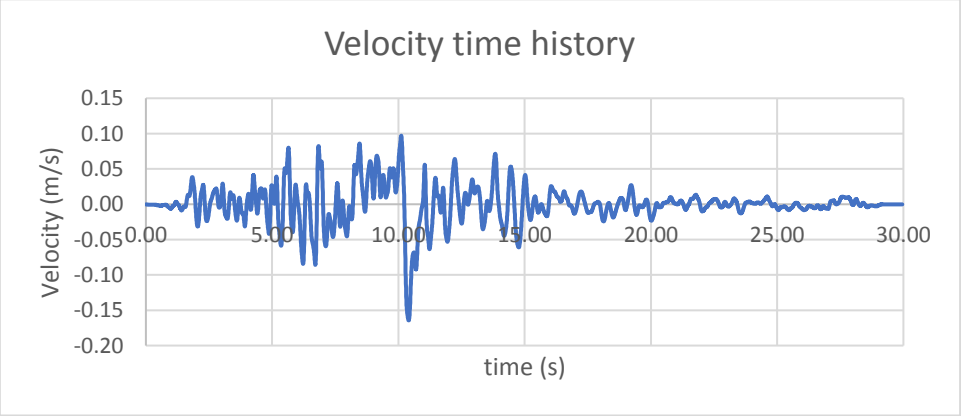

Fig 3.15: Mammoth-lake earthquake velocity-time history (0.3g)

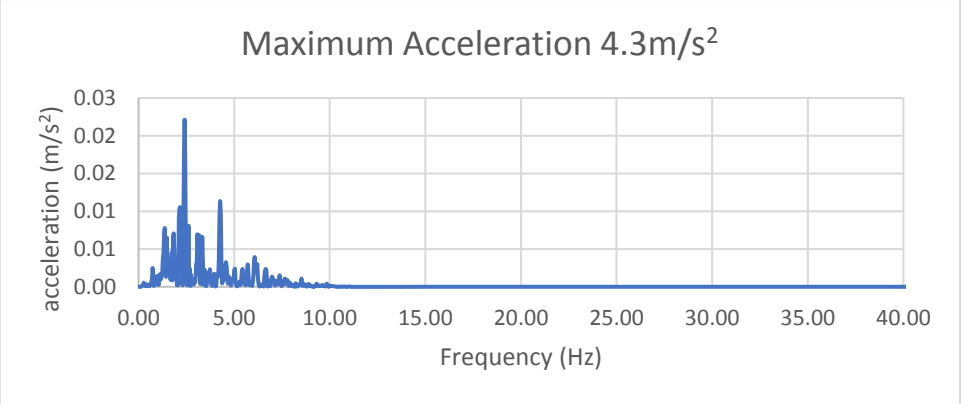

Fig 3.16: Power spectrum of Mammoth-lake (PGA 0.43g)

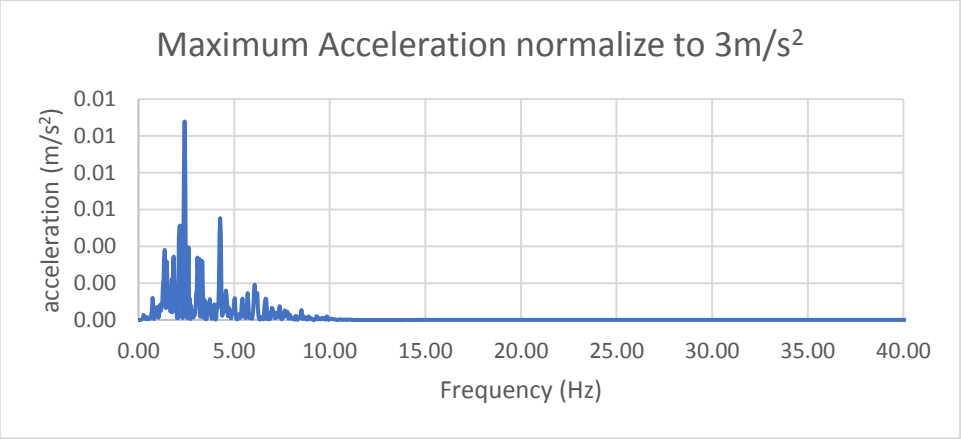

Fig 3.17: Power spectrum of Mammoth-lake (PGA 0.3g)

Comparing all the above Fig, it is clear that power spectrum pattern for all cases are same and peak differs due to normalization of the acceleration; but in all cases, the peaks reach at the frequency at approximately 2.5 Hz. The other peaks are formed at frequency range 0.5 to 2Hz in all cases. So, it can be concluded that the frequency contents associated with significant power dissipation are similar in all cases. But this two-input motion is derived from the raw data that was recorded in the site and also all the cases, the major power dissipation happens within 10 Hz frequency range. Usually, when raw data from sites are used for numerical modeling, the acceleration history is brought through some correction i.e. baseline correction to make the data compatible with the numerical model and the software. Also, if the acceleration is filtered with a filter that filters out the acceleration above the 10 Hz frequency range, it would be suitable for the calculation purpose and conform to our mesh size (Mesh size is designed for calculation upto10 Hz accurately.

3.10 Mode of application of input motion

The seismic input motion can be applied to the model in three different ways like in forms of acceleration-time history, velocity-time history, shear stress wave history etc. In the FLAC 2D version 8.1, all these modes of seismic load application are available. But the dynamic boundaries discussed in 3.6.1 and 3.6.2 cannot be applied suitably along with all modes of application of dynamic loading. For example, if the input motion is applied in the form of velocity-time history or acceleration-time history along the base, the quiet boundary cannot be along the base; it is a limitation of the software. The dynamic boundary is very important in the analysis of the seismic behavior of embankment. So, the shear stress-wave history is used as input loading and the quiet boundary and input stress-wave history both can be applied along the same base grid of the model that is necessary for the accurate study of the embankment. But the originally the record is being used is recorded and normalized acceleration time history. So, the acceleration time history will have to be converted into stress wave history. The conversion procedure is described below considering the boundary condition as well.

i. First, the acceleration time history is integrated to convert it into shear particle velocity history (vs).
ii. Then the shear velocity time history is converted into shear stress-time history by the following relationship.

$$\sigma = -2.\rho.Cs.\ vs \quad \ldots\ldots\ldots\ldots\ldots\ldots\ldots\ldots\ldots\ldots (3.4)$$

Where, σ= shear stress

3.11 Wave Filtration and Base-line correction

Wave filtration is necessary because certain high frequency of the original wave create a disturbance while propagating. So, before doing the base line correction, the first step is the wave filtration. The baseline correction an acceleration time-history or velocity-time history needs to be done if raw data of those time histories are used in numerical input. This is because FLAC model may exhibit continuing velocity or residual displacements after the motion has finished. This condition arises from the integral of time -history is not zero. In our input motion acceleration-time history we need not to do base-line correction as it doesn't show any kind of residual displacement as shown below.

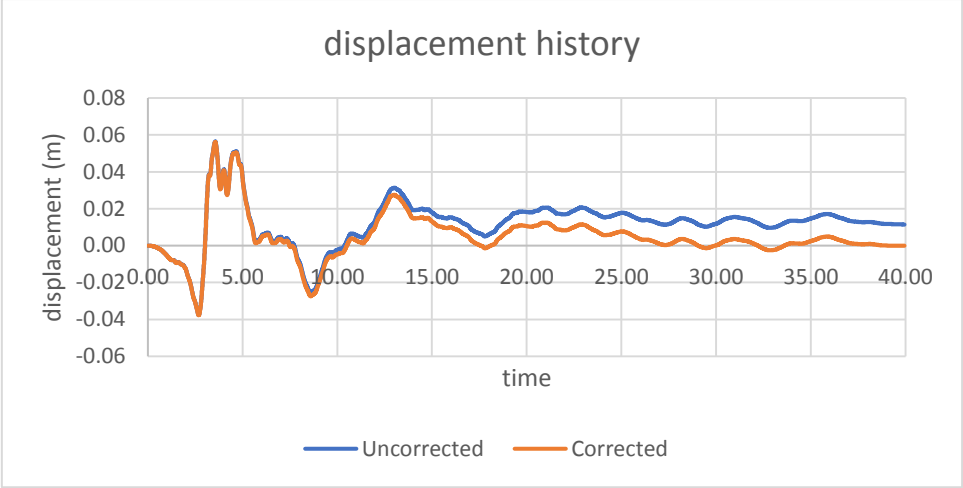

Fig. 3.18: Comparison between uncorrected and corrected displacement history (for Lomaprieta 0.3g acceleration)

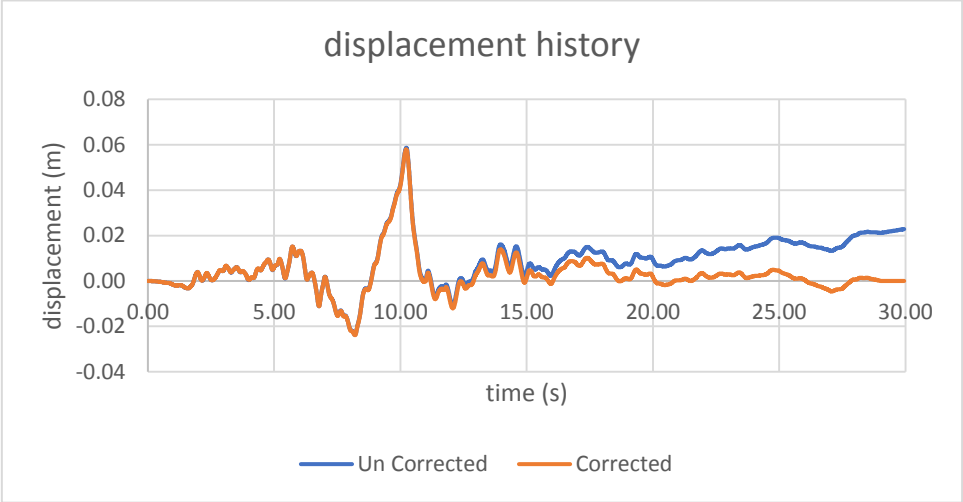

Fig. 3.19: Comparison between uncorrected and corrected displacement history (for Mammoth-lake 0.3g acceleration)

3.12 Damping of soil

Material damping in soil is generally because of its viscosity, friction and plasticity development (Ebrahimian,2012). The damping in the numerical dynamic analysis should use to simulate energy dissipation due to material properties within the model under a dynamic load. The damping has a significant effect on the response of soil-structure under seismic loading. In reality, all soil material shows some degree of damping that modifies the propagating seismic wave differently than in the case of un-damped analysis. Now the damping can be incorporated in the soil foundation in two ways – (i) Hysteretic damping, (ii) Rayleigh damping which are discussed below.

In this study, the dynamic damping was provided by Hysteretic damping combined with 0.2% Rayleigh damping. Hysteric damping was used as a backbone curve by Seed and Idriss (1970) for cohesionless soil. Rayleigh damping is applied as a Stiffness Proportional Damping Coefficient.

3.12.1Modulus reduction curve for Sandy Soil

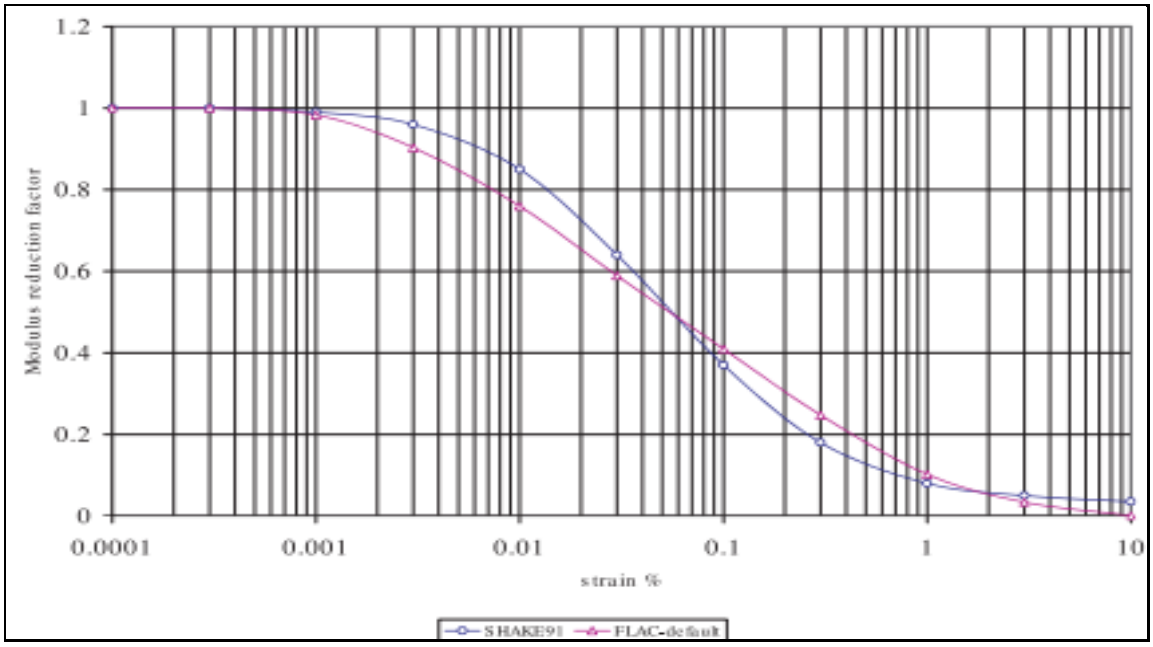

Fig. 3.20: Modulus reduction curve for sandy soils ($L_1 = -3.325$, $L_2 = 0.823$) (Seed & Idriss). (FLAC 2D 8.1, Dynamic Analysis manual)

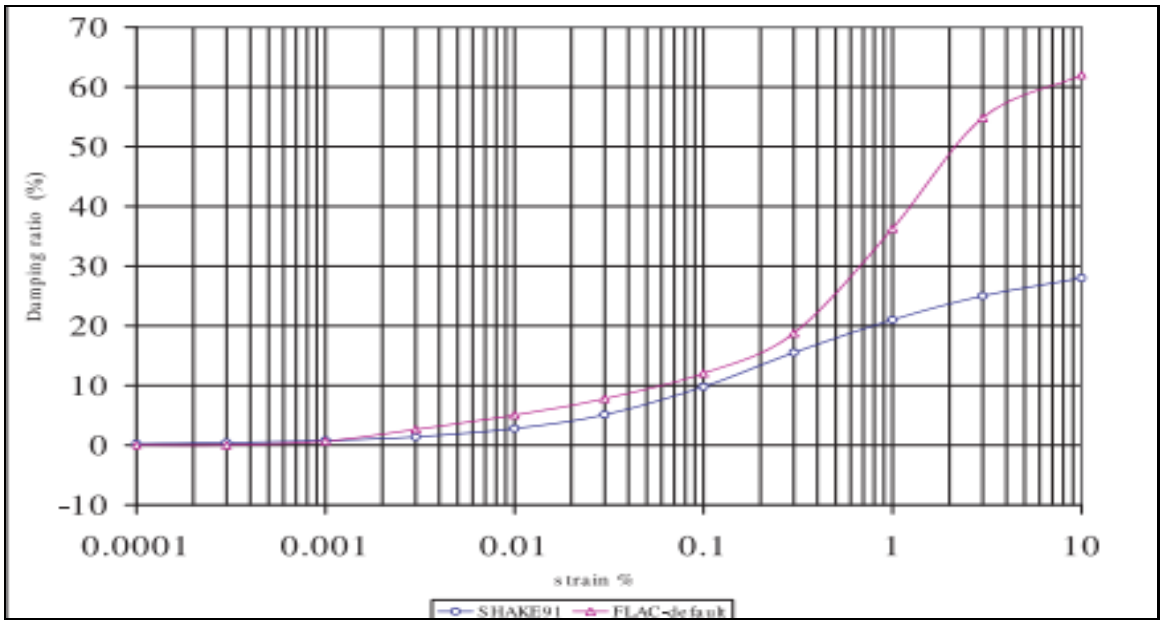

Fig. 3.21: Damping ratio curve for sandy soils ($L_1 = -3.325$, $L_2 = 0.823$) (Seed & Idriss). (FLAC 2D 8.1, Dynamic Analysis manual)

3.12.2 Modulus reduction curve for Stone Column

As stone column have different material other than sandy soil or cohesionless soil we must have provided the modulus reduction curve for stone column while applying Hysteretic damping. Stone column made with compact and high stiff gravel. So, we take modulus reduction curve for gravel materials.

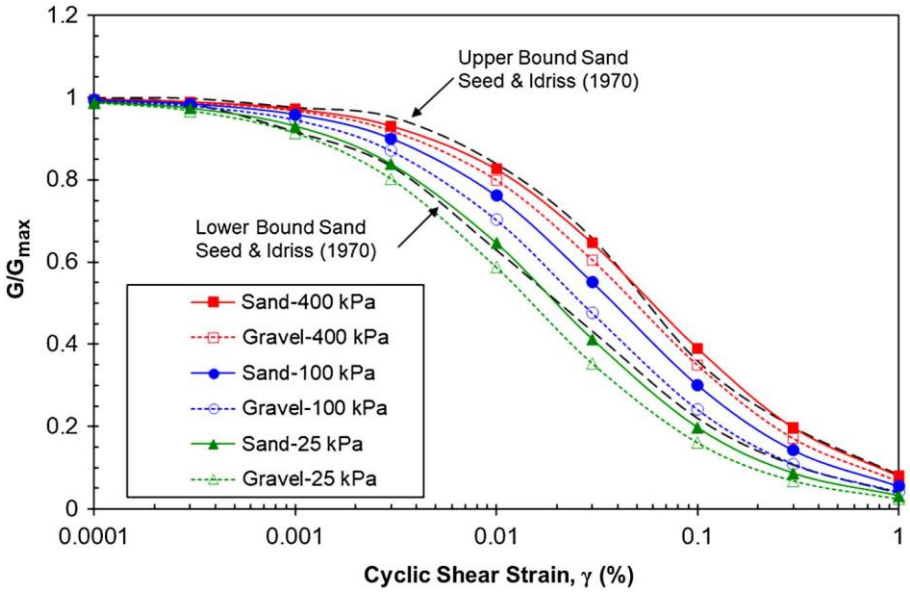

Fig. 3.22: Comparison of G=Gmax versus γ curves for sand (Darendeli 2001) and gravel (Rollins et al. 1998) relative to upper and lower bound curves for sand developed by Seed and Idriss (1970). (Rollins et. al.)

$$\frac{G}{G_{\max}} = \frac{1}{\left[1 + \left(\frac{\gamma}{0.0039 * \sigma_0'^{0.42}}\right)^{0.84}\right]} \dots\dots\dots\dots\dots\dots (3.5)$$

Above equation_ taken from Rollins et. al. paper

where G/Gmax = modulus reduction curve,

σ'_0 = effective stress at depth of gravel,

γ = % shear strain

Using the above equation G/G_{max} Vs γ are plotted. Then the sigma3 model given in FLAC 2D dynamic part is best fitted with the modulus reduction curve. The fitted constant is used as input while applying hysteretic damping for Stone column.

a	1.001	b	-0.43	x_0	-1.365

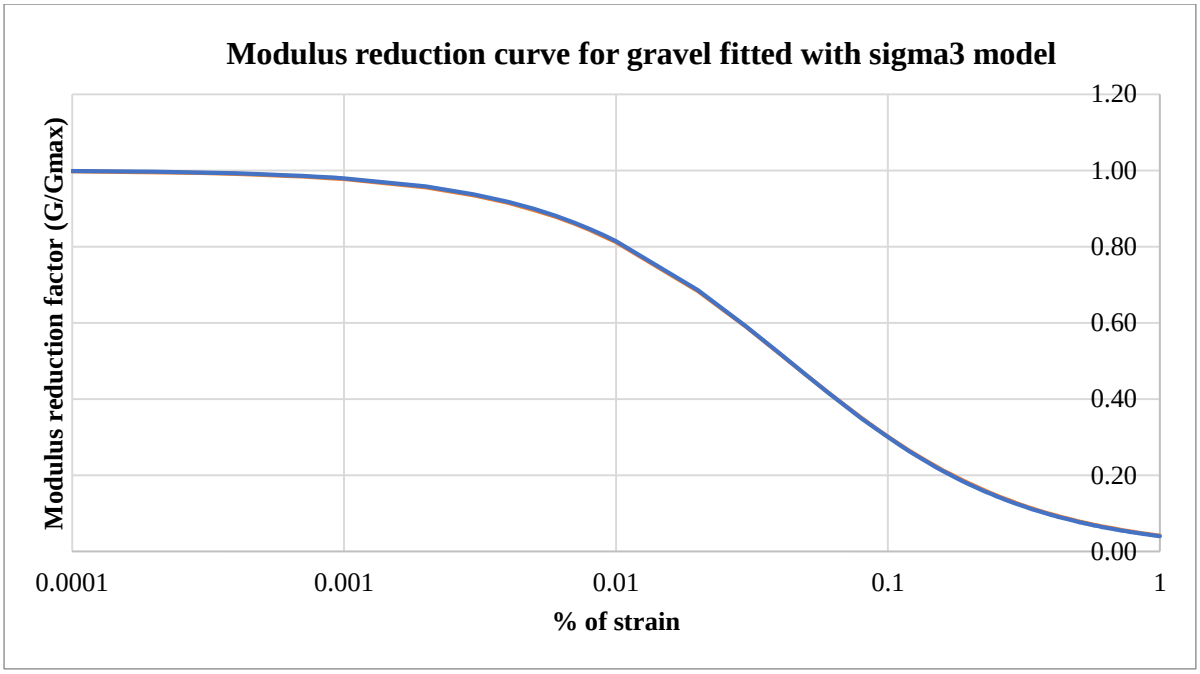

Fig. 3.23: Modulus reduction curve for gravel fitted with sigma3 model

3.12.3 Modulus reduction curve for bedrock

Similarly, the Modulus reduction curve for bedrock is generated using previous study [**Hanumantha Rao Ch 2014].** The Modulus reduction and strain relationship that is used in this study for rock is shown in Figure 3.24

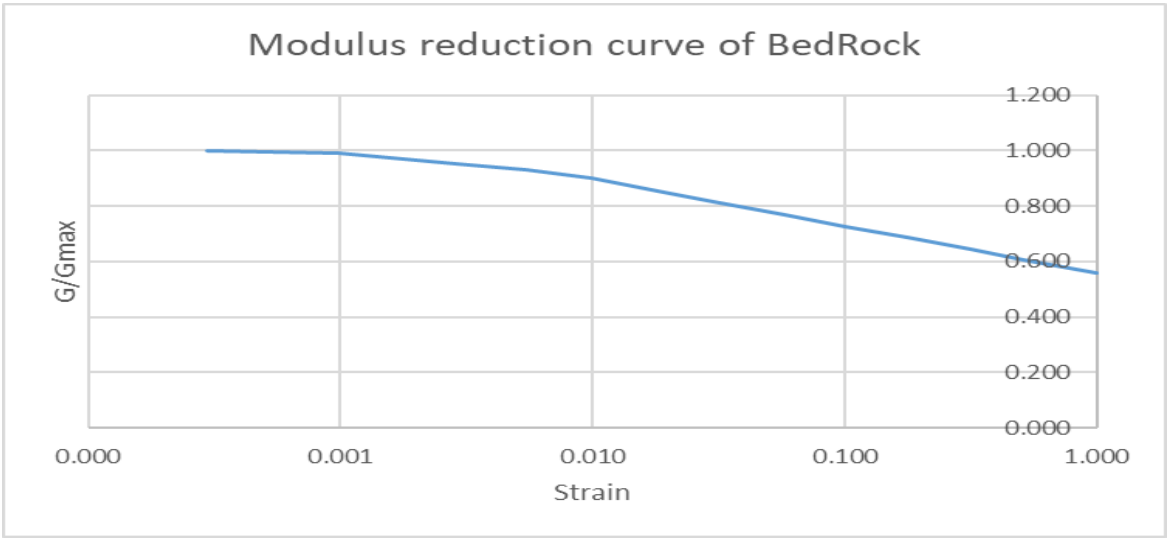

Fig 3.24: Modulus reduction curve of Bedrock used for this study

These curves are numerically linked with the basic constitutive algorithm of the Mohr-Coulomb model to simulate the actual condition of the soil materials under dynamic loading.

CHAPTER –4

RESULTS & DISCUSSION

This chapter presents the various results and findings which are obtained by simulation of different combinations of model at different earthquake loading and interpretation of the results are also briefly discuss below. The results are divided into two categories:

i. Static Analysis Result.

The static portion cover only for the case of without stone column. Here static pore pressure, Total Stress and Effective stress are shown in following section.

ii. Dynamic Analysis Result.

In the dynamic portion excess pore water pressure (EPWP) generation without stone column and dissipation with stone column are shown with detailed.

4.1 Static Analysis Results: (Without Stone Column)

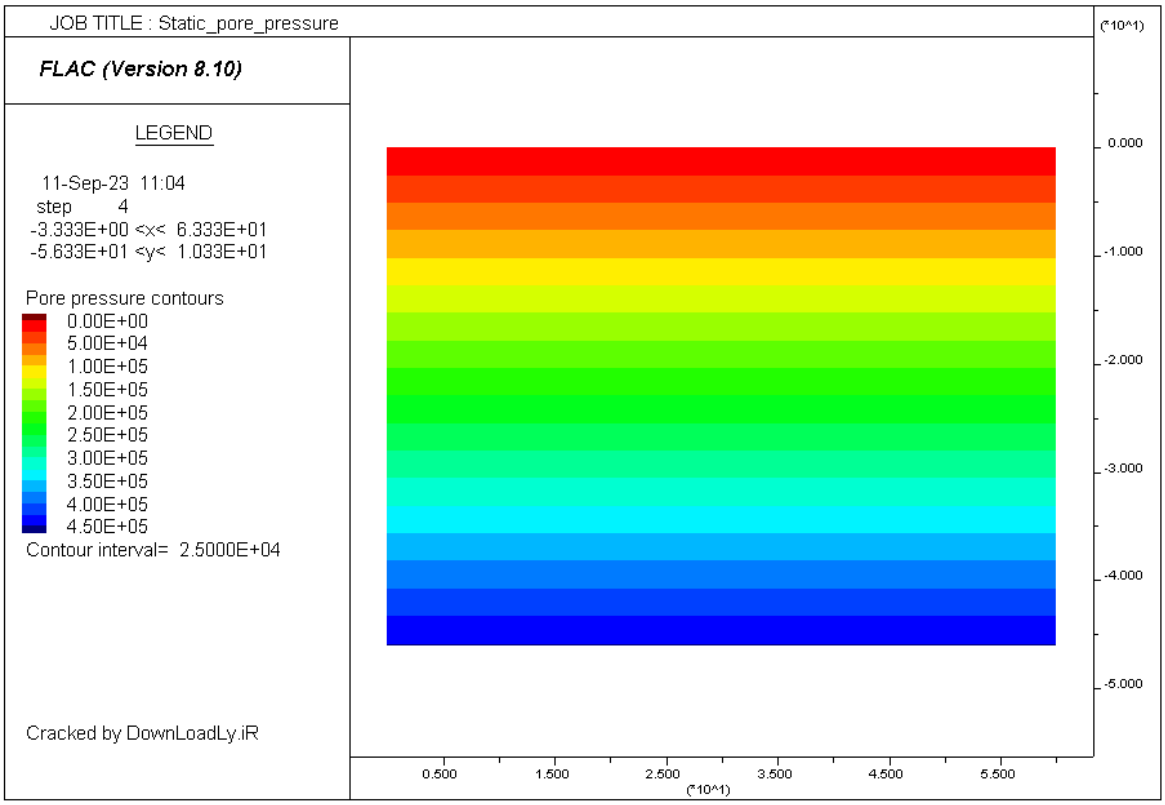

Fig 4.1: Static pore pressure distribution contour on stratified sandy soil layer

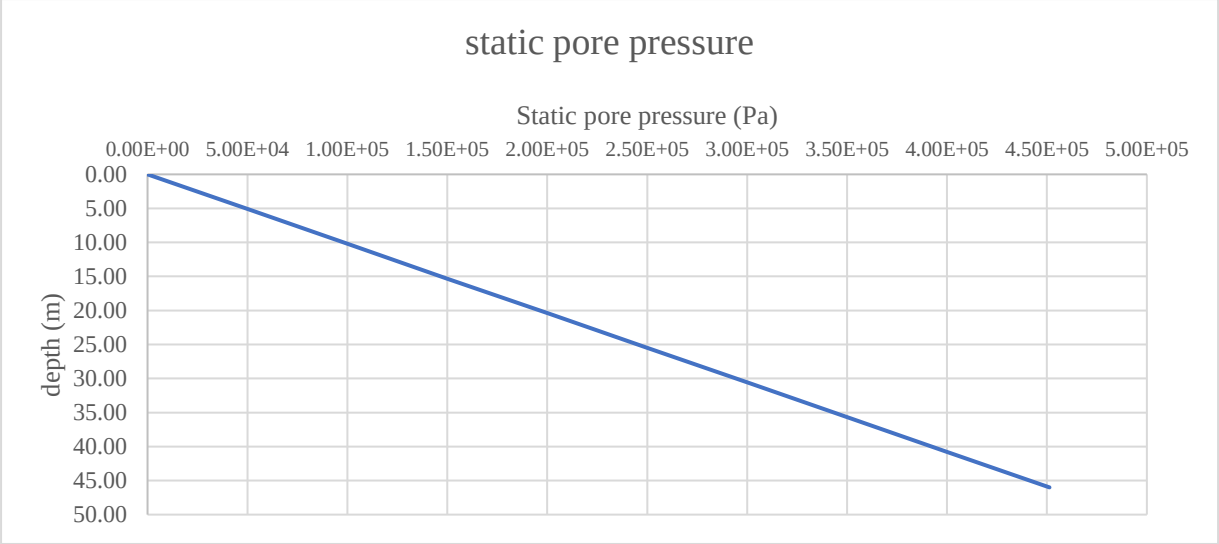

Fig 4.2: Pore pressure distribution with depth

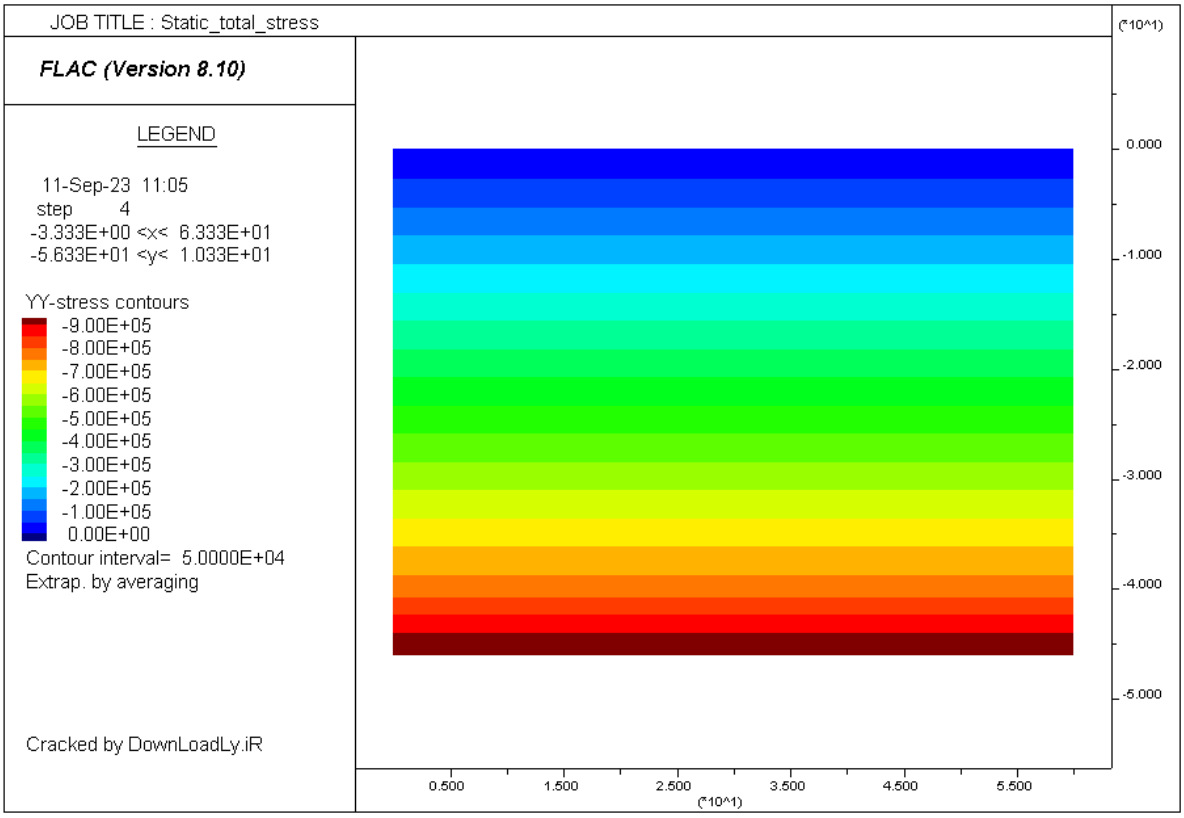

Fig 4.3: Static Total Stress distribution contour on stratified sandy soil layer

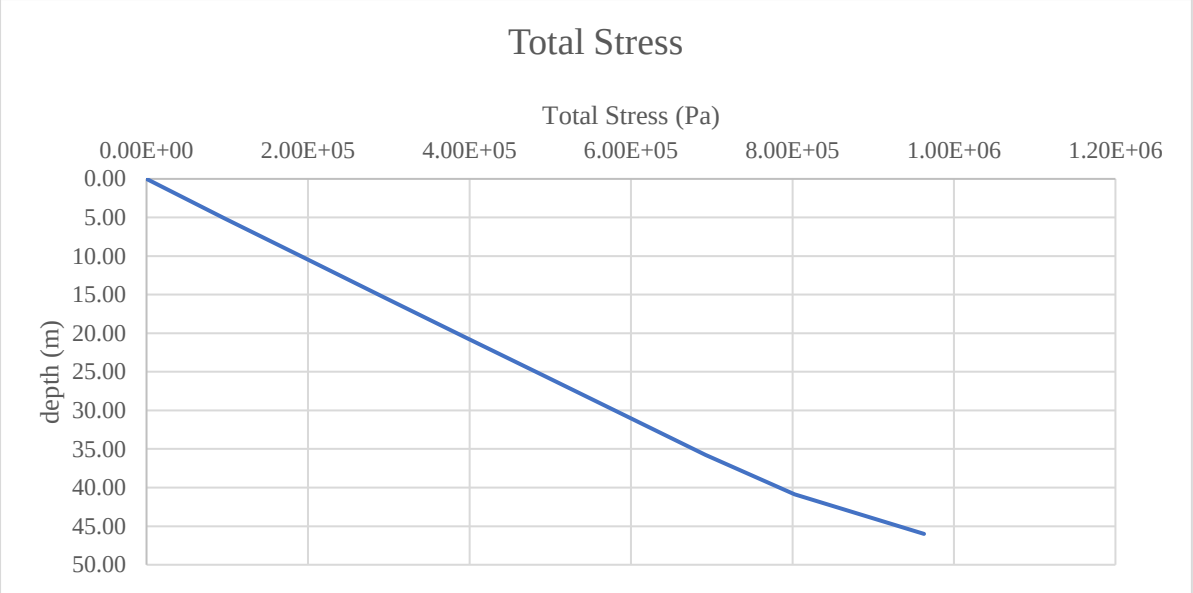

Fig 4.4: Total Stress distribution with depth

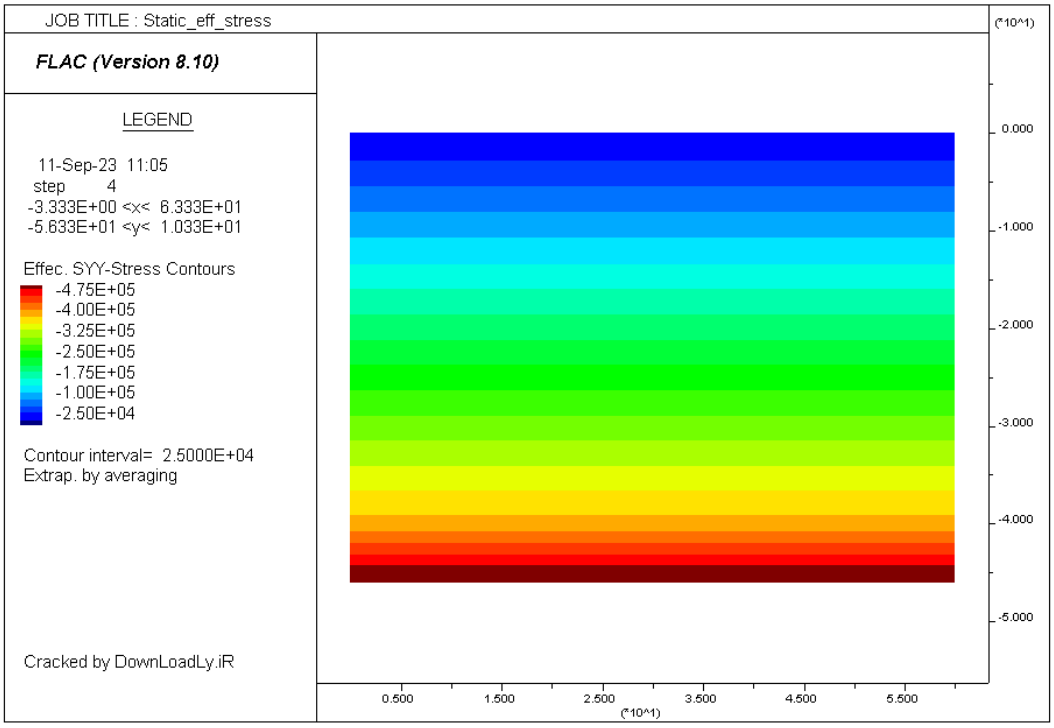

Fig 4.5: Static Effective Stress distribution contour on stratified sandy soil layer

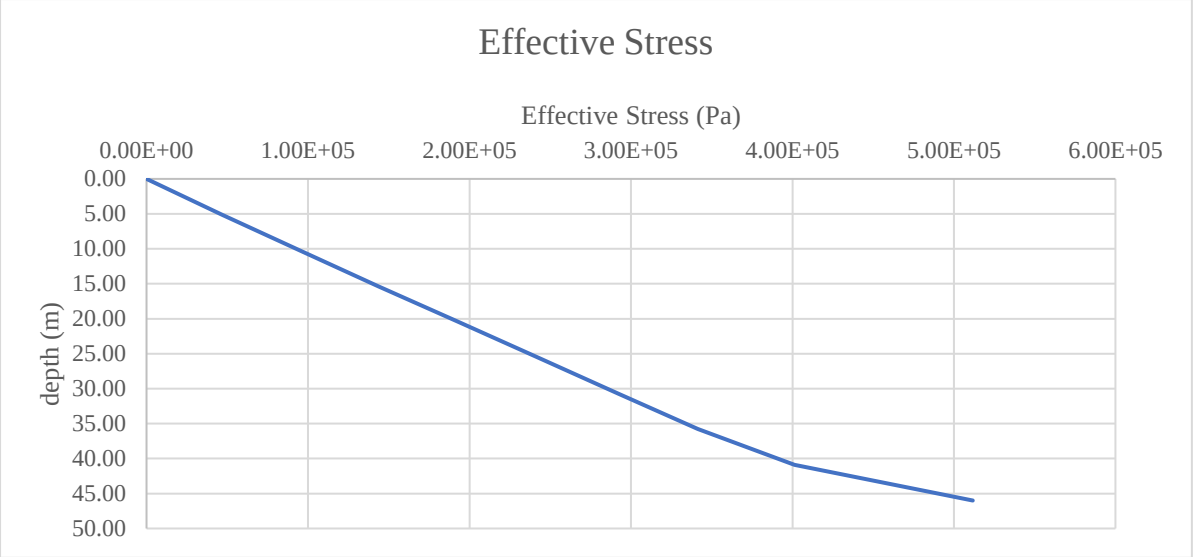

Fig 4.6: Total Effective Stress distribution with depth

Hand Calculation

The soil stratification is 60 m wide and 46 m deep which was discuss in methodology part. First 40 m is a fine sandy layer with different densification, after that 6 m bedrock. The Ground water table is at the ground surface. In the static analysis FLAC 2D first run with elastic stable condition. Then static calculation is run with considering bulk modulus of water is 2 x 10^9 Pa.

The pore water pressure is at a bottom depth of dense sand layer is

= 40*9810

=36400 Pa

= 36.4 kPa

Total stress at the bottom depth of dense sand layer

$$= (1785 - 981) * 1.5 + (1931 - 981) * 12 + (1955 - 981) * 26.5$$

=1206 + 11400 + 25811

=38417 kg/m^2

= 384.17 kPa

So, Effective stress at the bottom depth of dense sand layer = 384.17 – 36.4 = 347.77 kPa

The static pore pressure, total stress and effective stress calculated by FLAC 2D software is showing on fig 4.1 to fig 4.6.

4.2 Dynamic Analysis Result:

4.2.1 [MOD1] Without Stone Column – Lomaprieta (a_{max}=0.3g)

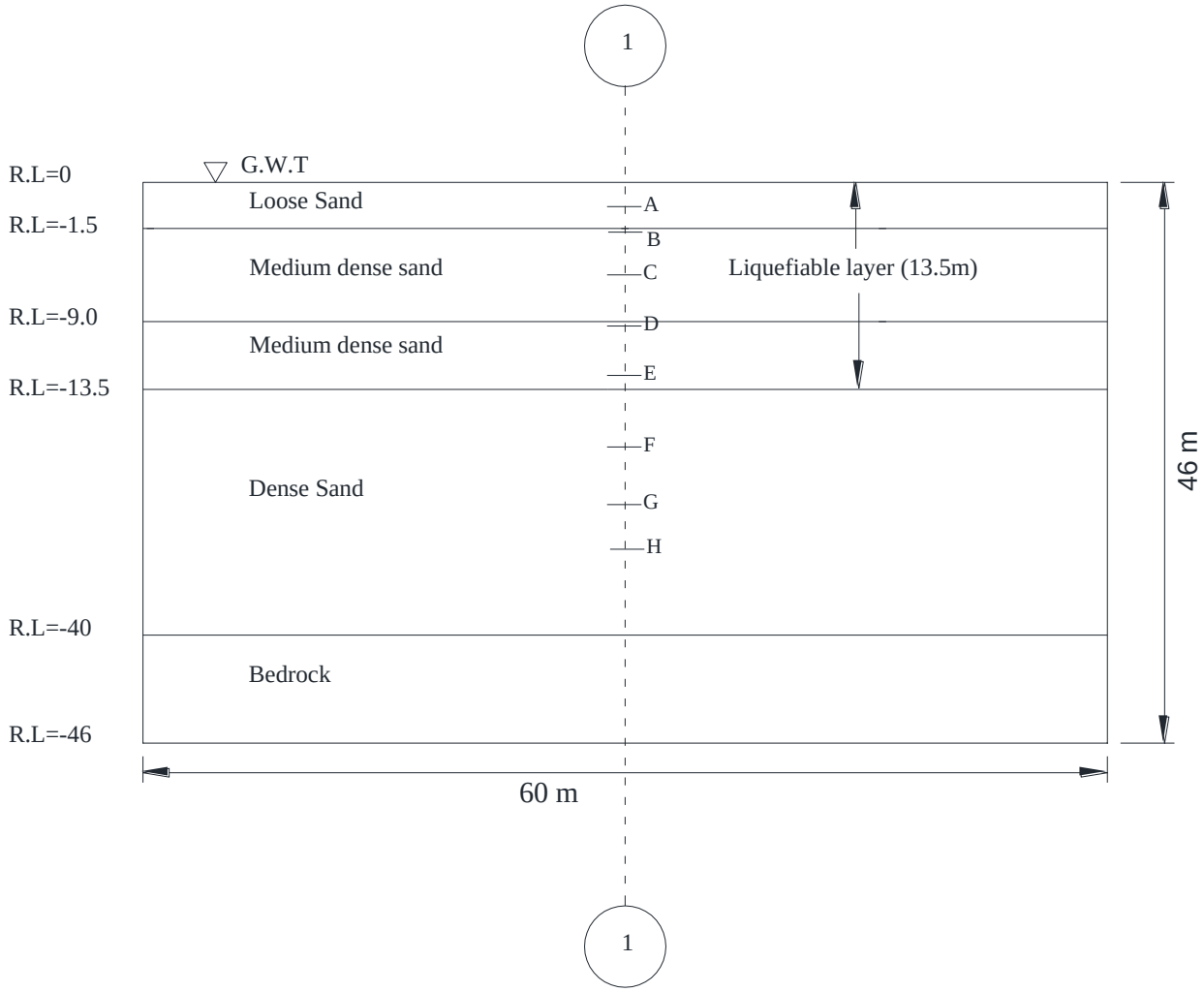

Fig. 4.7 Schematic diagram of MOD1 showing different section and observation points where excess pore pressure parameter calculated

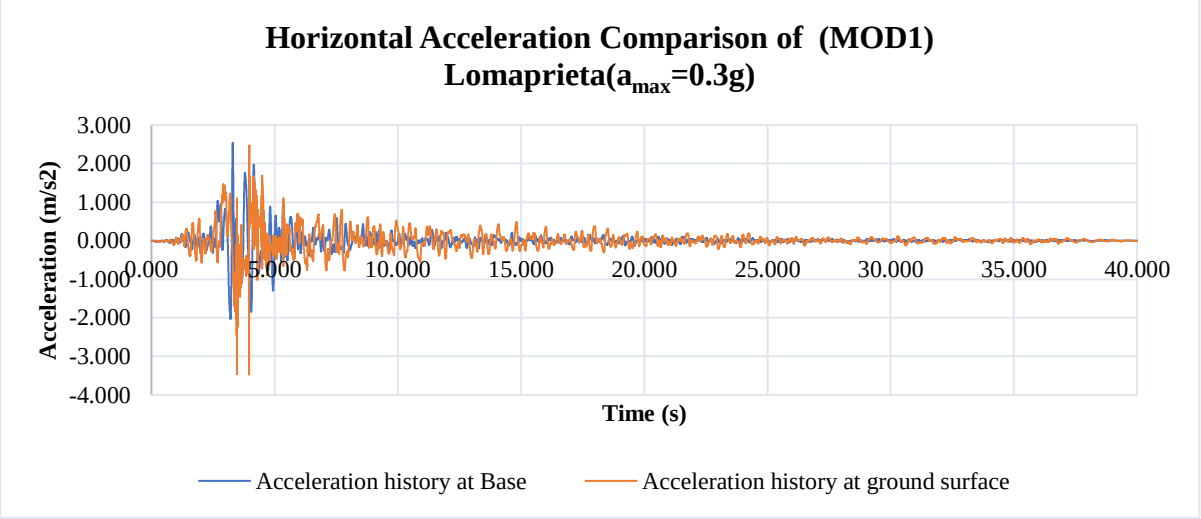

Fig. 4.8 Horizontal Acceleration Comparison of MOD1

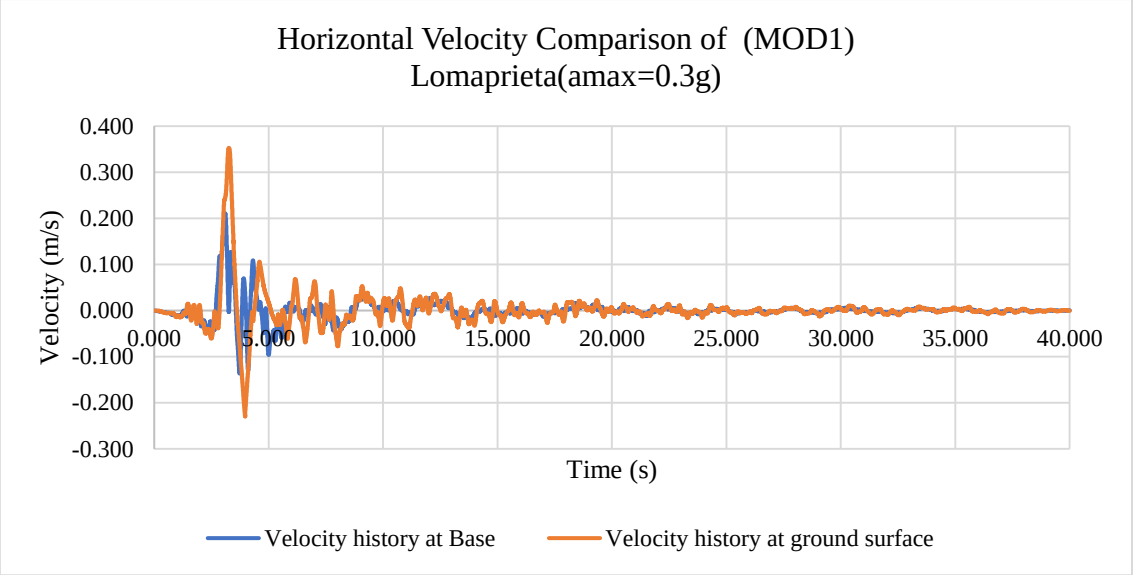

Fig. 4.9 Horizontal Velocity Comparison of MOD1

4.2.1.1 Horizontal acceleration and velocity amplification

When a shear wave or a seismic wave is propagating from one soil medium to another soil medium, the shear wave properties like acceleration amplitude, velocity amplitude etc. gets modified depending upon its frequency content and input motion. This modification or variation is best represented as amplification ratio, i.e. ratio of modified amplitude to original amplitude (a/a_{max}).

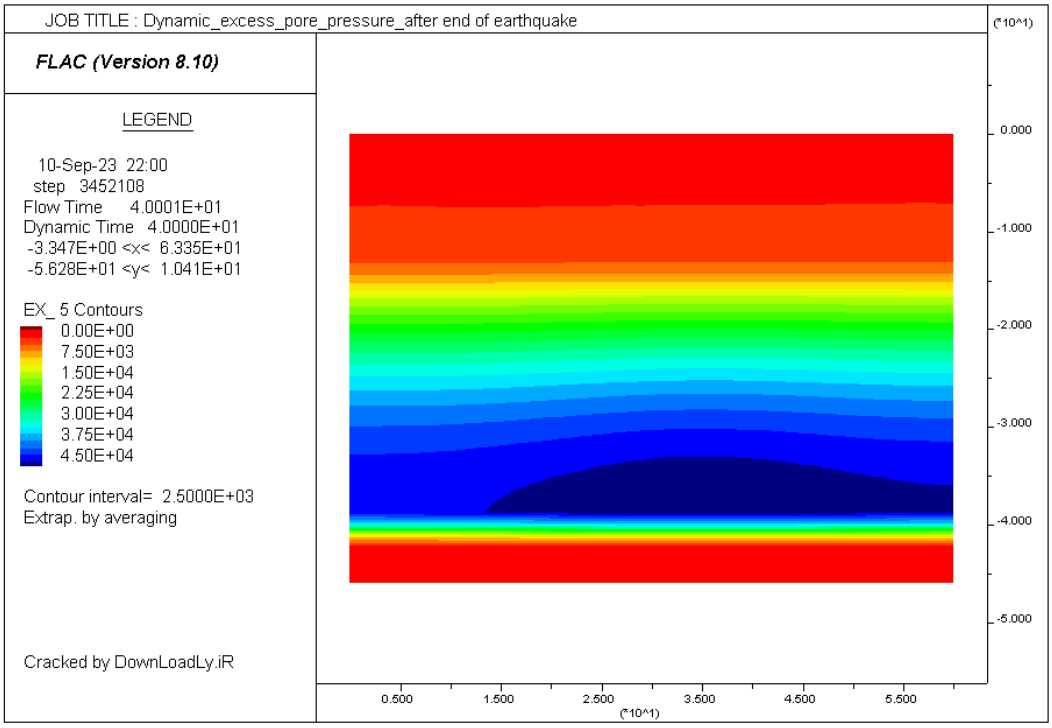

Fig. 4.10 Excess pore water pressure contour (EPWP) at the end of earthquake MOD1

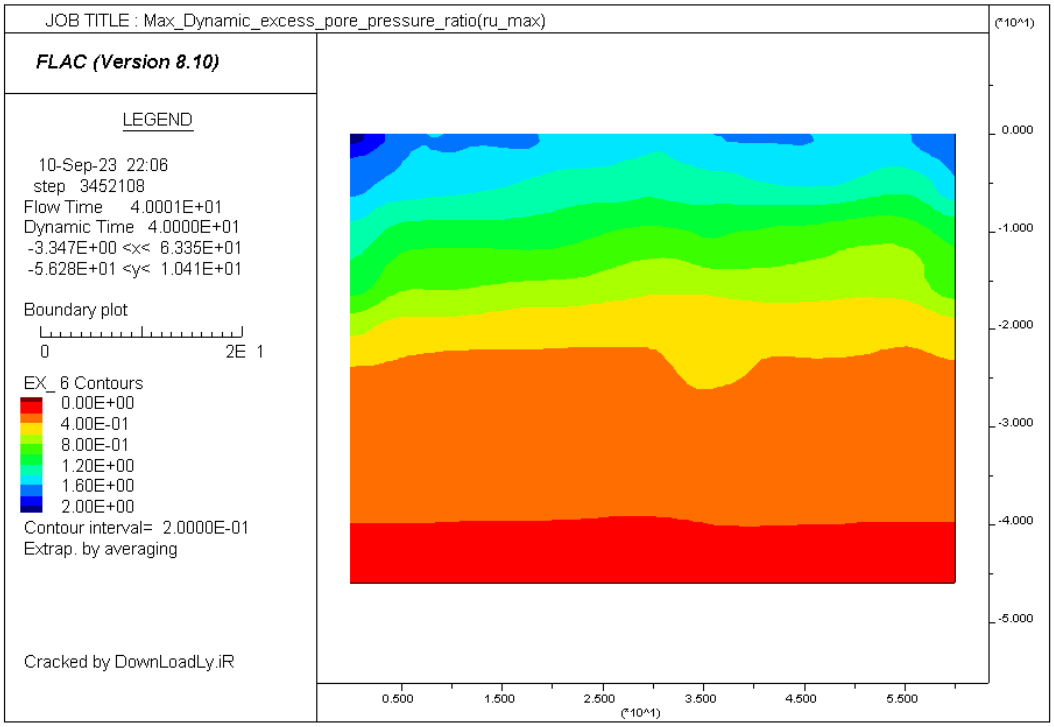

Fig. 4.11 Maximum Excess pore pressure ratio contour MOD1

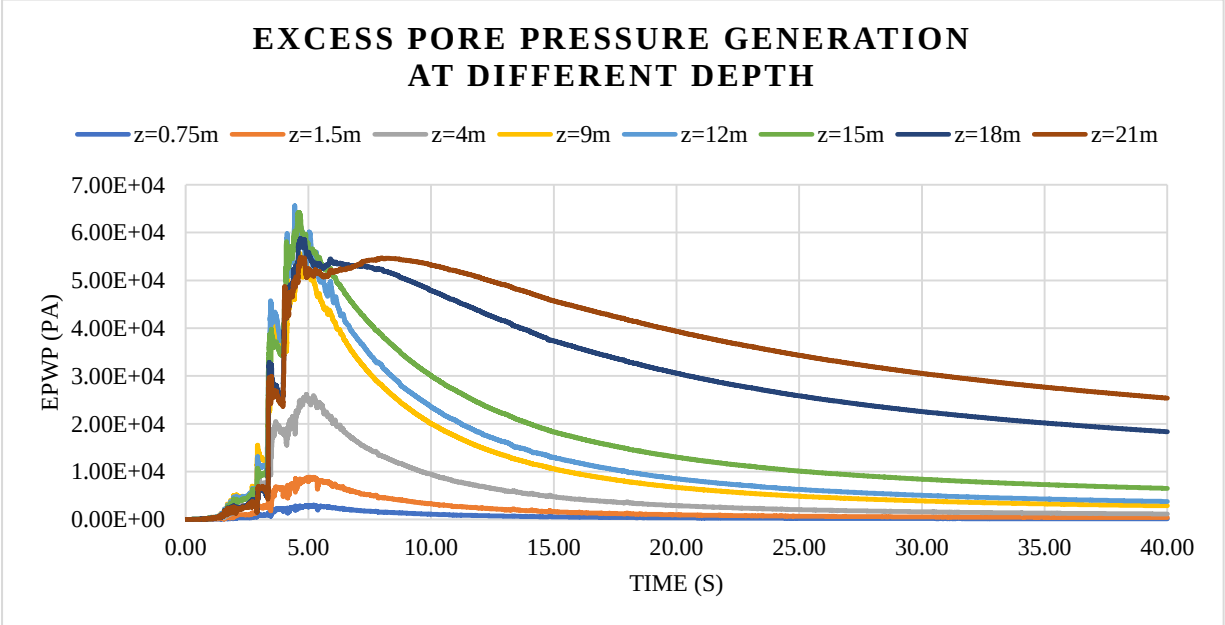

Fig. 4.12 Excess pore water pressure (EPWP) MOD1 at 1-1 section and different depth (A-H) (without stone column)

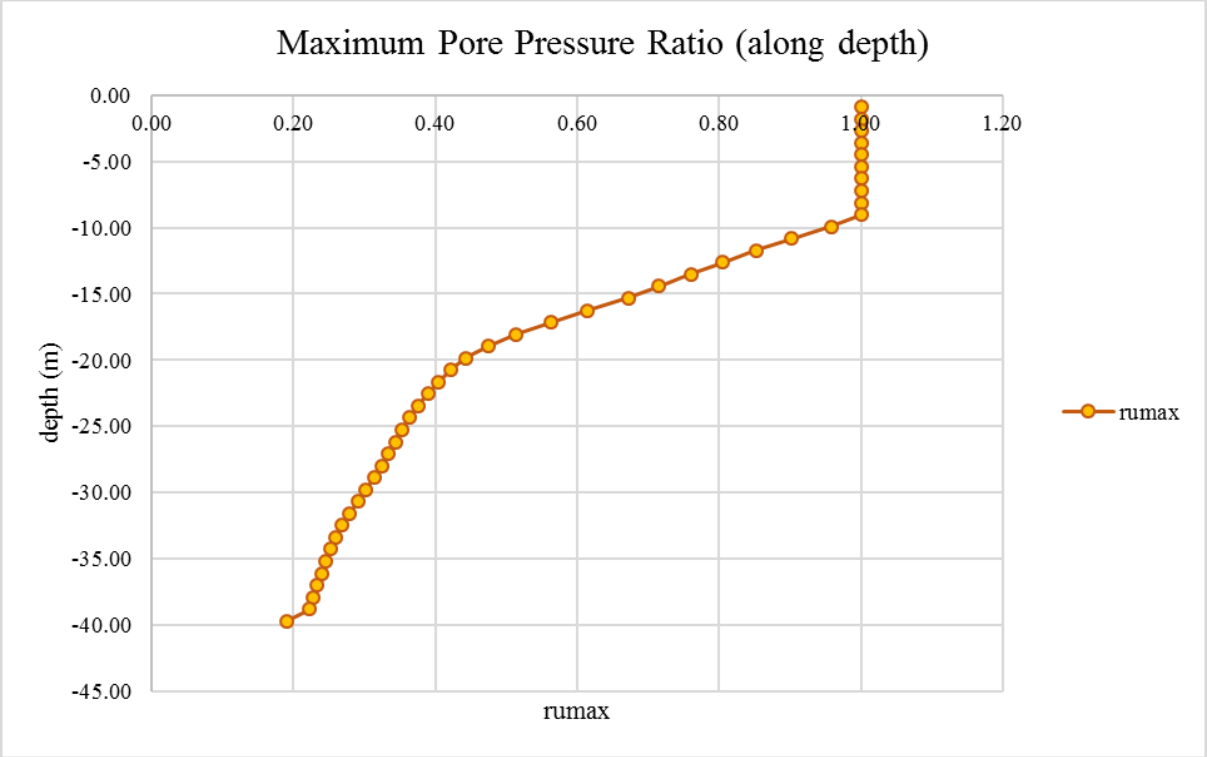

Fig. 4.13 Maximum Excess pore pressure ratio comparison at 1-1 section (without stone column)

4.2.1.2 Discussion on Results of dynamic analysis [MOD-1]:

In this case, model have without stone column, simulate with Lomaprieta (0.3g).

In fig. 4.8 and fig. 4.9 showing acceleration and velocity comparisons in between at base and ground surface. In both cases we observed the acceleration is amplified at ground surface and also velocity is amplified. The acceleration amplification ratio is 1.67 times. And velocity amplification ratio is about 1.68 times.

From fig. 4.10 we get the EPWP is generated at the end of the seismic excitation is 45kPa and the maximum EPWP generation is at bottom But initial time of excitation (first 10 seconds out of 40s time record as major acceleration peak is covered within first 10s) the EPWP is generated about 60-65kPa and the location of the maximum generation is at 9m to 15m depth from the ground surface. In the next time record the generated EPWP is dissipated slowly as this simulation is run on flow-on condition and upper layer boundary is permeable. If we observed carefully, we can see the bottom dense sand layer have lower permeability as compared to top layer of permeable sand. So top layer of sand is fast dissipated as compared to bottom sand layer. So, the EPWP is generation is showing maximum value at the end of earthquake.

Fig. 4.12 shows the maximum excess pore pressure is generated at depth 12m is 65.5kPa after that the EPWP is decreasing, at depth 15m excess pore pressure generate 62.7kPa, at depth 18m EPWP is 58.2kPa, and at depth 21m EPWP is 54.6kPa.

Fig. 4.11 showing maximum pore pressure ratio contour, ru_{max}. Pore pressure ratio is the representation of liquefaction. It is indicate the ratio of excess pore water pressure to the initial effective stress. When this pore pressure ratio is reached to 1, the excess pore pressure equal to effective stress, the soil termed as liquefy. Figure 4.11 shows due the seismic excitation the liquefaction reached to 11m depth on a 13.5m liquefiable layer.

Fig. 4.13 showing maximum pore pressure ratio along the depth at 1-1 cross section of MOD1. From this graph it is clear that the $ru_{max} \geq 1$ for a depth of 9 m. So, under the lomaprieta 0.3g PGA soil layer got liquefied the depth up to 9m.

4.2.2 [MOD2] With Stone Column (L = 5m) – Lomaprieta (a_{max}=0.3g)

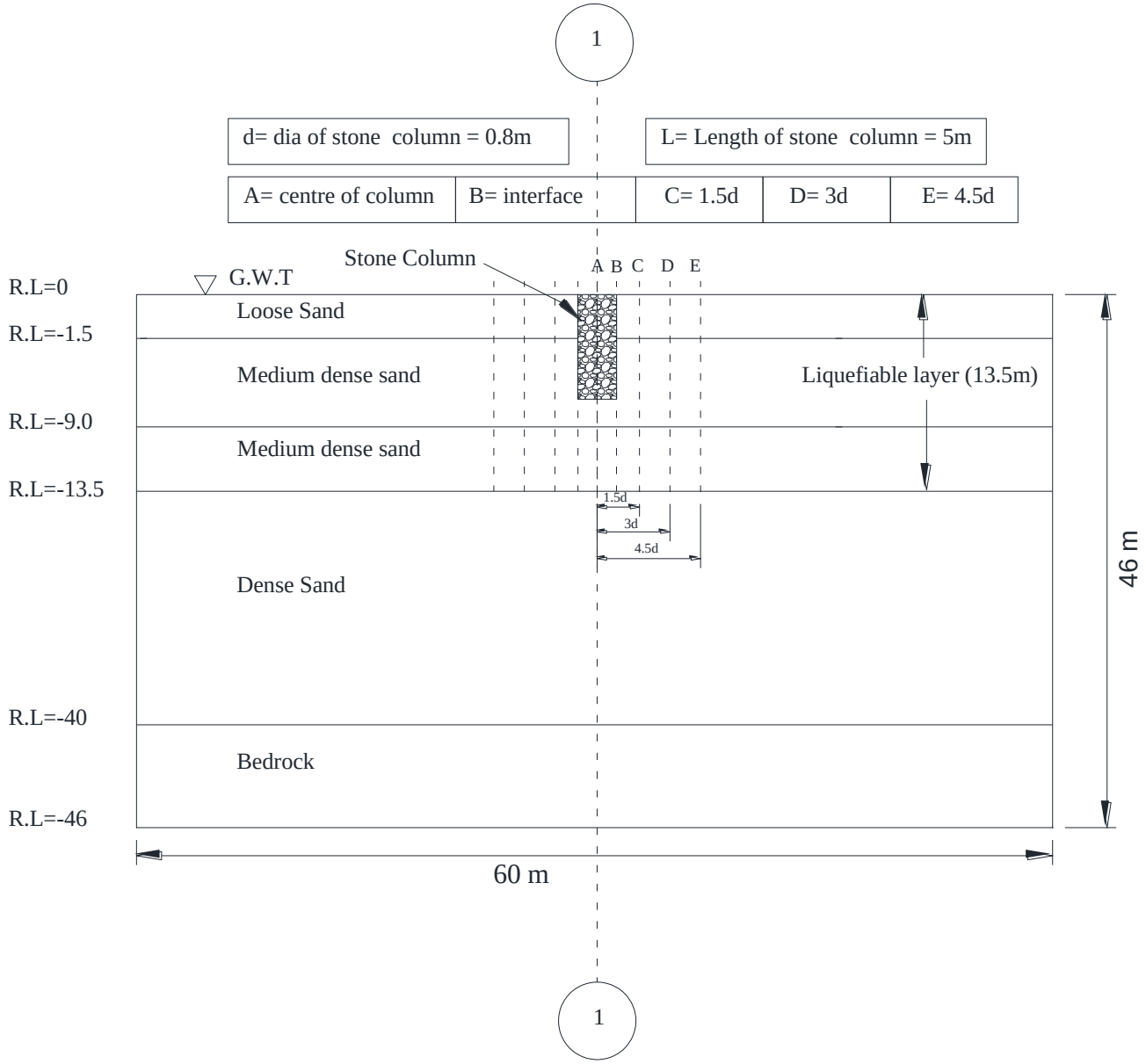

Fig. 4.14 Schematic diagram of MOD2 showing different observation points where excess pore pressure parameter calculated

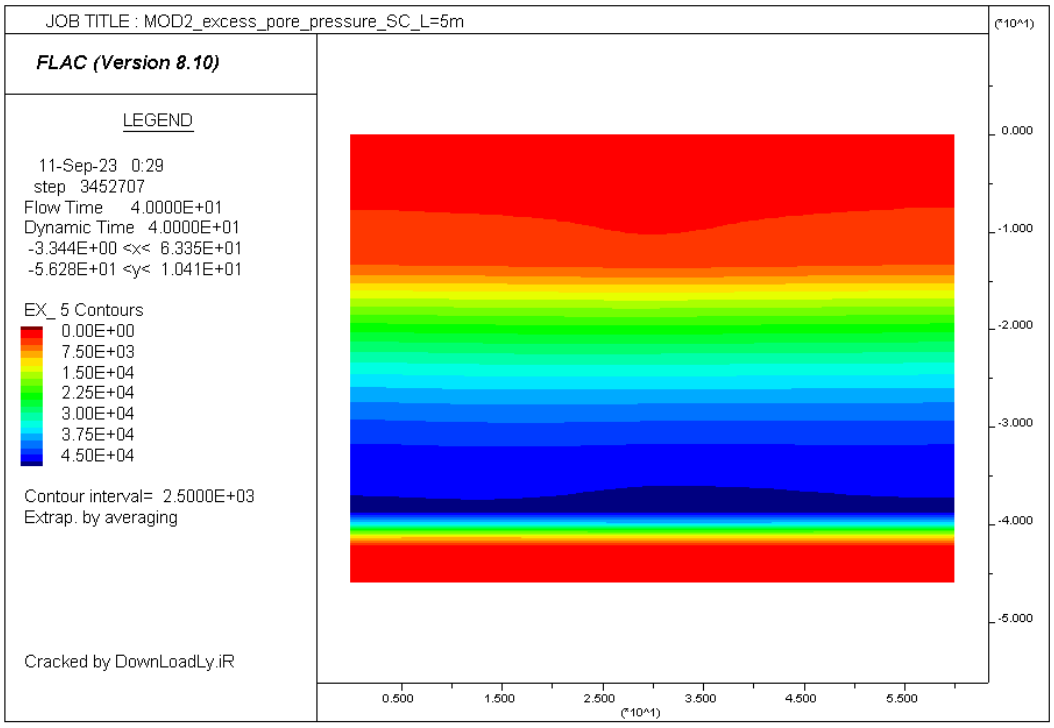

Fig. 4.15 Excess pore water pressure contour (EPWP) at the end of earthquake (with stone column, L=5m)

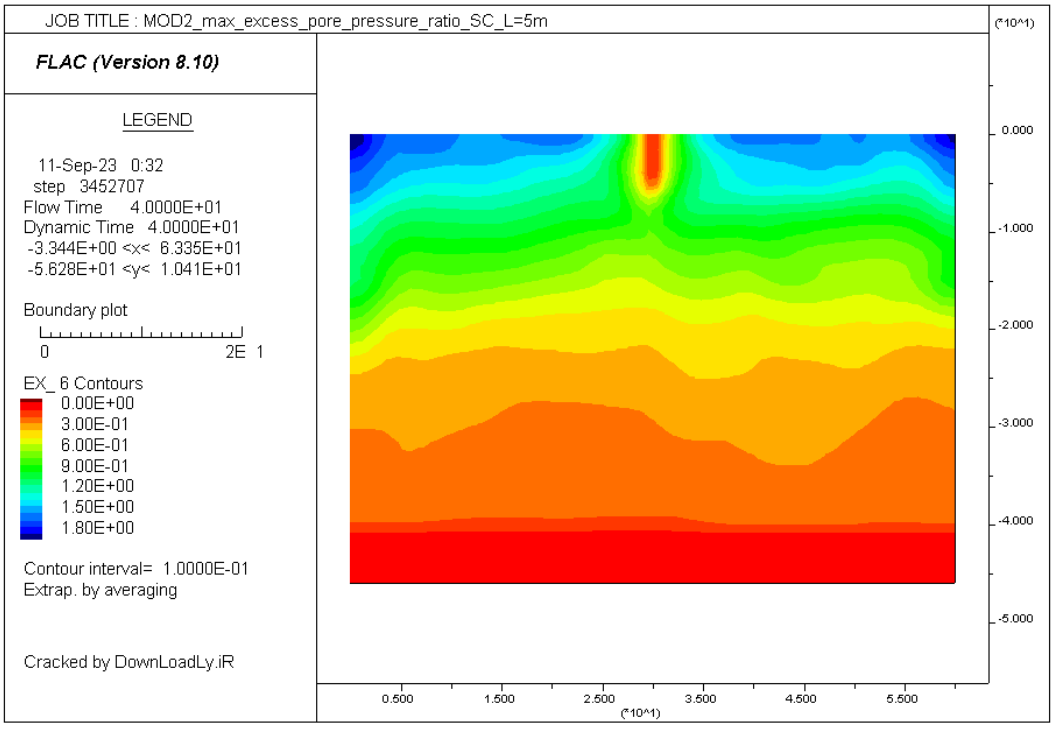

Fig. 4.16 Maximum Excess pore pressure ratio contour (with stone column, L=5m)

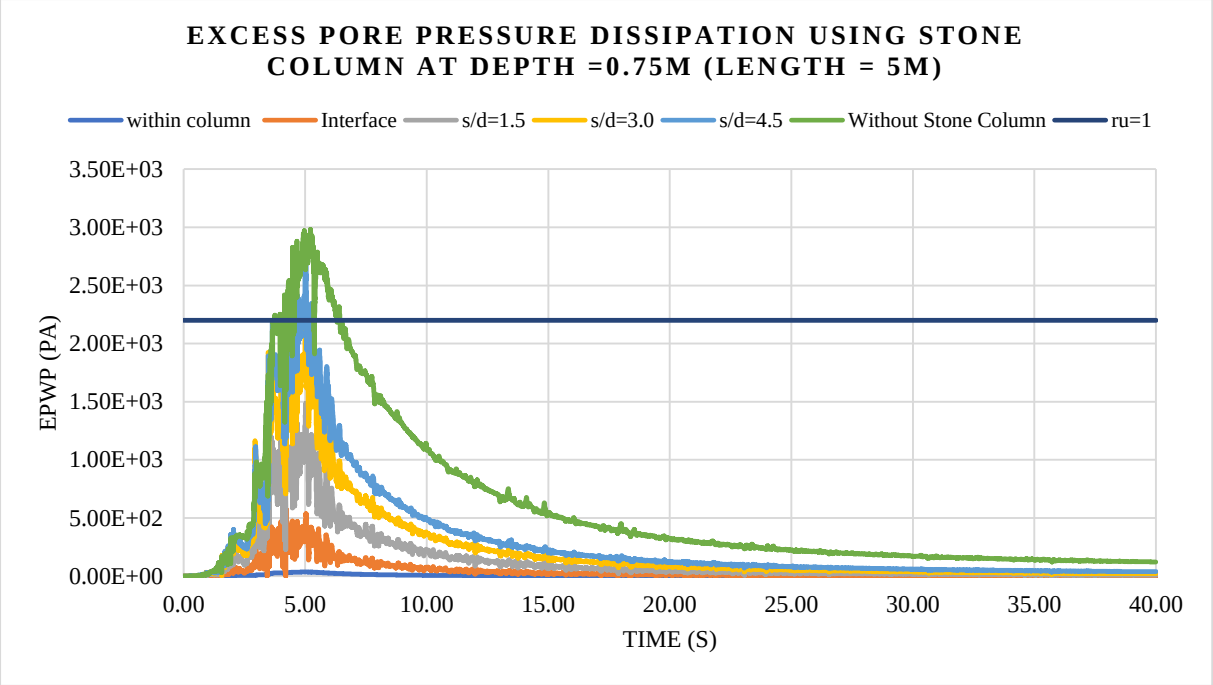

Fig. 4.17 Pore pressure dissipation comparison at lateral distances from center of stone column depth=0.75m from G.L (with stone column, L=5m)

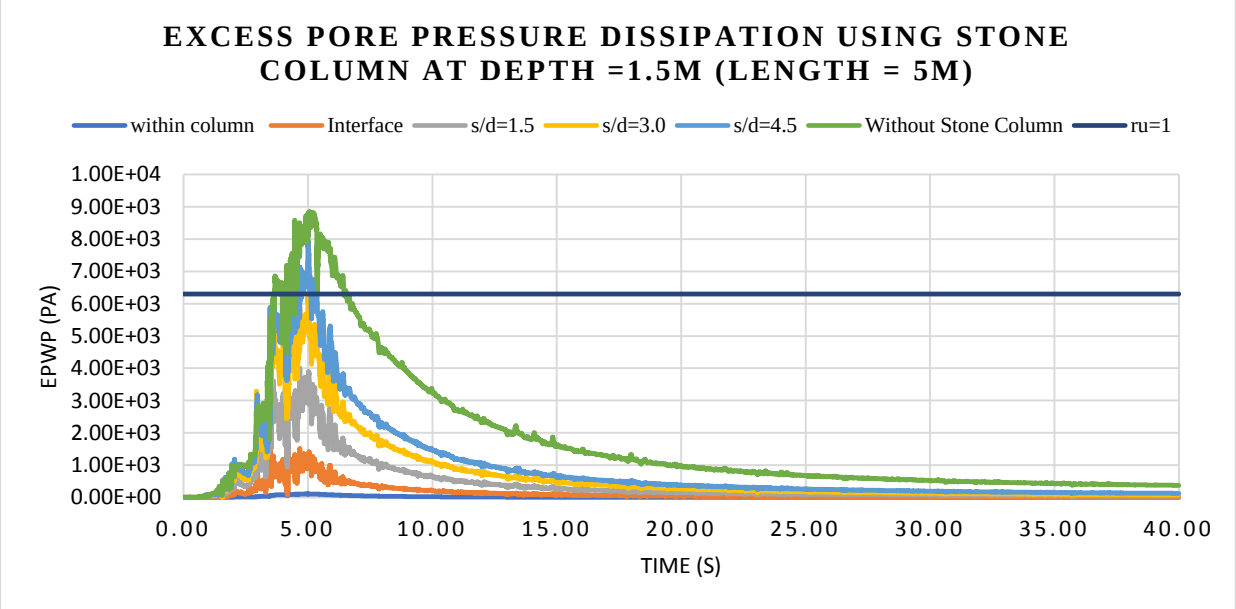

Fig. 4.18 Pore pressure dissipation comparison at lateral distances from center of stone column depth=1.5m from G.L (with stone column, L=5m)

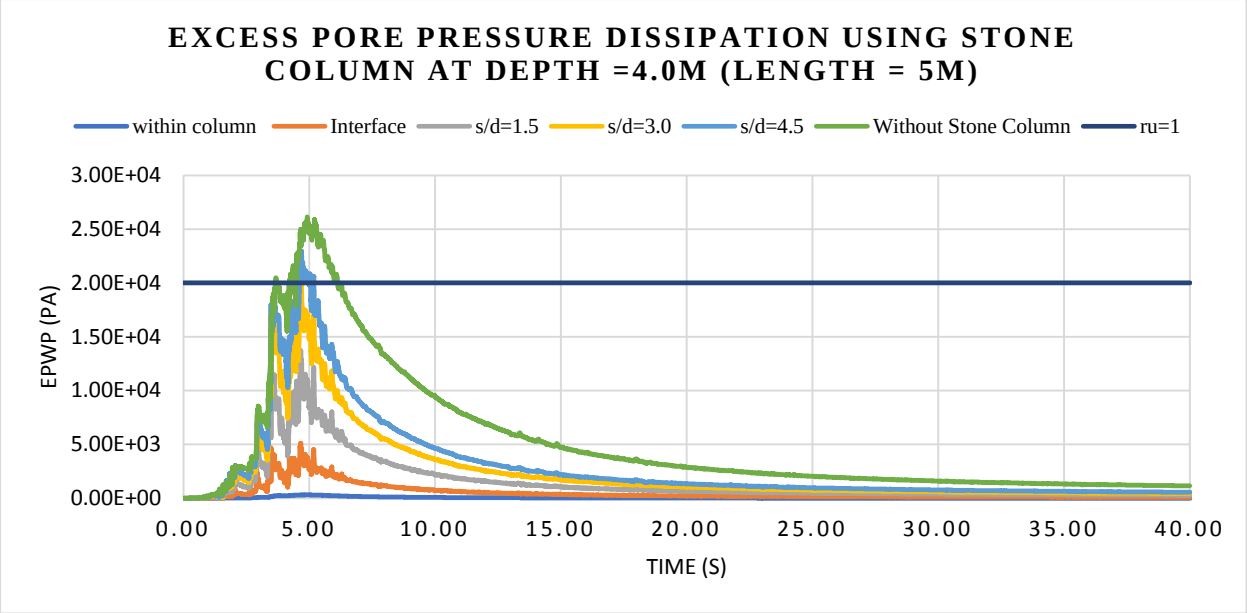

Fig. 4.19 Pore pressure dissipation comparison at lateral distance from center of stone column depth=4m from G.L (with stone column, L=5m)

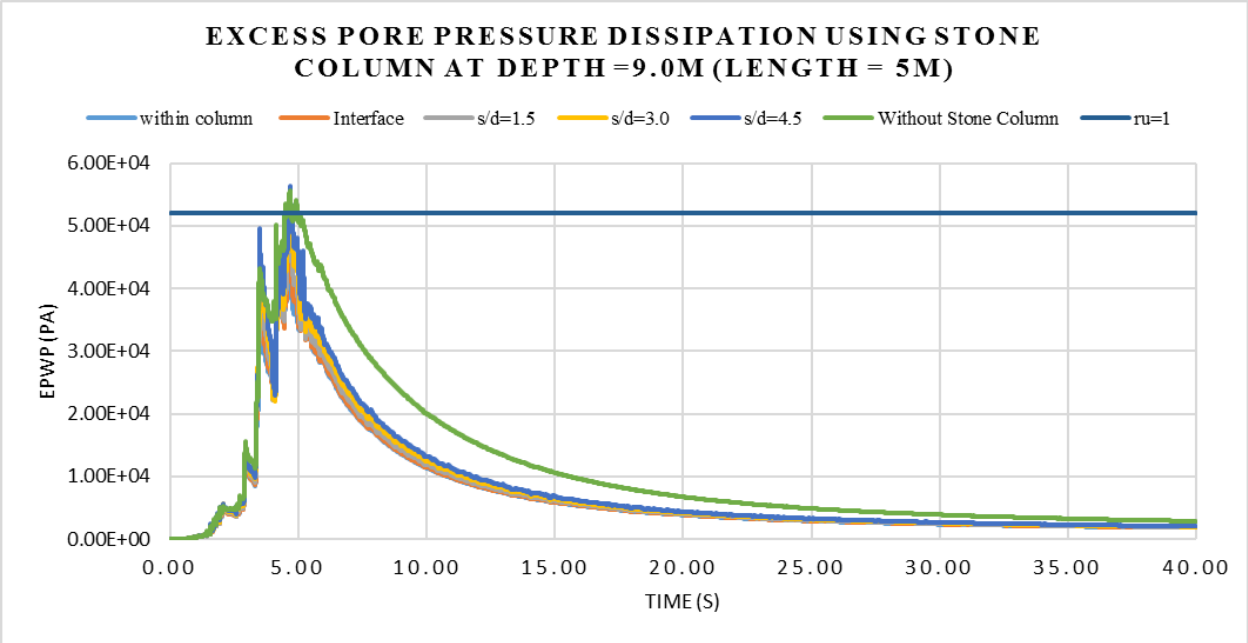

Fig. 4.20 Pore pressure dissipation comparison at lateral distance from center of stone column depth=9m from G.L (with stone column, L=5m)

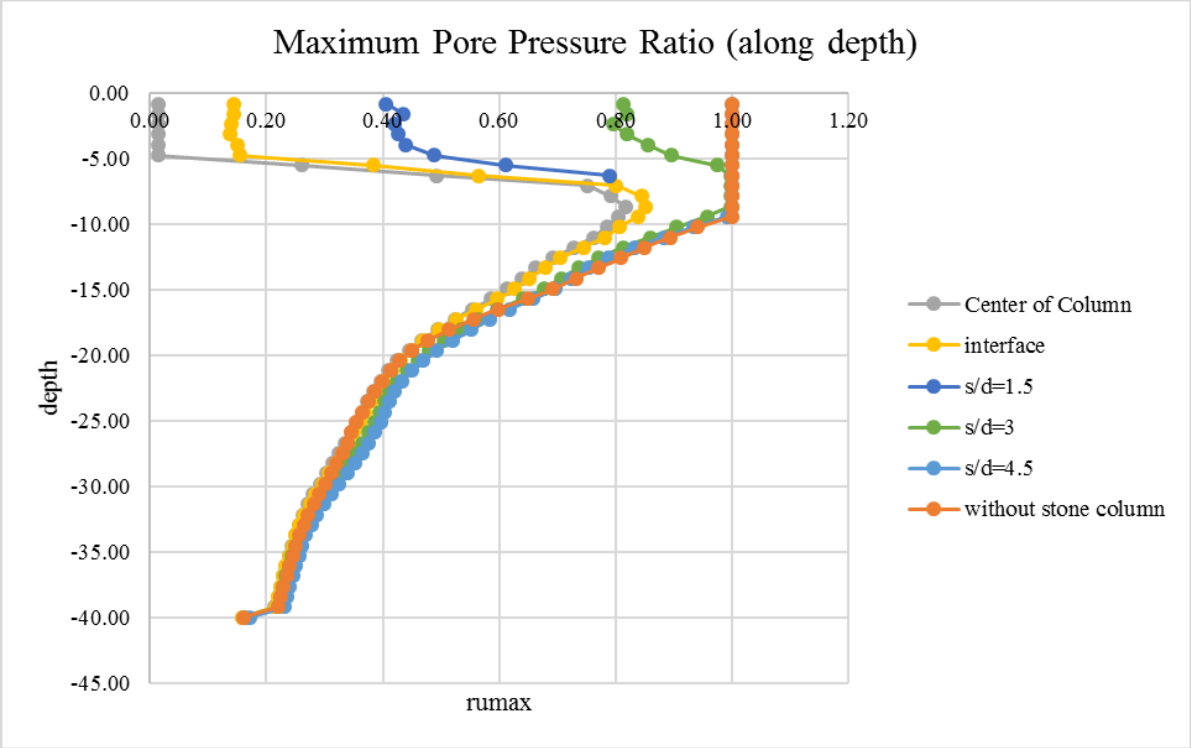

Fig. 4.21 Maximum Excess pore pressure ratio along with depth comparison at different lateral distance (with stone column, L=5m)

4.2.2.1 Discussion on Results of dynamic analysis [MOD-2]:

Fig. 4.15 showing excess pore pressure generation for stone column length, L=5m is 45kPa after the end of earthquake. In without stone column case that was 45kPa at the bottom. That's means no pore pressure dissipation at bottom depth 25m to 40m.

Fig. 4.16 showing the pore pressure ratio is reduce around the column and up to a depth of 5-6m from ground level.

Fig. 4.17 showing the comparison result of excess pore pressure with stone column of length 5m and without stone column. At depth of 0.75m from ground level. Excess pore water pressure at the center of stone column is negligible. At interface reached 0.5kPa. And at a distance 1.2 m distance from center indicated as s/d =1.5 or distance of 1.5 times diameter of stone column is reach 1.5 kPa. at these three distances stone column worked properly. But after s/d=1.5 m, excess pore pressure is not dissipated as compare to the above cases, and excess pore pressure reached to 1.

Fig. 4.18 and Fig. 4.19 showing similar pattern as Fig. 4.17, stone column of length 5 m dissipates excess pore water pressure up to a distance of 1.5d from the center of column. After that distance liquefaction is not reduce.

Fig. 4.20 showing the liquefaction not mitigate at depth of 9m as we used in MOD 2 length of stone column is 5m.

Fig. 4.21 shows that up to the distance of 1.5d from the stone column, liquefaction is mitigated by stone column effectively.

4.2.3 [MOD3] With Stone Column (L=10m) – Lomaprieta (a_{max}=0.3g)

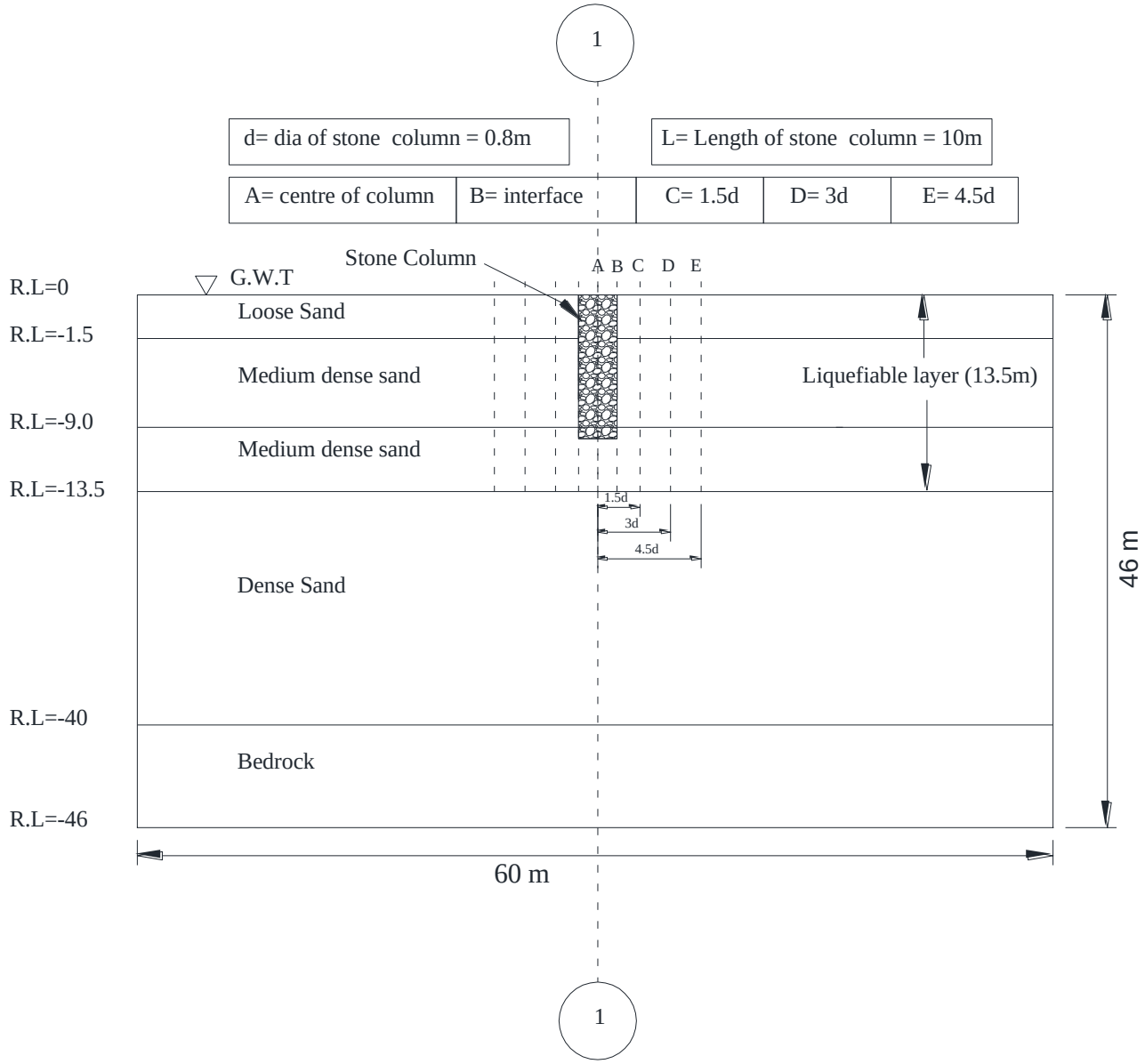

Fig. 4.22 Schematic diagram of MOD3 showing different observation points where excess pore pressure parameter calculated

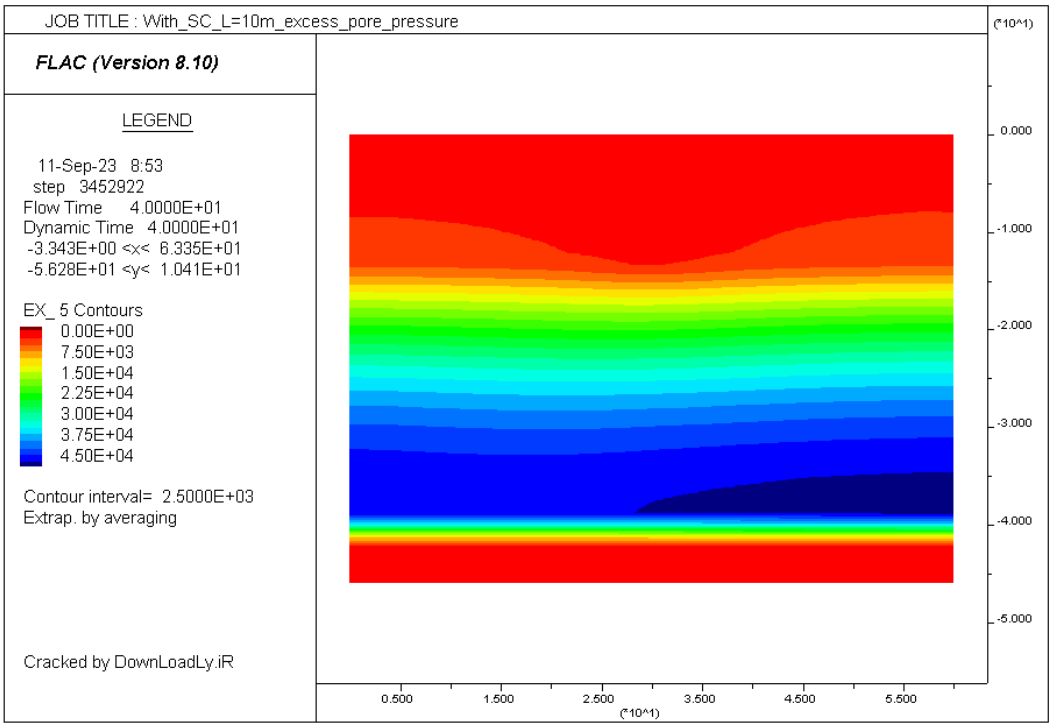

Fig. 4.23 Excess pore water pressure contour (EPWP) at the end of earthquake (with stone column, L=10m)

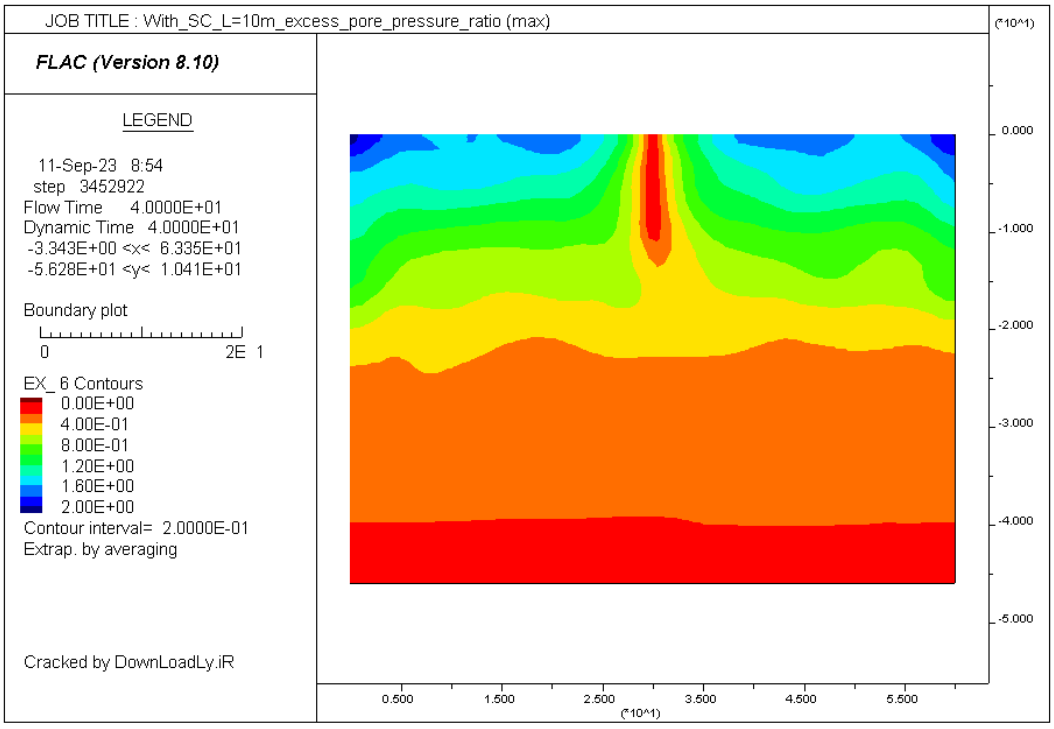

Fig. 4.24 Maximum Excess pore pressure ratio contour (with stone column, L=10m)

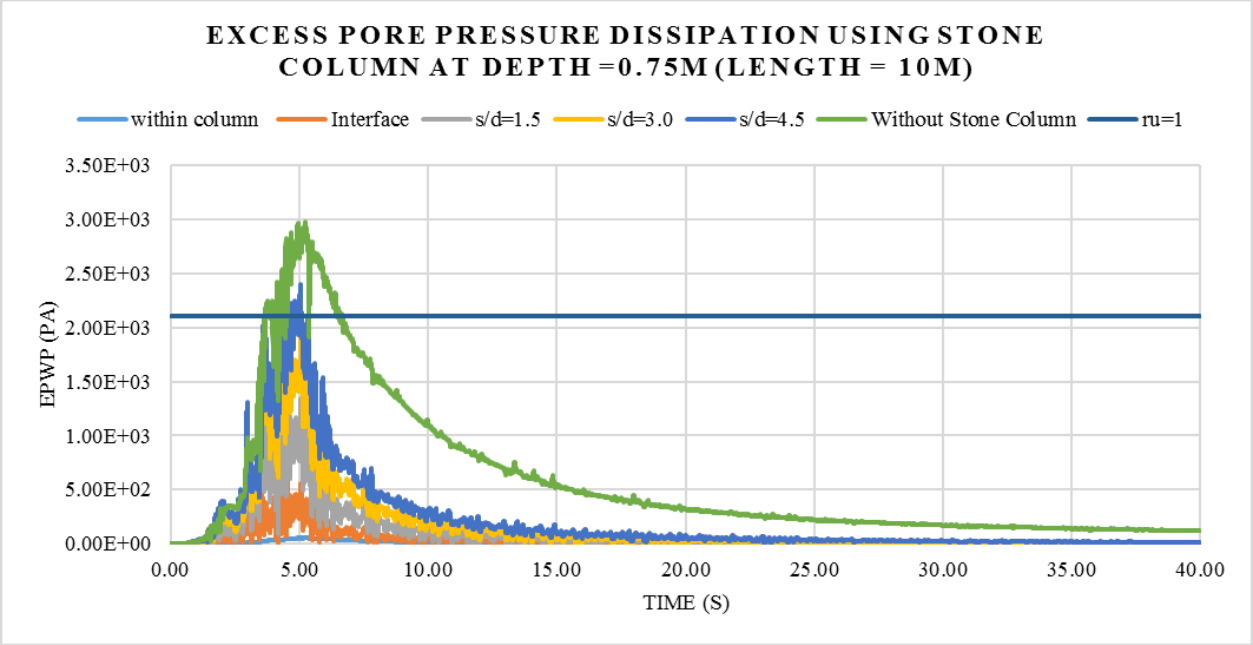

Fig. 4.25 Pore pressure dissipation comparison at lateral distance from center of stone column depth=0.75 m from G.L (with stone column, L=10m)

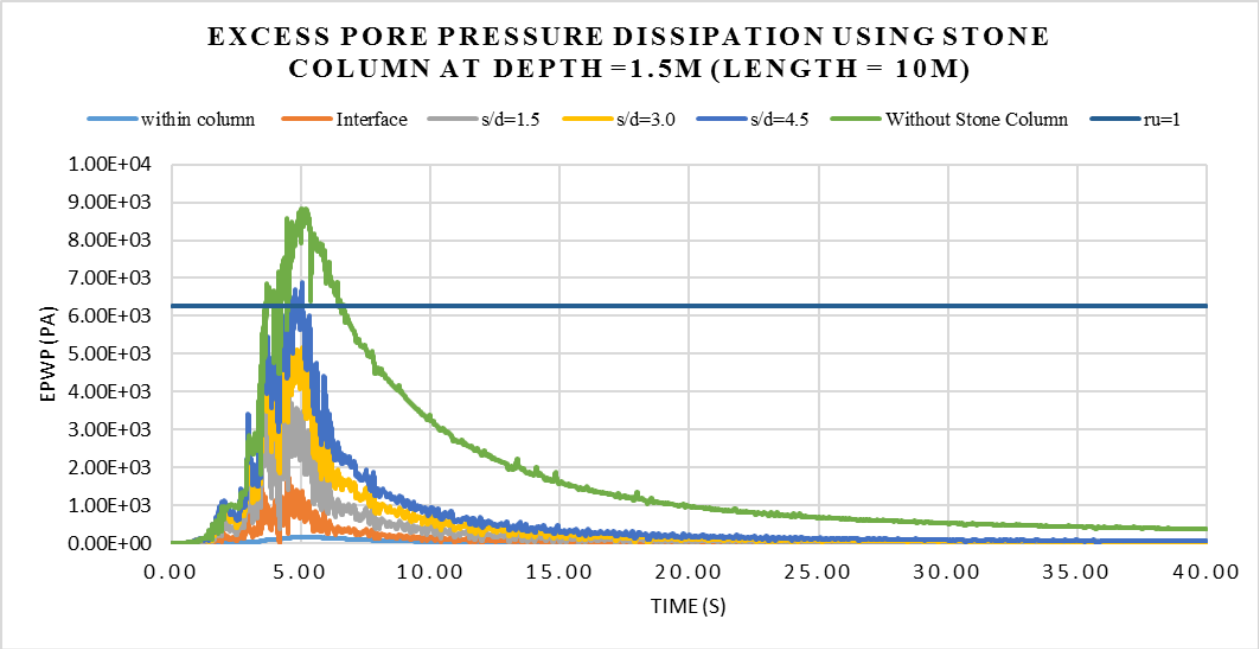

Fig. 4.26 Pore pressure dissipation comparison at lateral distance from center of stone column depth=1.5m from G.L (with stone column, L=10m)

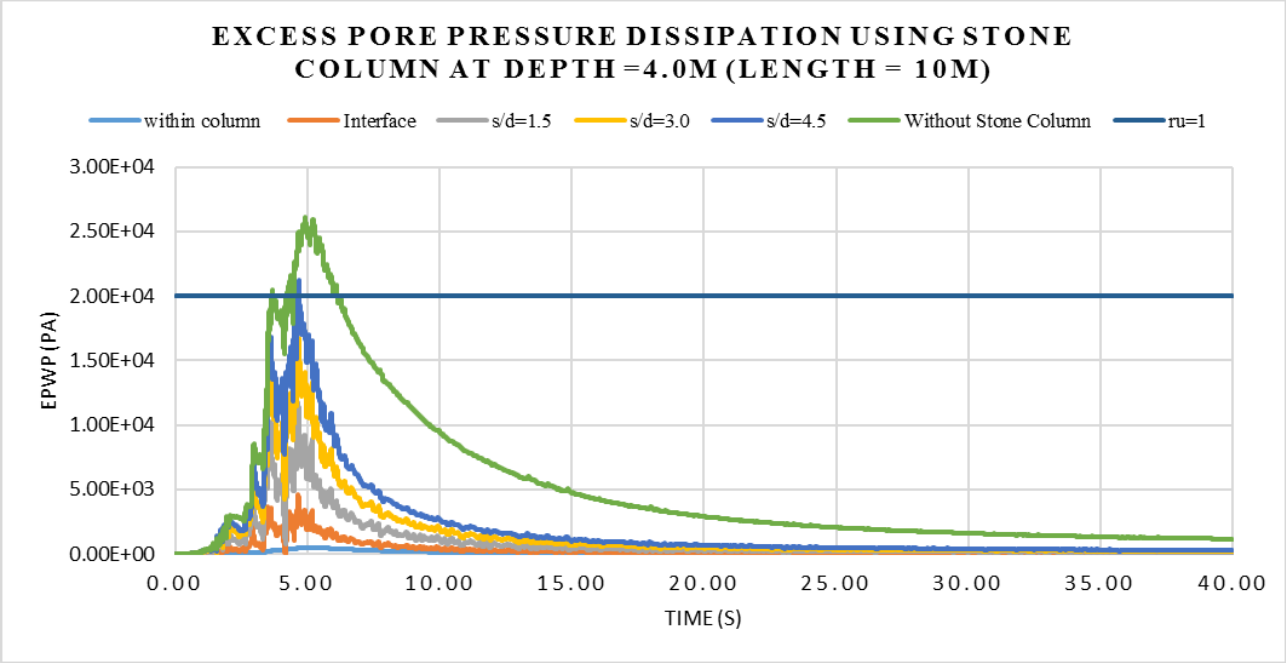

Fig. 4.27 Pore pressure dissipation comparison at lateral distance from center of stone column depth=4m from G.L (with stone column, L=10m)

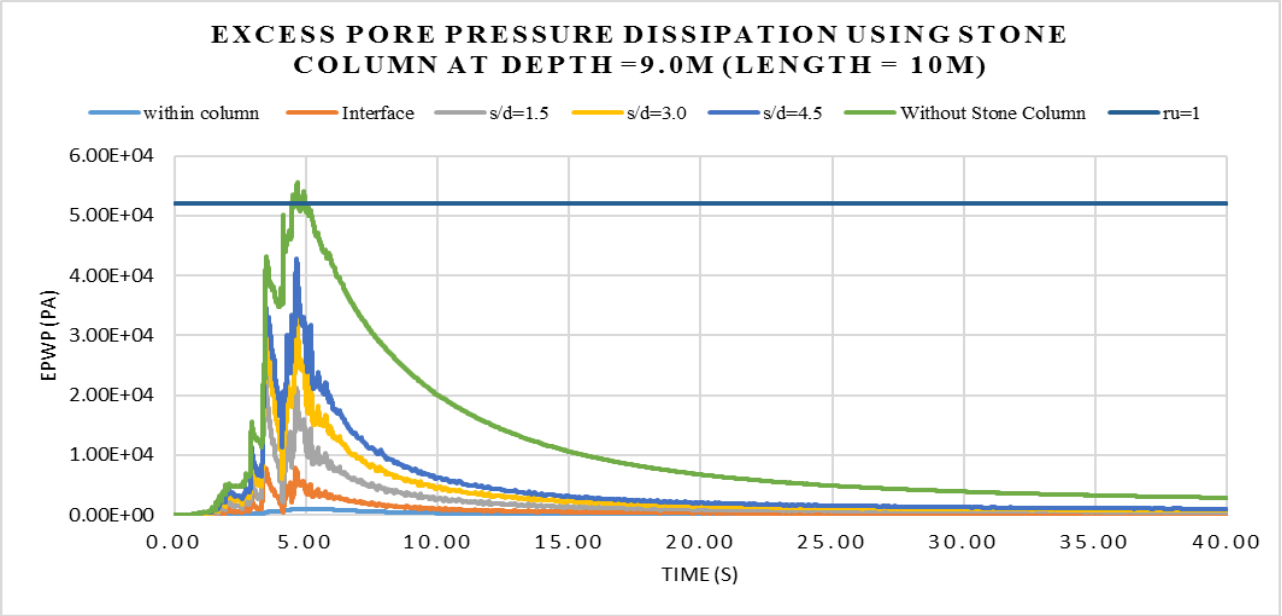

Fig. 4.28 Pore pressure dissipation comparison at lateral distance from center of stone column depth=9m from G.L (with stone column, L=10m)

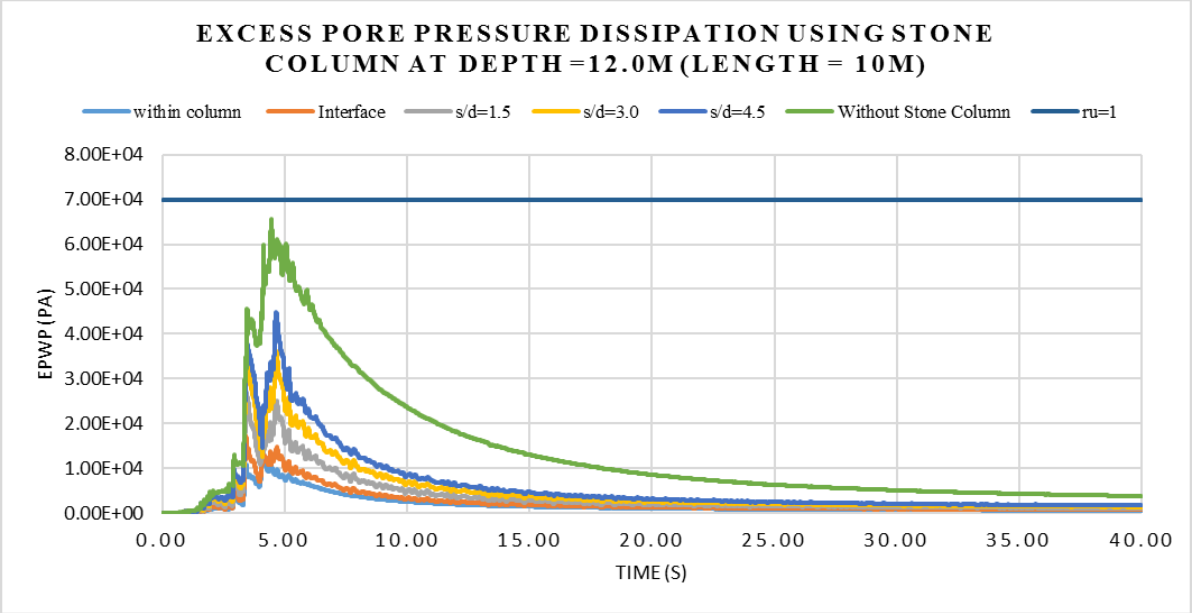

Fig. 4.29 Pore pressure dissipation comparison at lateral distance from center of stone column depth=12m from G.L (with stone column, L=10m)

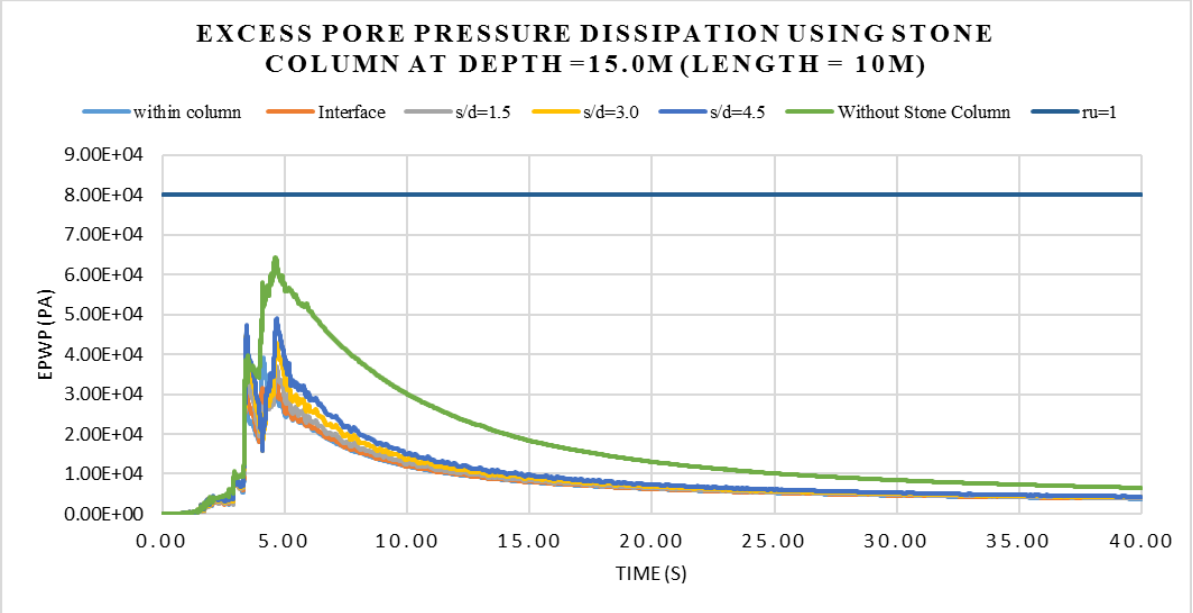

Fig. 4.30 Pore pressure dissipation comparison at lateral distance from center of stone column depth=15m from G.L (with stone column, L=10m)

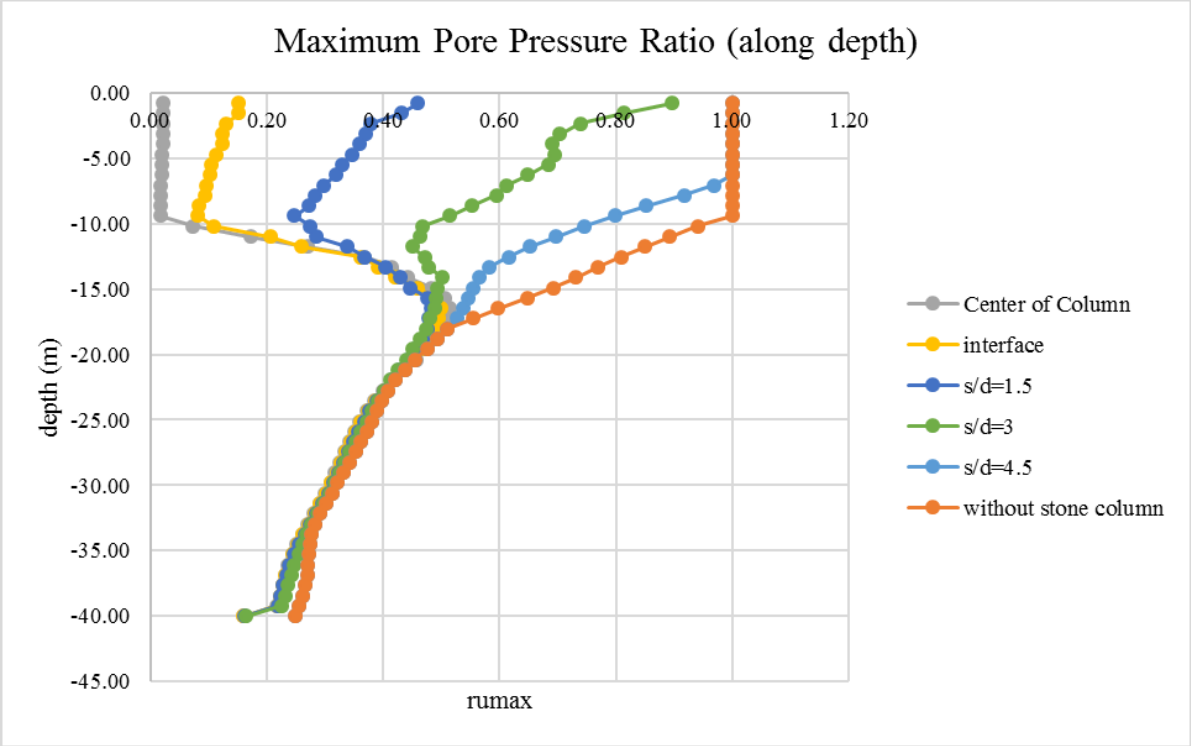

Fig. 4.31 Maximum Excess pore pressure ratio along with depth comparison at different lateral distance (with stone column, L=10m)

4.2.3.1 Discussion on Results of dynamic analysis (MOD-3)

Fig. 4.23 showing excess pore pressure contour is quite similar with the previous model. The EPWP on top 12m layer is fully dissipated and the maximum excess pore water pressure is at bottom.

Fig. 4.24 showing the pore pressure ratio is reduce around the column and up to a depth of 13 m from ground level. In this model stone column length used is 10m.

Fig. 4.25 showing the comparison result of excess pore pressure with stone column of length 10m and without stone column. At depth of 0.75m from ground level, Excess pore water pressure at the center of stone column is negligible because stone column have very high permeability, so when water from the surrounding reach just the column, instantly dissipated. At interface EPWP reached 0.5kPa. And at a distance 1.2 m distance from center indicated as s/d =1.5 or distance of 1.5 times diameter of stone column is reach 1.3 kPa. at these three distances stone column worked properly. But after s/d=1.5 m, excess pore pressure is not dissipated as compare to the above cases, and excess pore pressure reached closed to 1.

Fig. 4.26, Fig. 4.27, Fig. 4.28 and Fig. 4.29 showing similar pattern as Fig. 4.25, stone column of length 10 m dissipates excess pore water pressure up to a distance of 1.5d from the center of column. After that distance liquefaction is not reduce as much as the first three cases (i.e. within column, interface and s/d=1.5).

Fig. 4.30 showing that stone column of having length 10m not work properly at a depth of 15m even, in that depth liquefaction is not triggered as the depth of liquefaction is only 11m for the 0.3g Lomaprieta earthquake. So, 10m length of stone column can sufficiently mitigate liquefaction of 11-12m soil layer.

Fig. 4.31 shows that very clearly up to the distance of 1.5d from the stone column, liquefaction is mitigated by stone column effectively.

4.2.4 [MOD4] With Stone Column (L=15m) – Lomaprieta (a_{max}=0.3g)

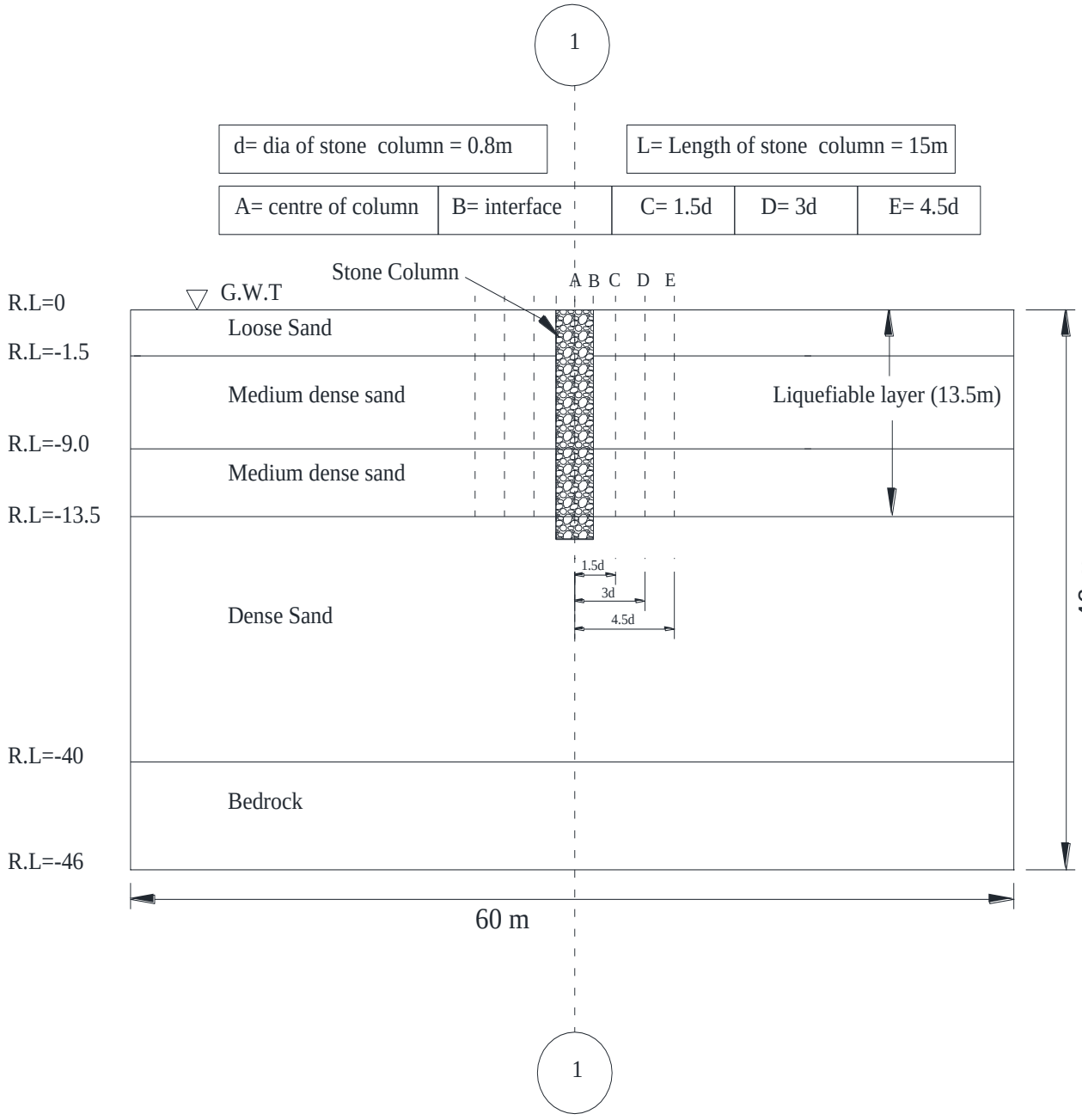

Fig. 4.32 Schematic diagram of MOD4 showing different observation points where excess pore pressure parameter calculated

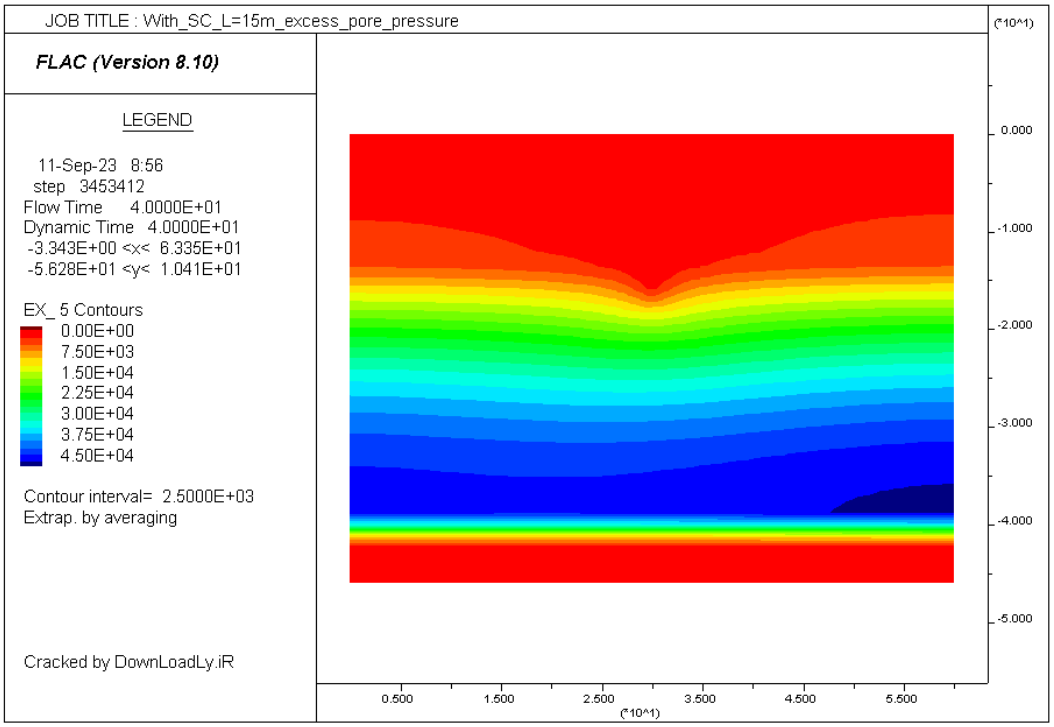

Fig. 4.33 Excess pore water pressure contour (EPWP) at the end of earthquake (with stone column, L=15m)

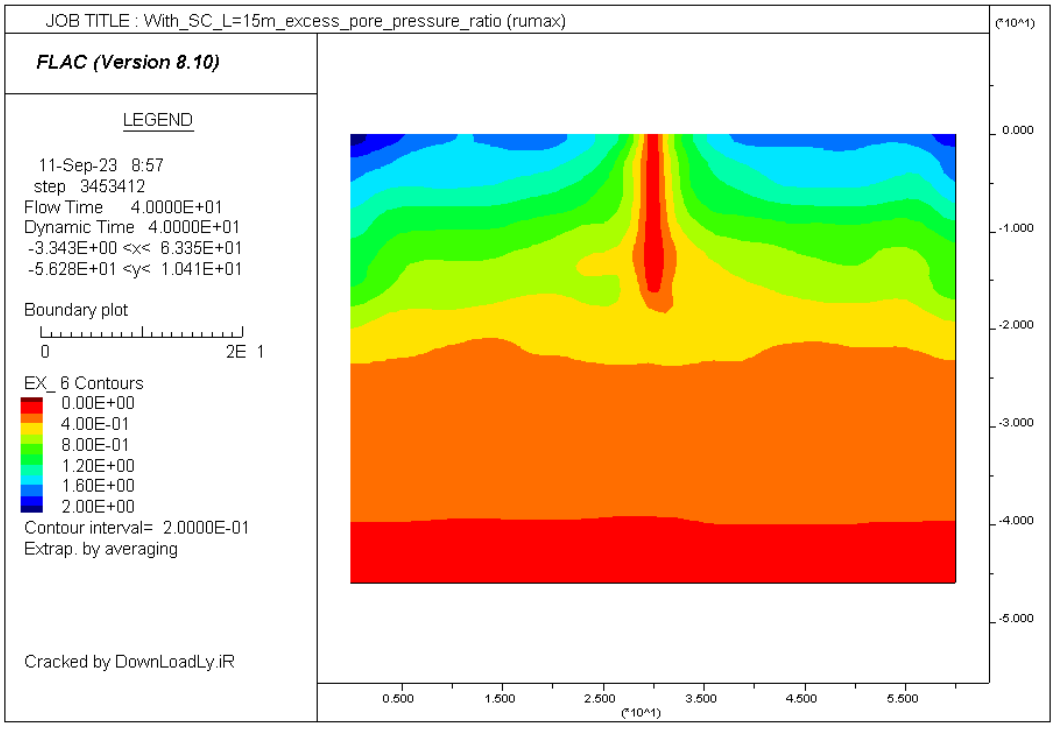

Fig. 4.34 Maximum Excess pore pressure ratio contour (with stone column, L=15m)

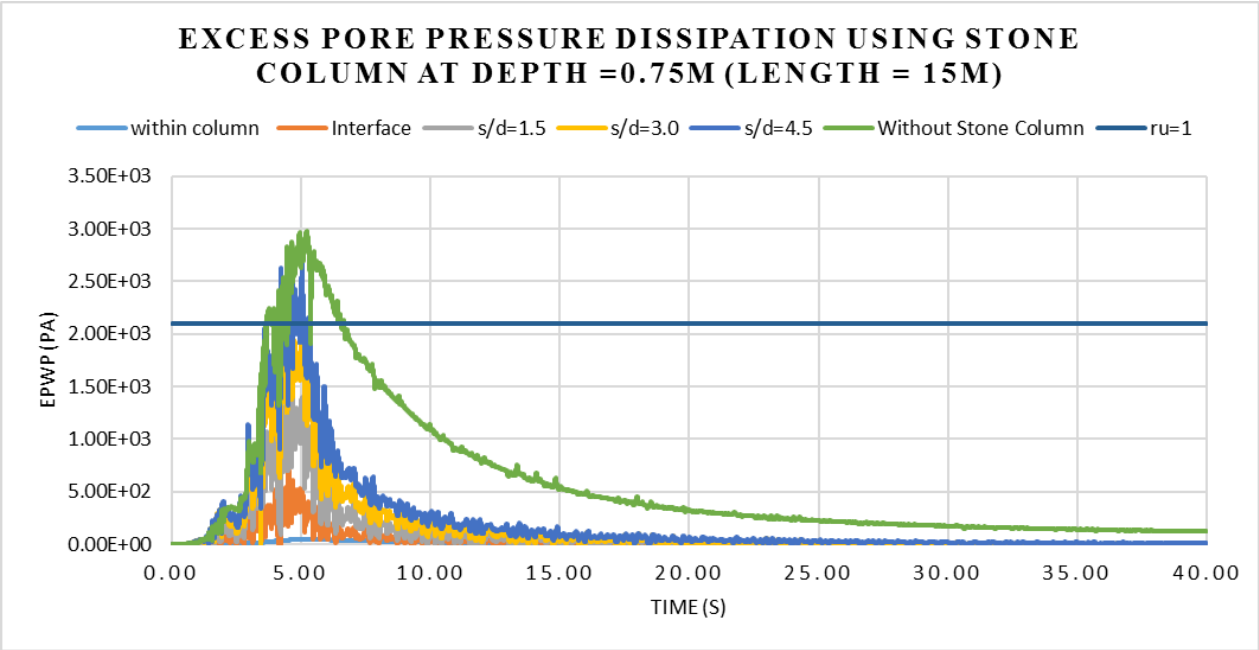

Fig. 4.35 Pore pressure dissipation comparison at lateral distance from center of stone column depth=0.75m from G.L (with stone column, L=15m)

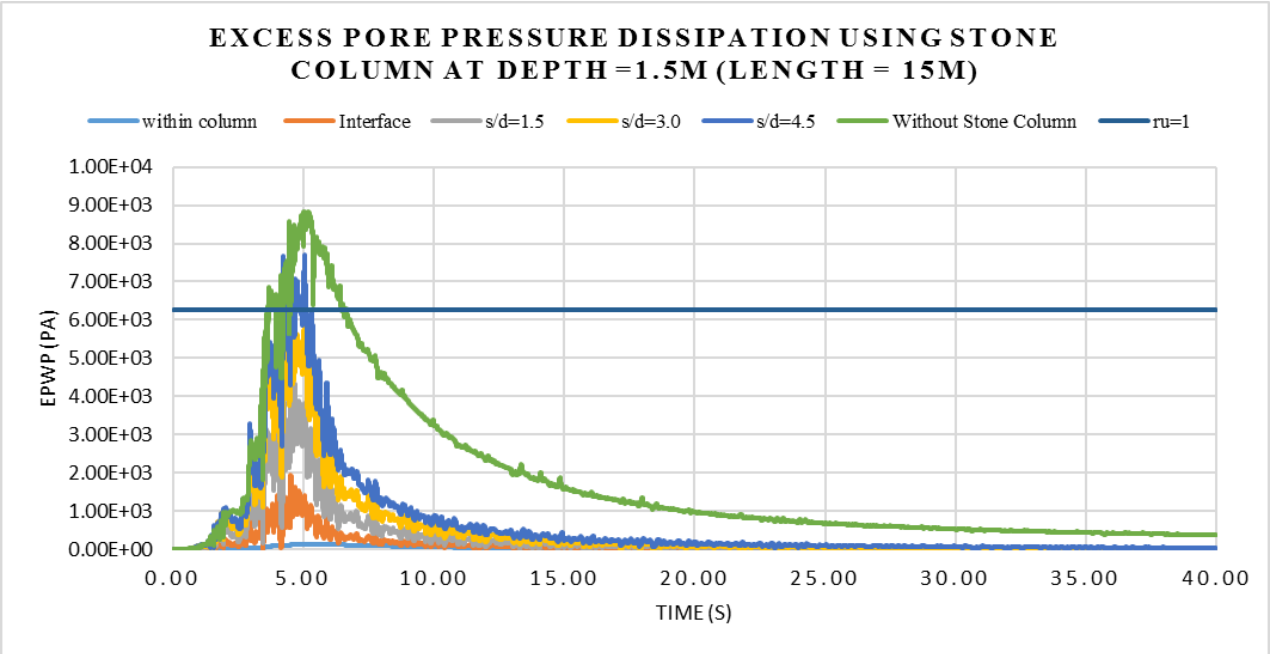

Fig. 4.36 Pore pressure dissipation comparison at lateral distance from center of stone column depth=1.5m from G.L (with stone column, L=15m)

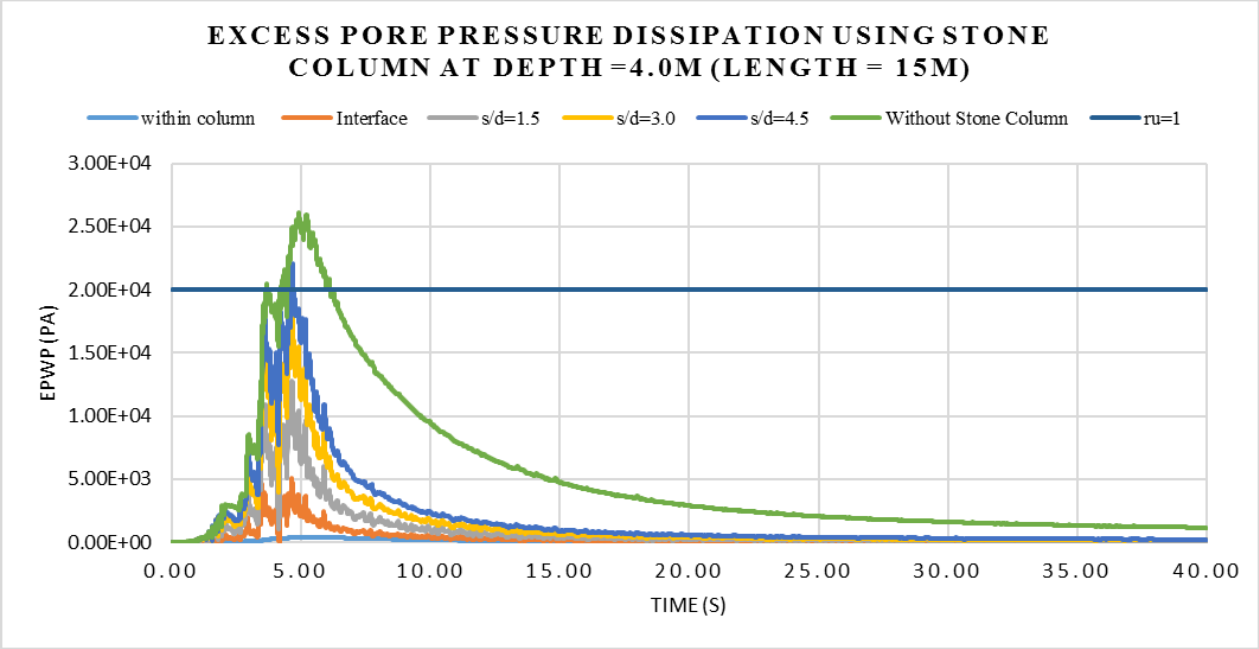

Fig. 4.37 Pore pressure dissipation comparison at lateral distance from center of stone column depth=4m from G.L (with stone column, L=15m)

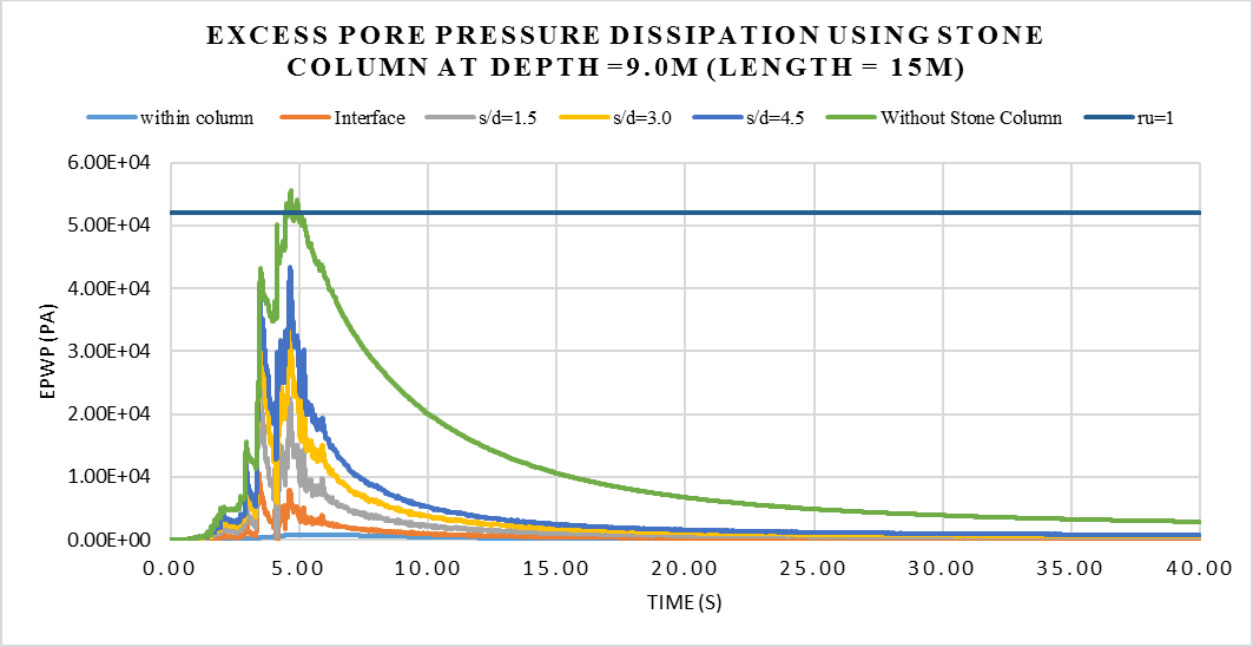

Fig. 4.38 Pore pressure dissipation comparison at lateral distance from center of stone column depth=9m from G.L (with stone column, L=15m)

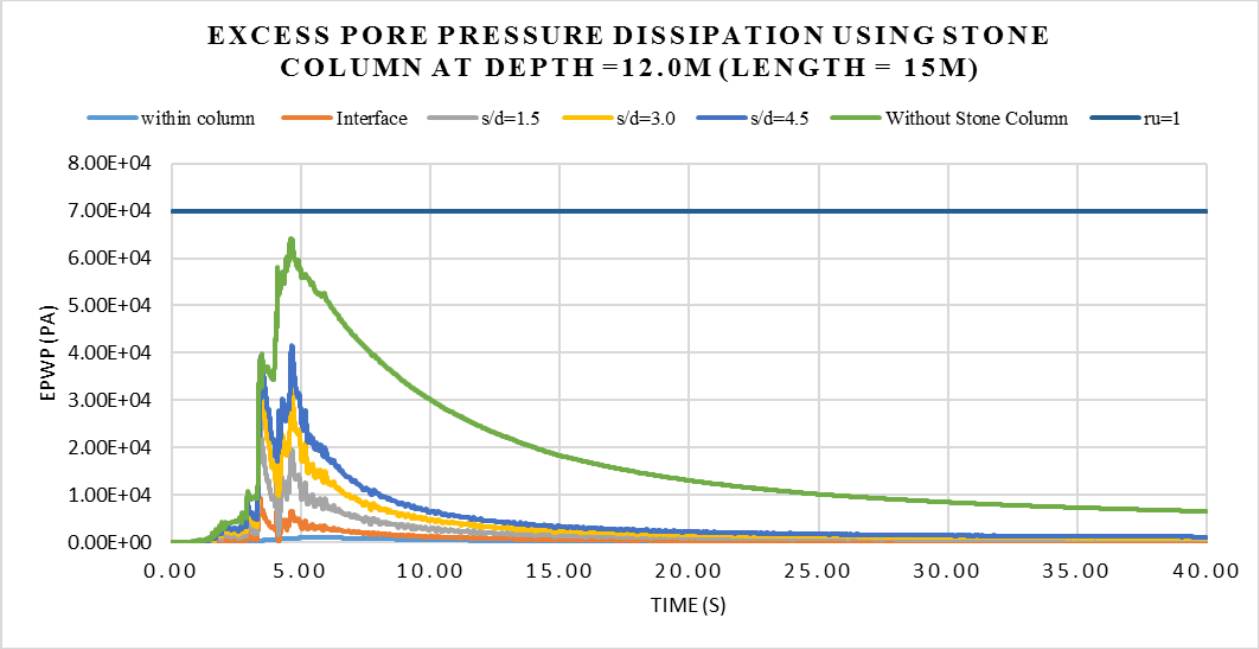

Fig. 4.39 Pore pressure dissipation comparison at lateral distance from center of stone column depth=12m from G.L (with stone column, L=15m)

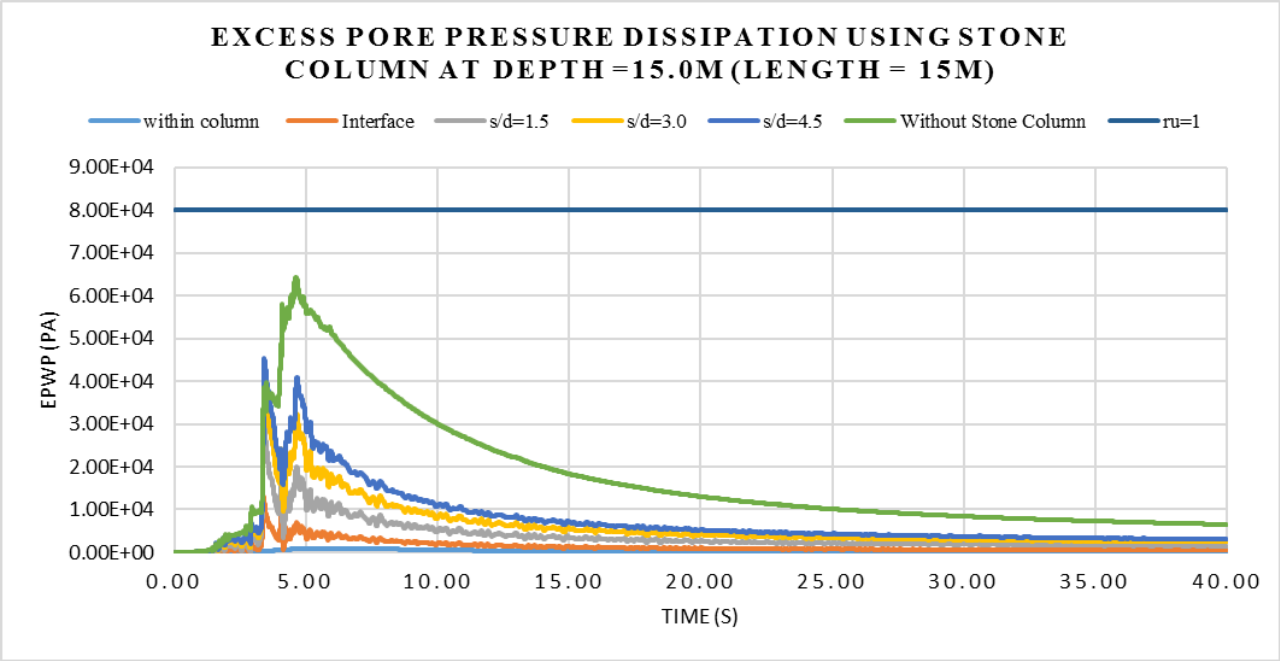

Fig. 4.40 Pore pressure dissipation comparison at lateral distance from center of stone column depth=15m from G.L (with stone column, L=15m)

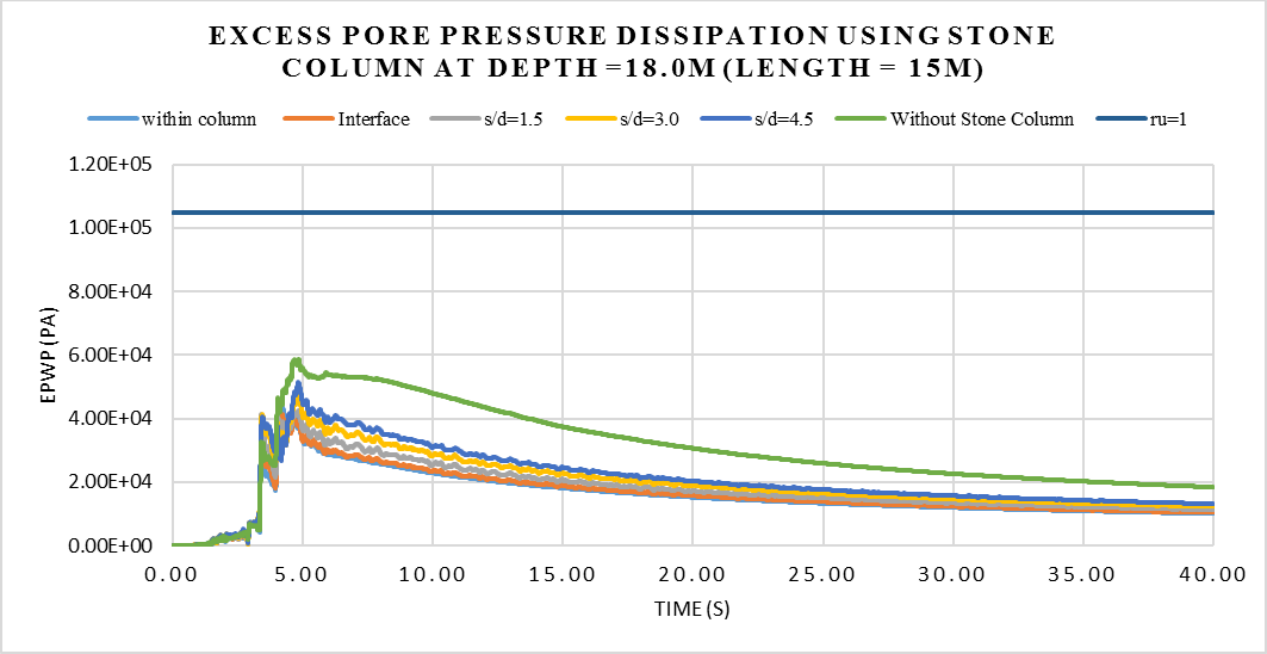

Fig. 4.41 Pore pressure dissipation comparison at lateral distance from center of stone column depth=18m from G.L (with stone column, L=15m)

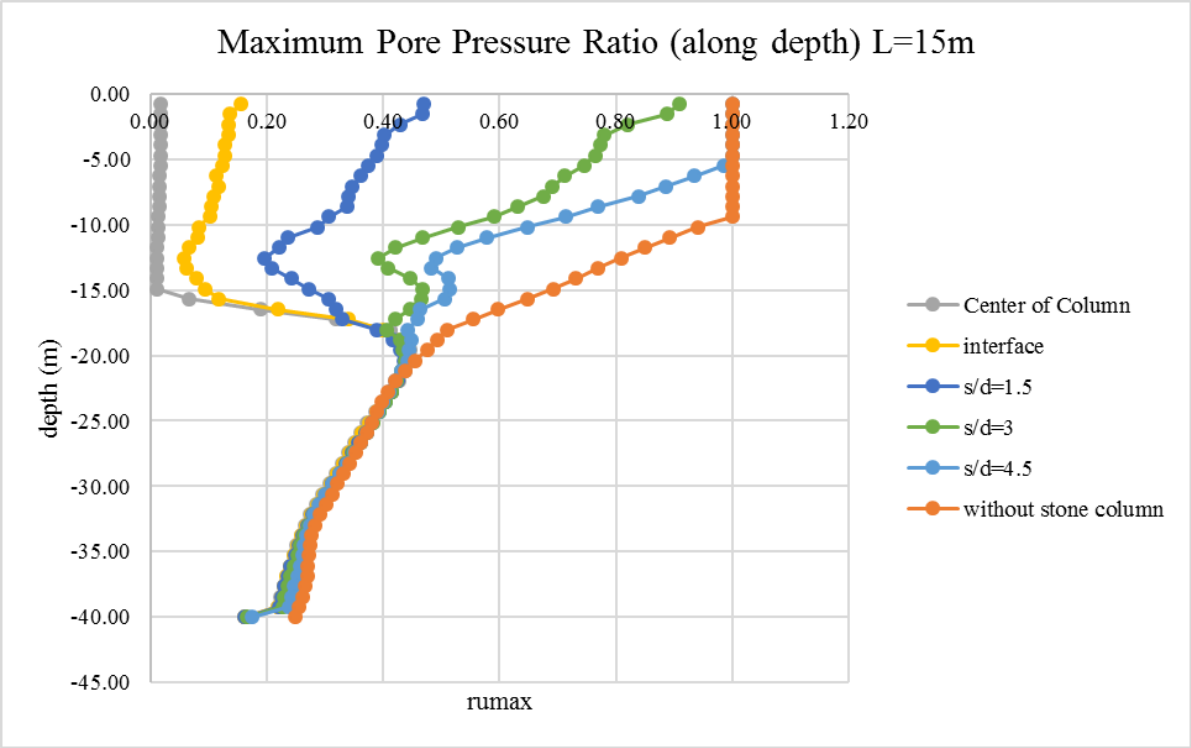

Fig. 4.42 Maximum Excess pore pressure ratio along with depth comparison at different lateral distance (with stone column, L=15m)

4.2.4.1 Discussion on Results of dynamic analysis (MOD-4)

Fig. 4.33 showing excess pore pressure is fully dissipated about top 15m layer and the maximum excess pore water pressure is at bottom.

Fig. 4.34 showing the pore pressure ratio is reduce around the column and up to a depth of 16 m from ground level. In this model stone column length used is 15m.

Fig. 4.35 showing the comparison result of excess pore pressure with stone column of length 15m and without stone column. At depth of 0.75m from ground level, Excess pore water pressure at the center of stone column is negligible because stone column have very high permeability, so when water from the surrounding reach just the column, instantly dissipated. At interface EPWP reached 0.5kPa. And at a distance 1.2 m distance from center indicated as s/d =1.5 or distance of 1.5 times diameter of stone column is reach 1.3 kPa. at these three distances stone column worked properly. But after s/d=1.5 m, excess pore pressure is not dissipated as compare to the above cases, and excess pore pressure reached closed to 1.

Fig. 4.36, Fig. 4.37, Fig. 4.38, Fig.4.39 and Fig. 4.40 showing similar pattern as Fig. 4.35, stone column of length 15 m dissipates excess pore water pressure up to a distance of 1.5d from the center of column. After that distance liquefaction is not reduce as much as the first three cases (i.e. within column, interface and s/d=1.5).

Stone column of having length 15m work properly at a depth up to 15-16m. Fig. 4.41 showing that in 18m depth EPWP is quite similar with stone column and without stone column as that depth, stone column not provided. So, 15m length of stone column can sufficiently mitigate liquefaction of 11-12m soil layer whereas 12m length of stone column also sufficiently reduce liquefaction.

4.2.5 [MOD5] Without Stone Column – Mammoth-lake (a_{max}=0.3g)

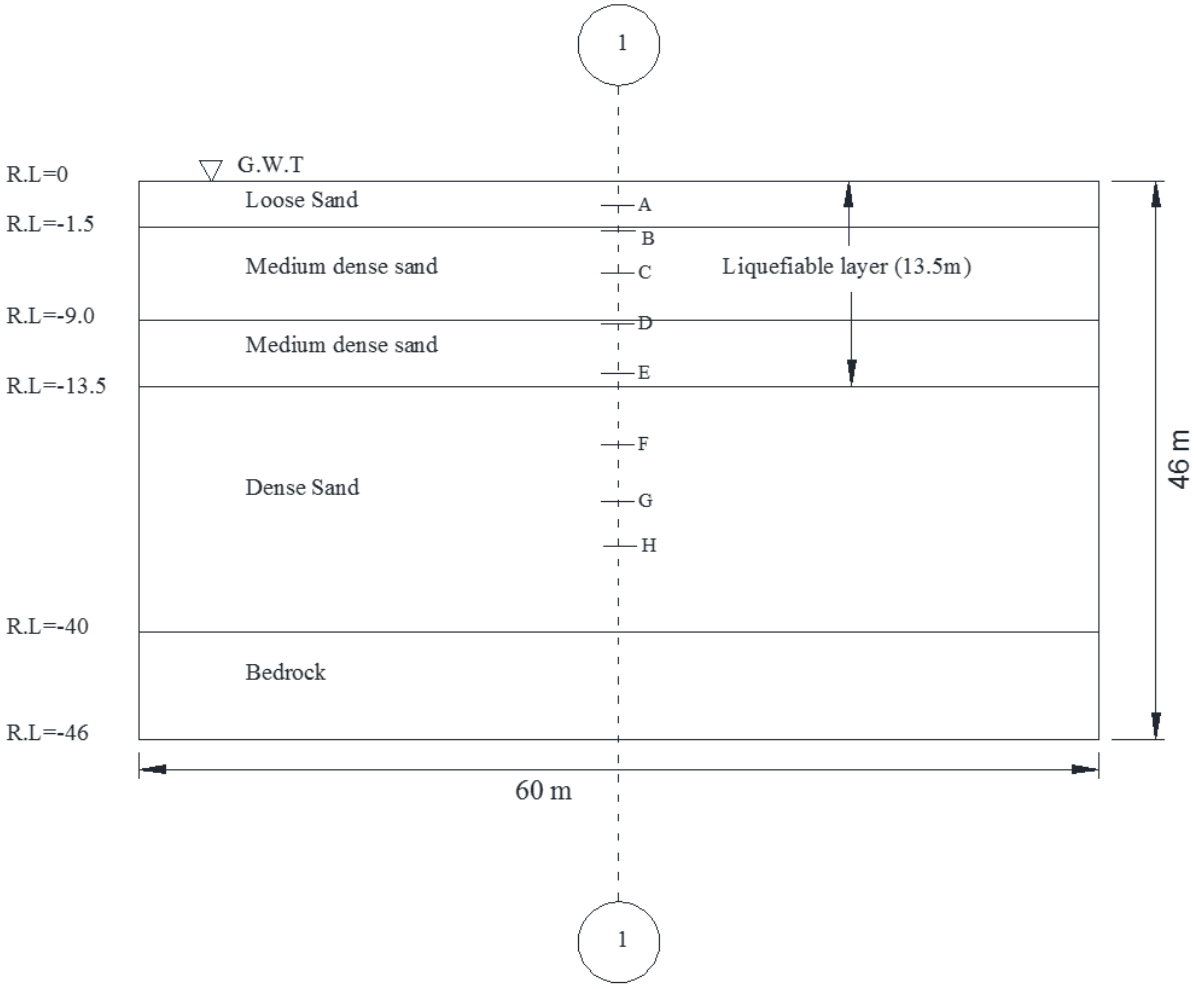

Fig. 4.43 Schematic diagram of MOD5 showing different section and observation points where excess pore pressure parameter calculated

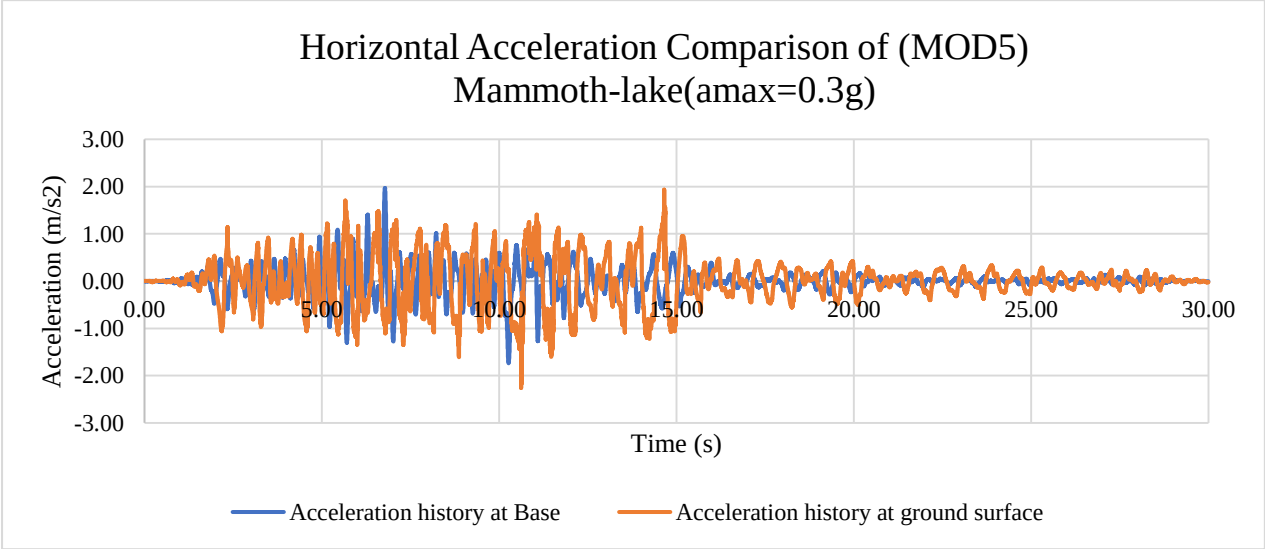

Fig. 4.44 Horizontal Acceleration Comparison of MOD5

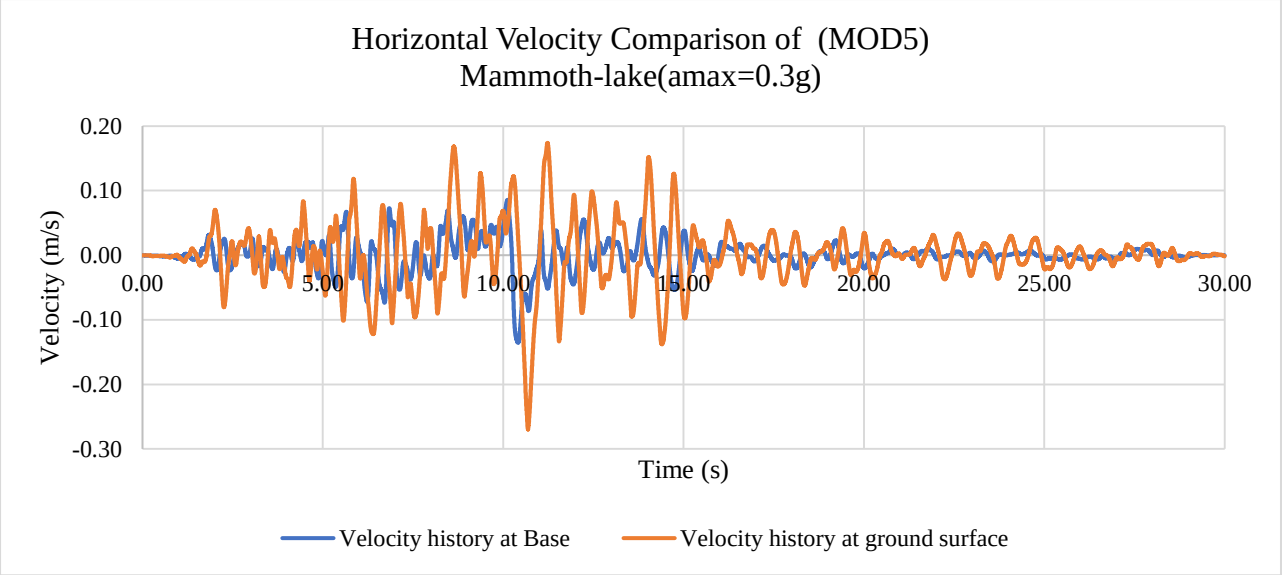

Fig. 4.45 Horizontal Velocity Comparison of MOD5

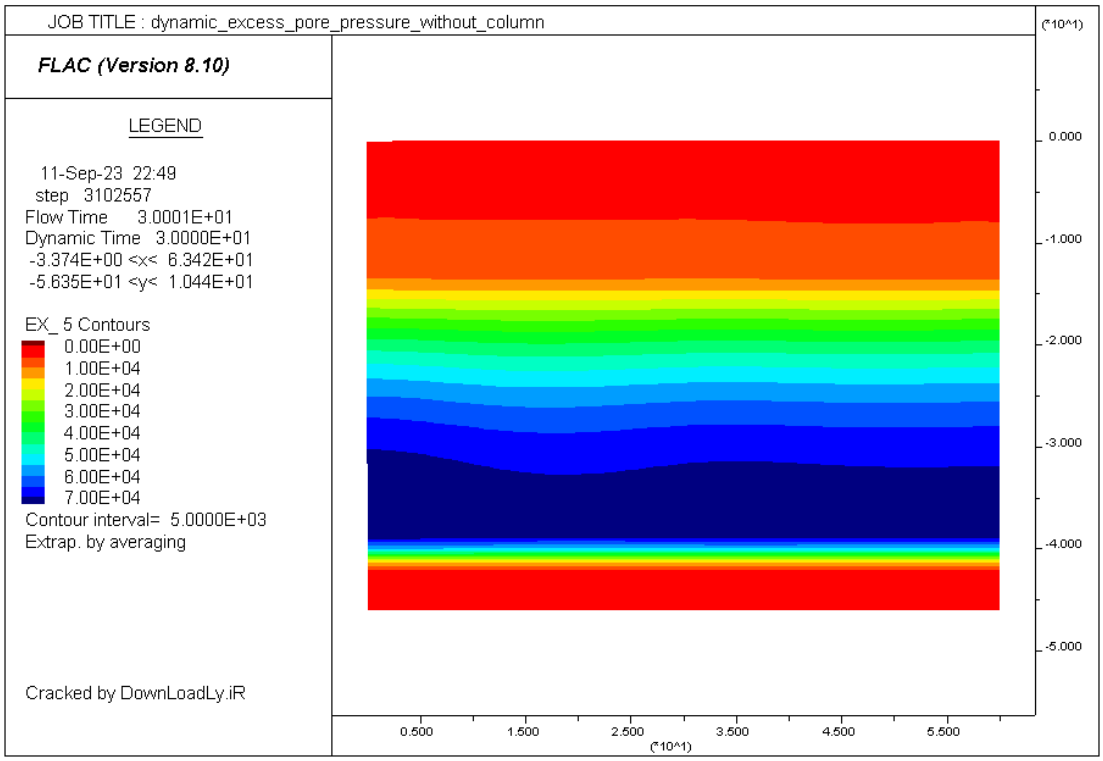

Fig. 4.46 Excess pore water pressure contour (EPWP) at the end of earthquake MOD5

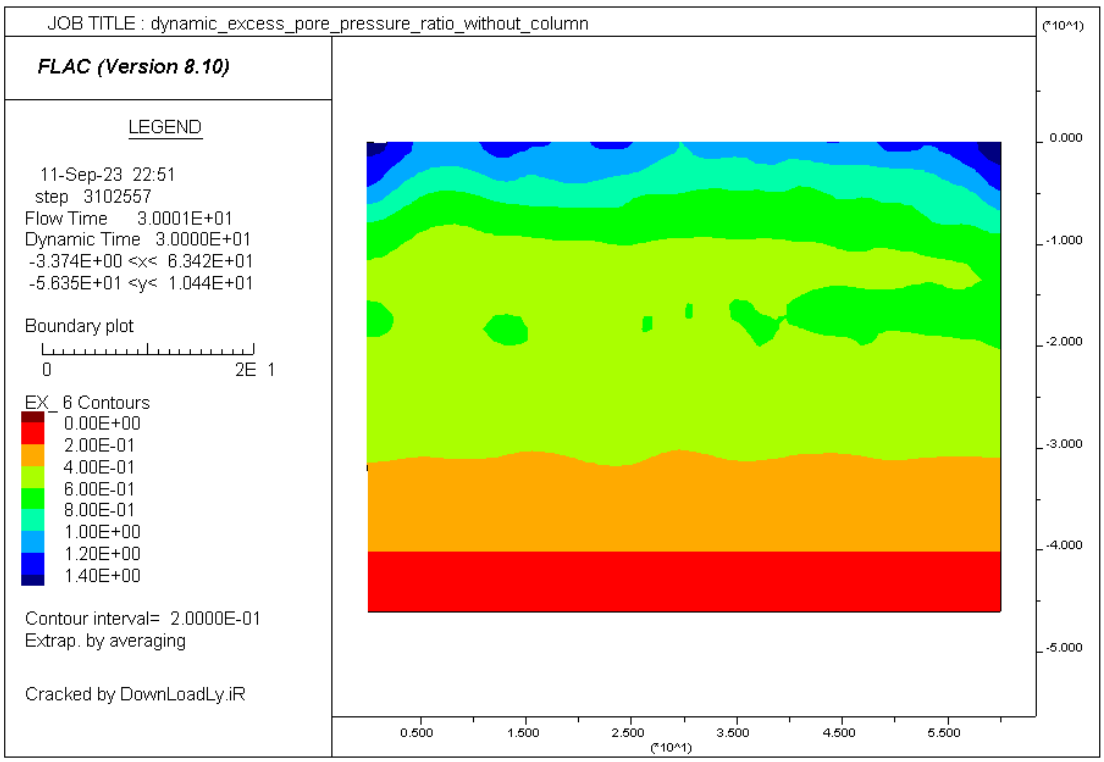

Fig. 4.47 Maximum Excess pore pressure ratio contour MOD5

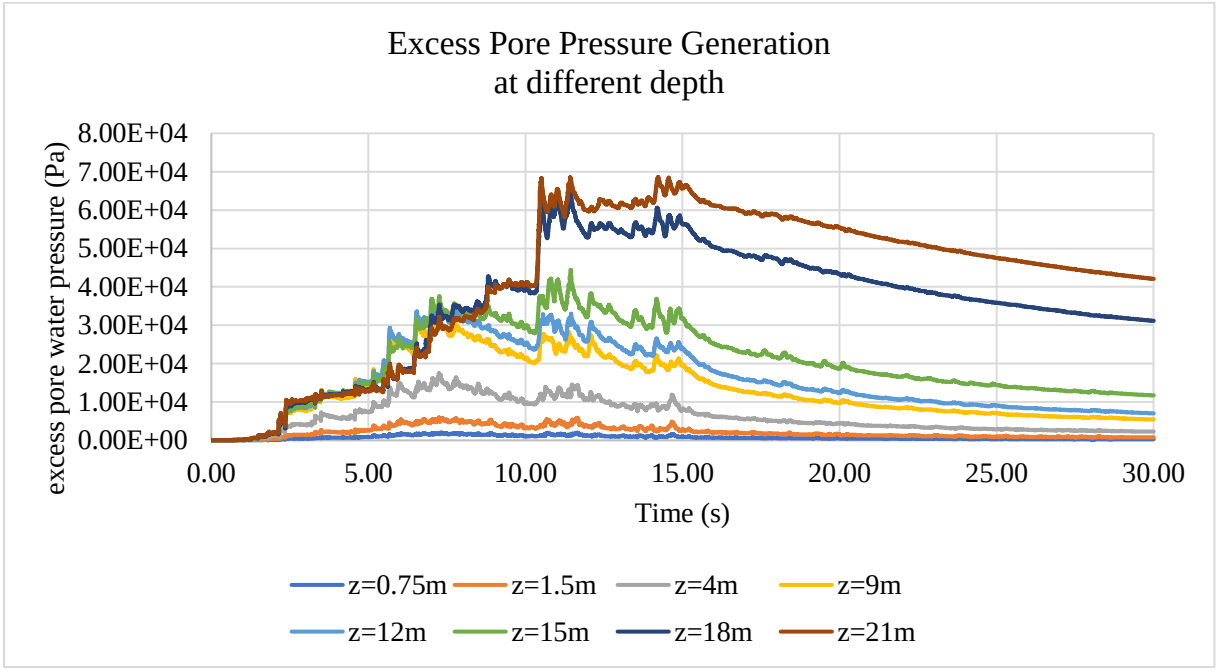

Fig. 4.48 Excess pore water pressure (EPWP) at 1-1 section and different depth (A-H) (without stone column) MOD5

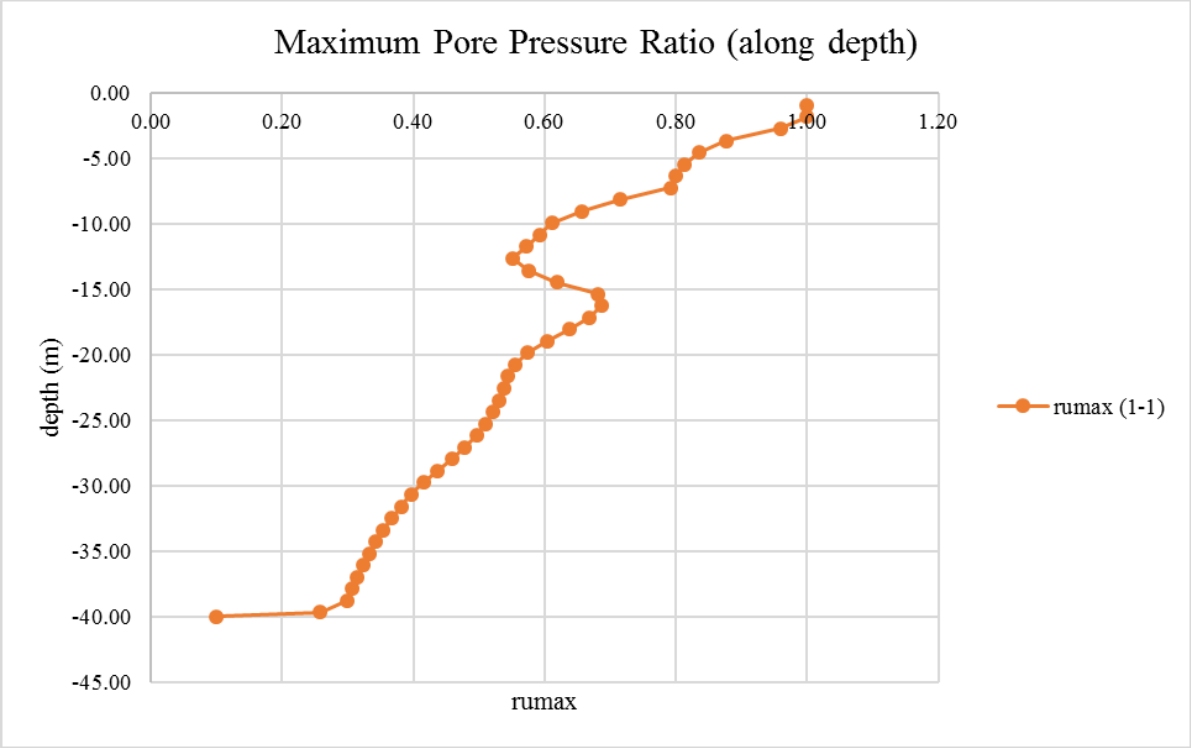

Fig. 4.49 Maximum Excess pore pressure ratio comparison at 1-1 section (without stone column) MOD5

4.2.5.1 Results of dynamic analysis (MOD-5)

In this case model have with-out stone column. Mammoth-lake 0.3g PGA Acceleration is used as a seismic excitation at the base of the model. This simulation is done with flow on condition or couple flow condition as the excess pore pressure is dissipate when stone column is installed on this soil stratification.

In fig. 4.44 and fig 4.45 shows acceleration and velocity comparisons in between at base and ground surface. In both cases we observed that acceleration is amplified at ground surface and velocity is also amplified. Acceleration is amplified 1.3 times and Velocity is amplified by 2.0 times.

Fig. 4.46 showing excess pore pressure contour. The excess pore water pressure (EPWP) is increasing with depth. The EPWP is 70kPa at bottom dense sand. But initially under the sharp acceleration the EPWP is generated at middle layer of depth 9m to 15m depth but latter stage, EPWP is dissipated as flow on condition from top layer but EPWP at bottom layer cant dissipate easily. So, this type of pattern is generated in fig.4.46.

Fig. 4.47 showing the maximum pore pressure ratio, from which we can predict the depth of liquefaction. The depth of liquefaction in this case is on an average 3m to 4m.

Fig. 4.48 showing the excess pore pressure generation at different depth. At depth 0.75m from the ground surface EPWP generation is 2kPa. At depth of 1.5m EPWP generates about 5kPa, At depth of 4m EPWP generates about 17kPa. At depth of 9m EPWP generates about 31kPa,

At depth of 12m EPWP is about 35kPa. At depth of 15m EPWP is about 44.5kPa. At depth of 18m the EPWP is about 62.5kPa. And lastly the EPWP at depth of 21m is about 68.5kPa.

Fig. 4.49 shows maximum pore pressure ratio along the depth at two different section mention in schematic diagram of this model. From this figure it is very clearly that up to the depth of liquefaction is about 3-4m.

4.2.6 [MOD6] With Stone Column (L=5m)– Mammoth-lake (a_{max}=0.3g)

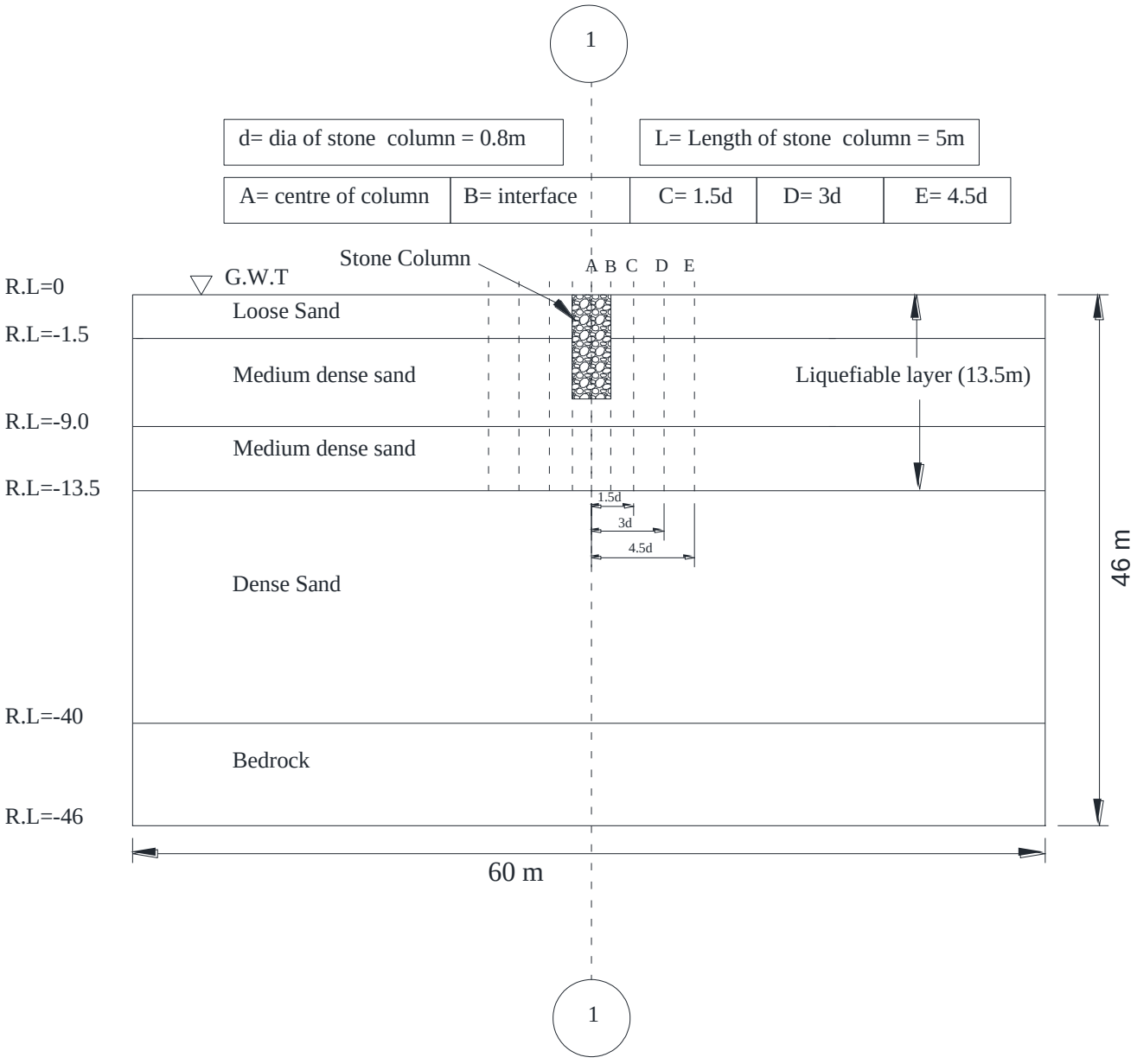

Fig. 4.50 Schematic diagram of MOD6 showing different observation points where excess pore pressure parameter calculated

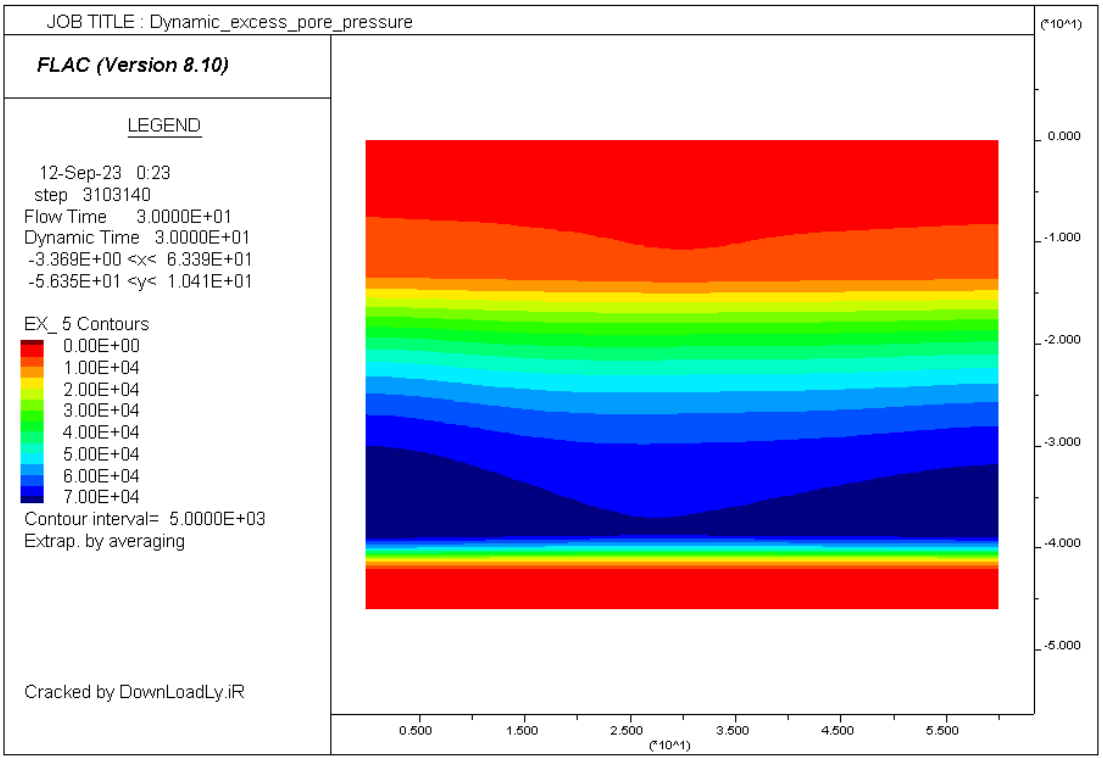

Fig. 4.51 Excess pore water pressure contour (EPWP) at the end of earthquake (with stone column, L=5m)

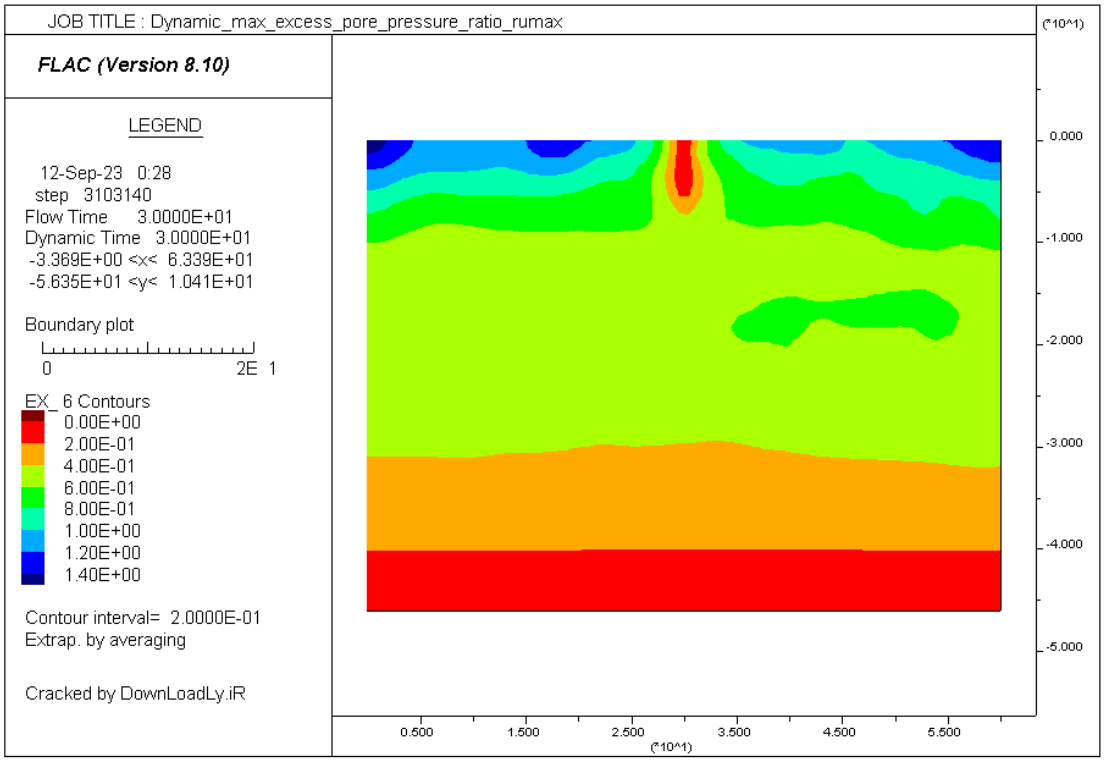

Fig. 4.52 Maximum Excess pore pressure ratio contour (with stone column, L=5m)

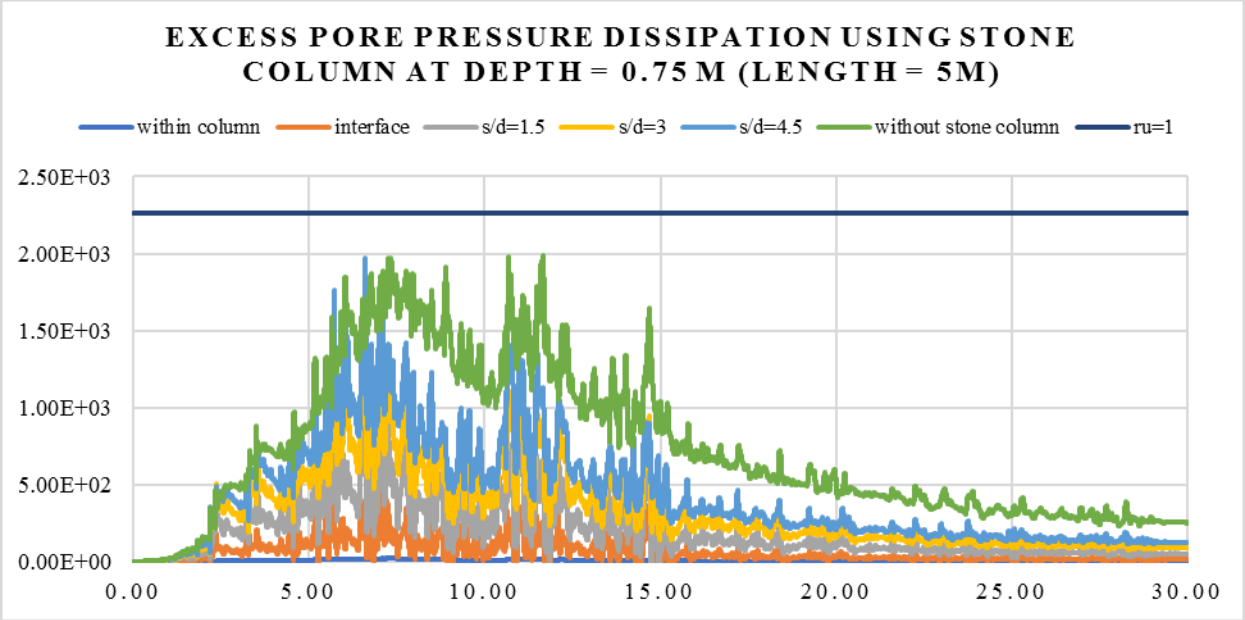

Fig. 4.53 Pore pressure dissipation comparison at lateral distances from center of stone column depth=0.75m from G.L (with stone column, L=5m)

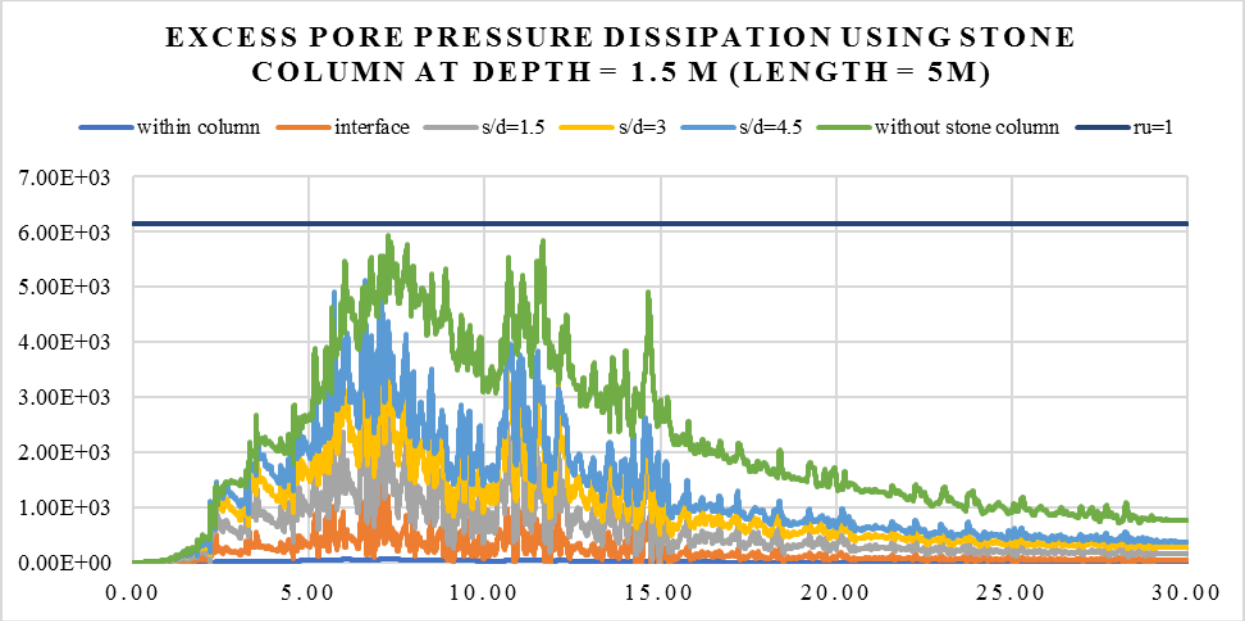

Fig. 4.54 Pore pressure dissipation comparison at lateral distances from center of stone column depth=1.5m from G.L (with stone column, L=5m)

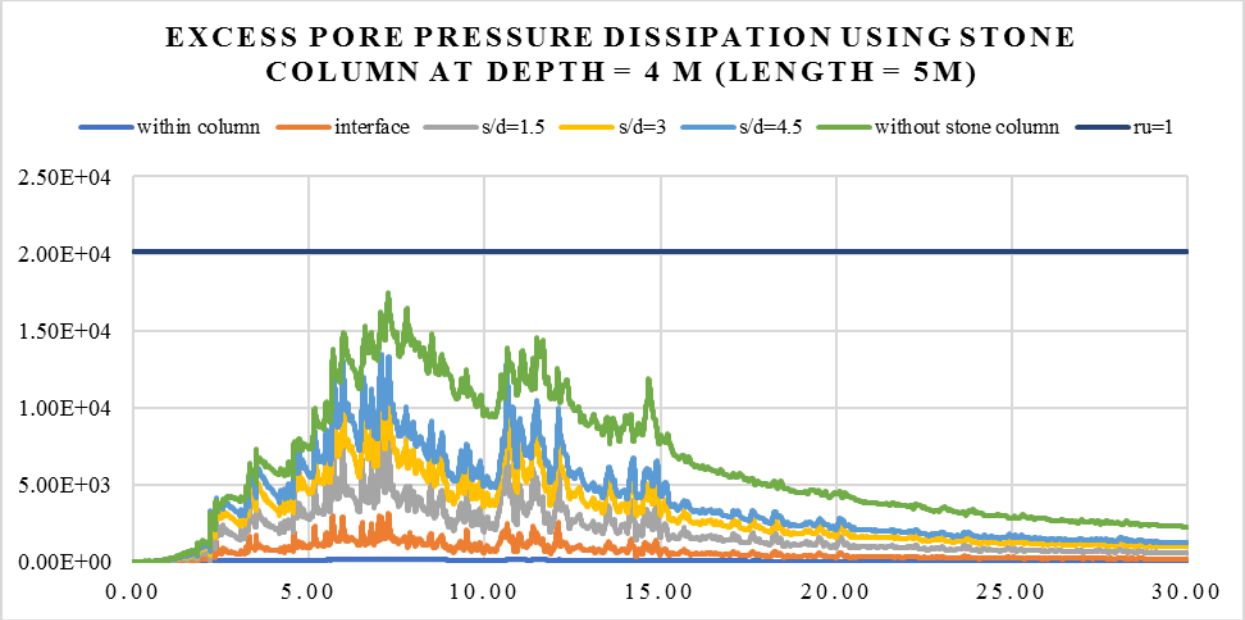

Fig. 4.55 Pore pressure dissipation comparison at lateral distance from center of stone column depth=4m from G.L (with stone column, L=5m)

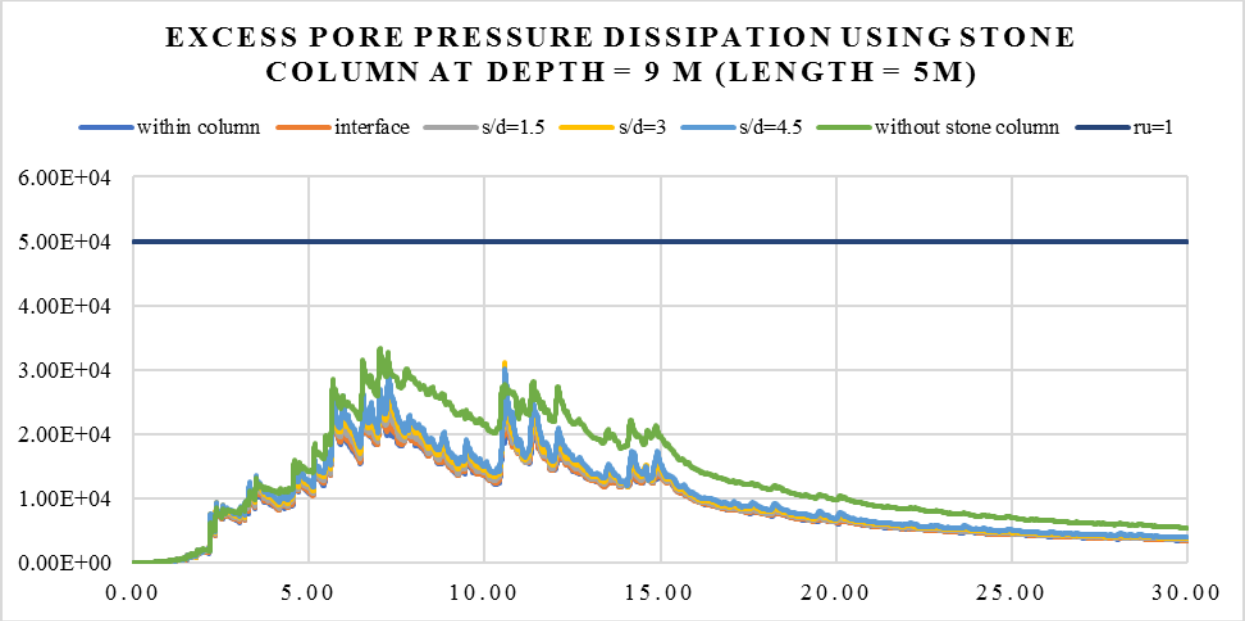

Fig. 4.56 Pore pressure dissipation comparison at lateral distance from center of stone column depth=9m from G.L (with stone column, L=5m)

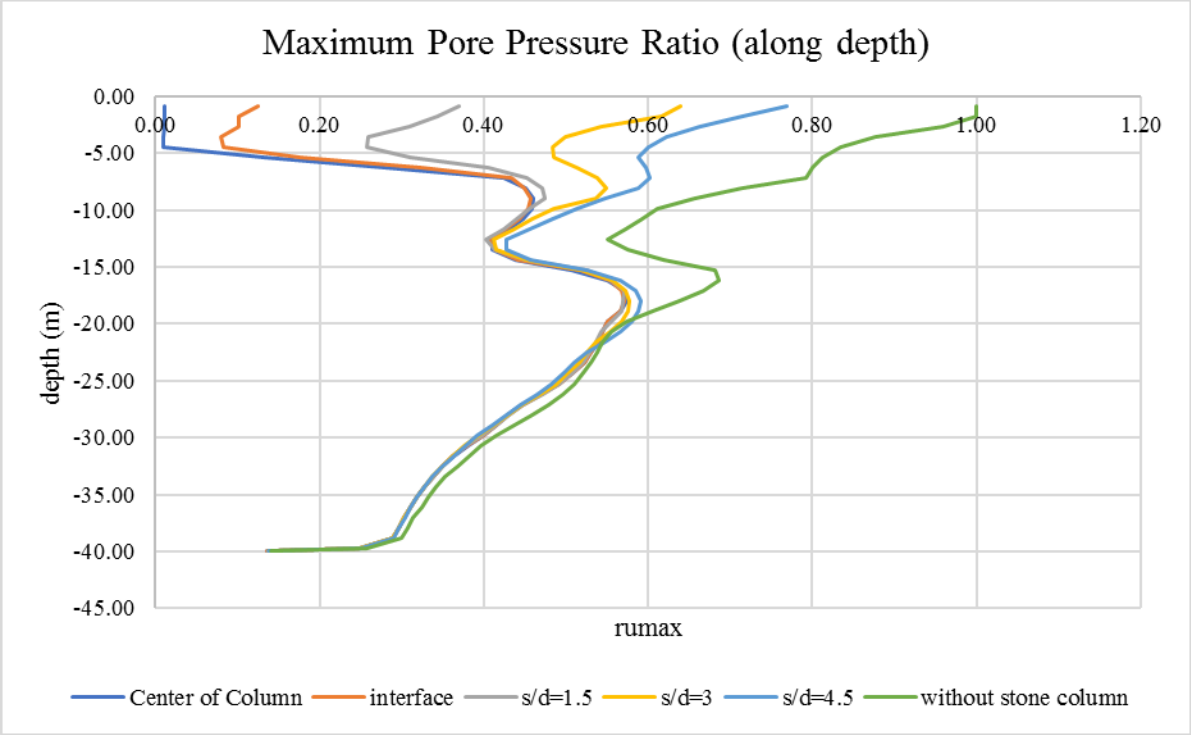

Fig. 4.57 Maximum Excess pore pressure ratio along with depth comparison at different lateral distance (with stone column, L=5m)

4.2.6.1 Discussion on Results of dynamic analysis (MOD-6)

In this case, model have stone column of length 5m shown in the schematic diagram. Mammoth-lake 0.3g PGA Acceleration is used as a seismic excitation at the base of the model. This simulation is done with flow on condition or couple flow condition as the excess pore pressure is dissipate by the stone column on this soil stratification.

Fig. 4.51 showing excess pore pressure contour. The excess pore water pressure (EPWP) is increasing with depth. The EPWP is 70kPa at bottom dense sand. But initially under the sharp acceleration the EPWP is generated at middle layer of depth 9m to 15m depth but latter stage, EPWP is dissipated as flow on condition from top layer but EPWP at bottom layer cant dissipate easily. So, this type of pattern is generated in fig.4.51.

Fig. 4.52 showing the pore pressure ratio is reduce around the column and up to a depth of 5-6 m from ground level. As In this model stone column length used is 5m.

Fig. 4.53 showing the comparison result of excess pore pressure with stone column of length 5m and without stone column. At depth of 0.75m, without stone column case EPWP was 2kPa. But when stone column is used, at depth of 0.75m from ground level, Excess pore water pressure at the center of stone column is negligible (20Pa) because stone column have very high permeability, so when water from the surrounding reach just the column, instantly dissipated. At interface EPWP reached 0.5kPa. And at a distance 1.2 m distance from center indicated as s/d =1.5 or distance of 1.5 times diameter of stone column, EPWP is reach 1.2 kPa. And at s/d=3.0, EPWP is reach 1.6 kPa. So, we observed, at first three distances stone

column worked properly (i.e. with center of column, interface, and s/d=1.5). But after s/d=1.5 m, excess pore pressure is not as dissipated as compare to the other cases, and excess pore pressure reached closed to 1.

Similarly, Fig. 4.54 and Fig. 4.55 showing similar pattern as Fig. 4.53, stone column of length 5 m dissipates excess pore water pressure up to a distance of 1.5d from the center of column. But in case fig.4.56, at depth 9m stone column not worked as stone column is a length of 5m only. Even liquefaction is not reached at that depth (9m form ground surface).

Fig. 4.57 shows maximum pore pressure ratio along the depth at various lateral distance from the center of stone column. From this figure it is very clearly that up to the distance of 1.5d distance from centre of column stone column dissipates EPWP effectively and mitigates liquefaction.

4.2.7 [MOD7] With Stone Column (L=10m)– Mammoth-lake (a_{max}=0.3g)

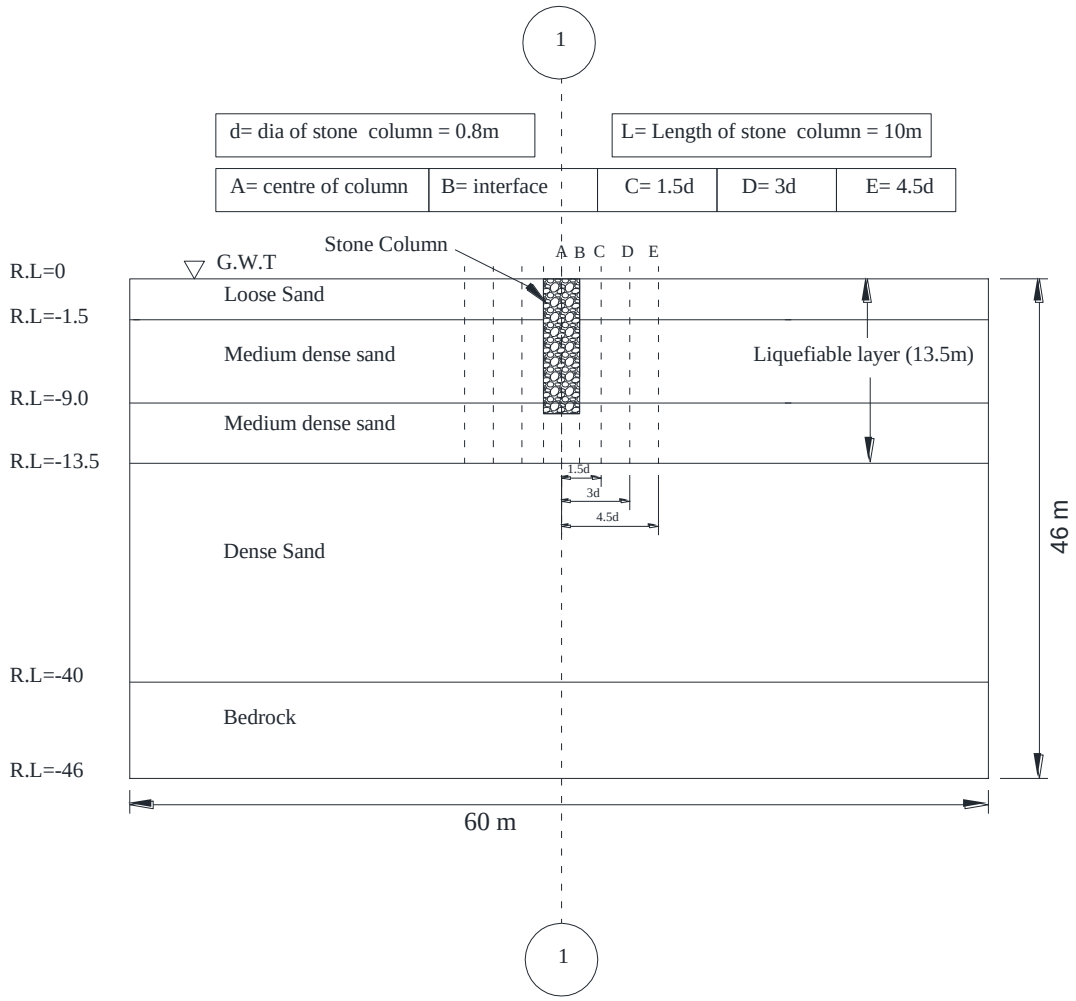

Fig. 4.58 Schematic diagram of MOD7 showing different observation points where excess pore pressure parameter calculated

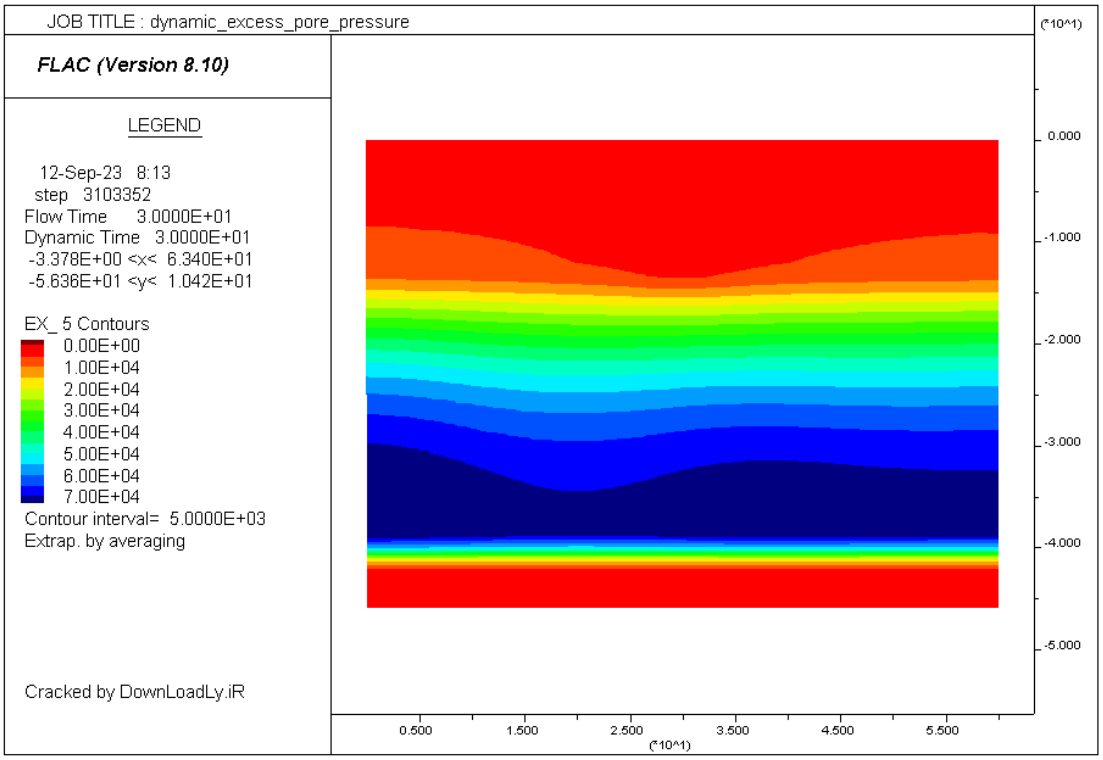

Fig. 4.59 Excess pore water pressure contour (EPWP) at the end of earthquake (with stone column, L=10m)

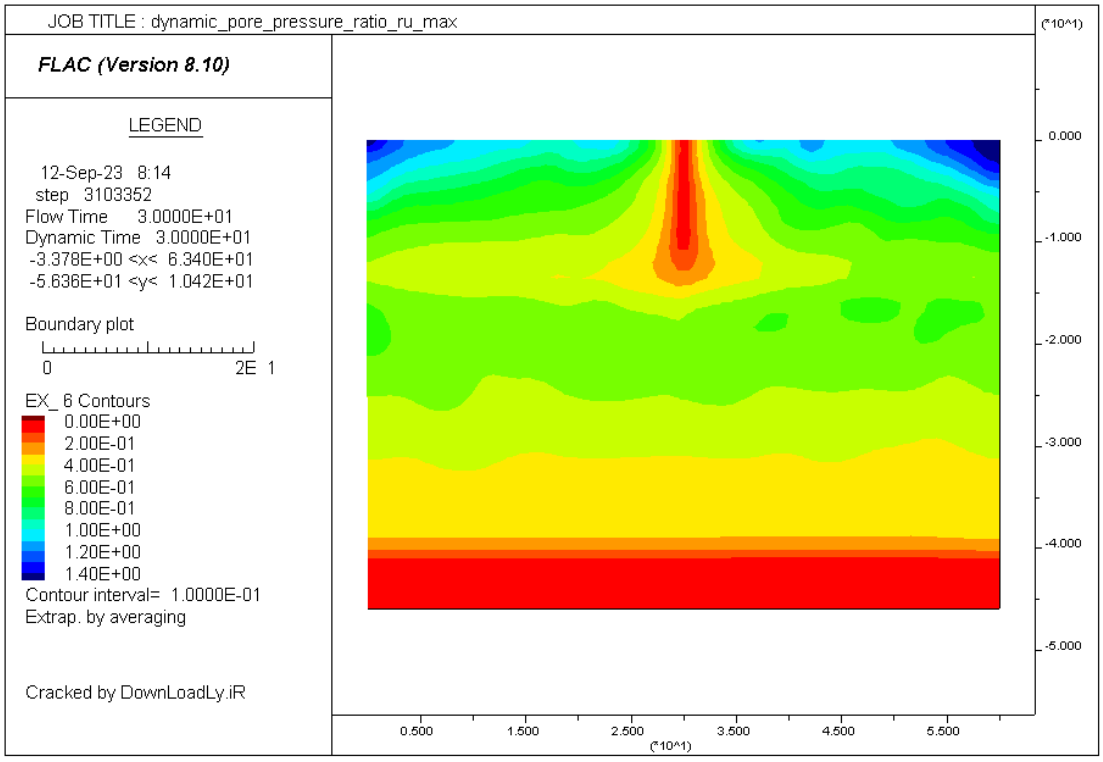

Fig. 4.60 Maximum Excess pore pressure ratio contour (with stone column, L=10m)

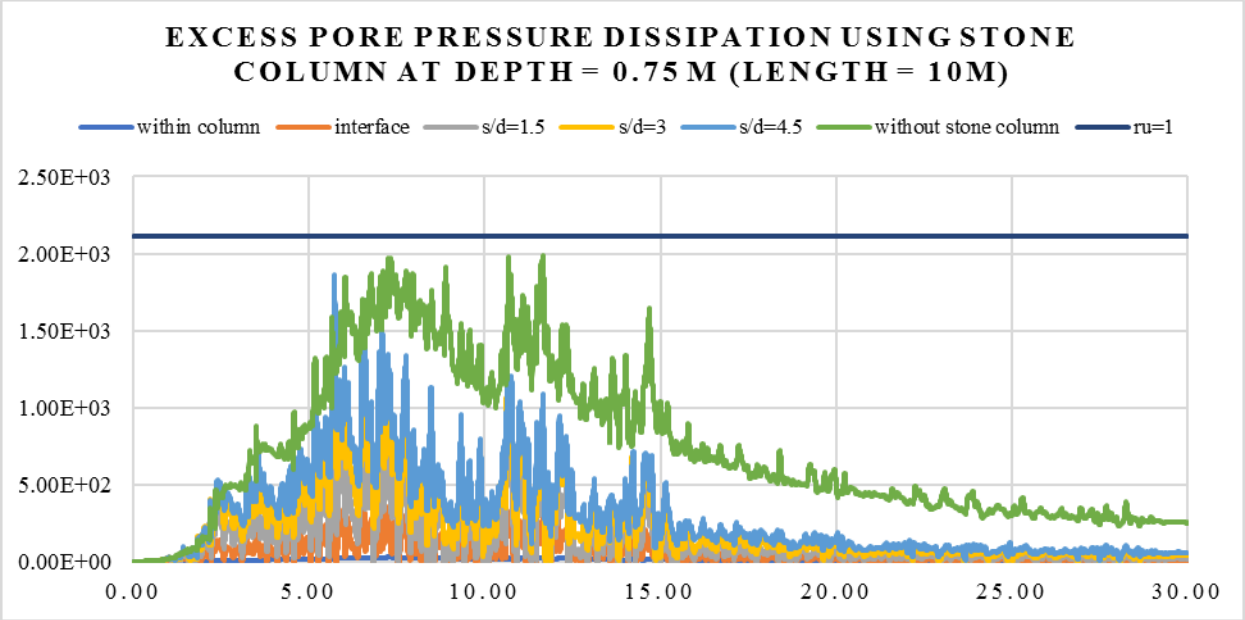

Fig. 4.61 Pore pressure dissipation comparison at lateral distance from center of stone column depth=0.75 m from G.L (with stone column, L=10m)

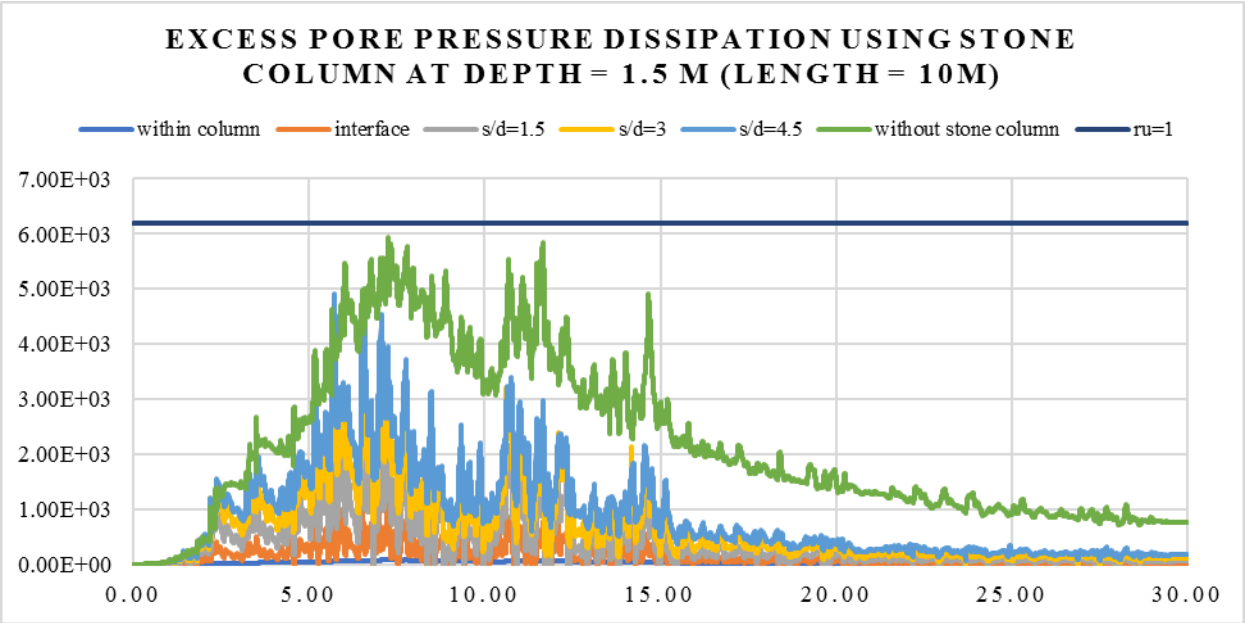

Fig. 4.62 Pore pressure dissipation comparison at lateral distance from center of stone column depth=1.5 m from G.L (with stone column, L=10m)

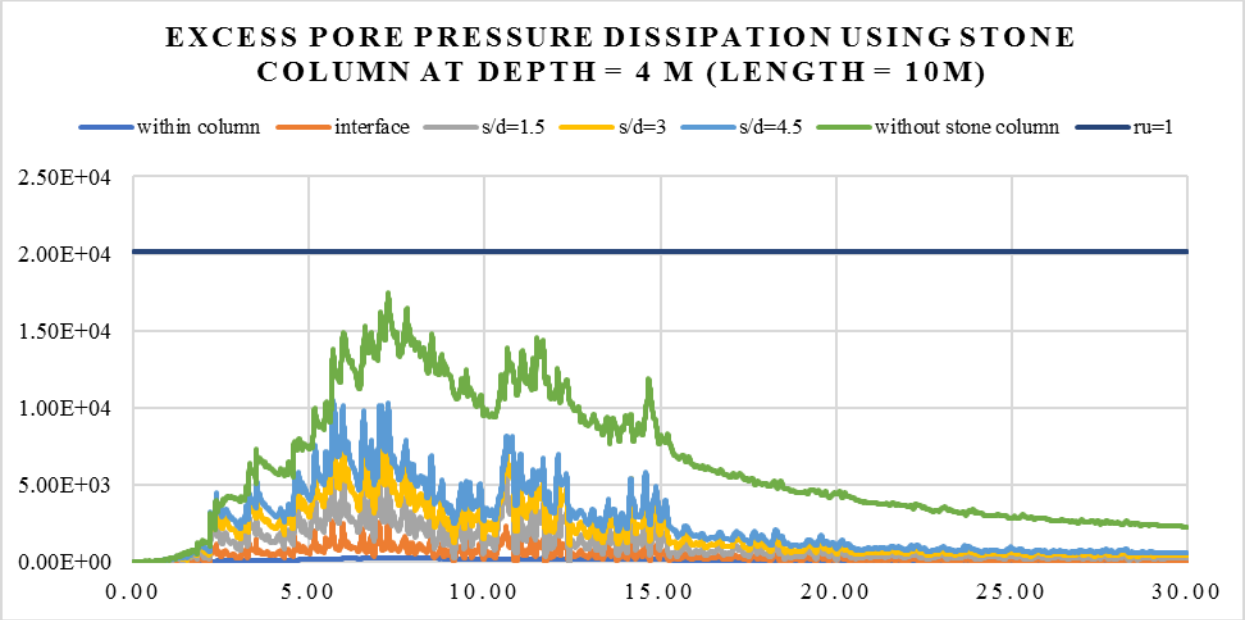

Fig. 4.63 Pore pressure dissipation comparison at lateral distance from center of stone column depth=4 m from G.L (with stone column, L=10m)

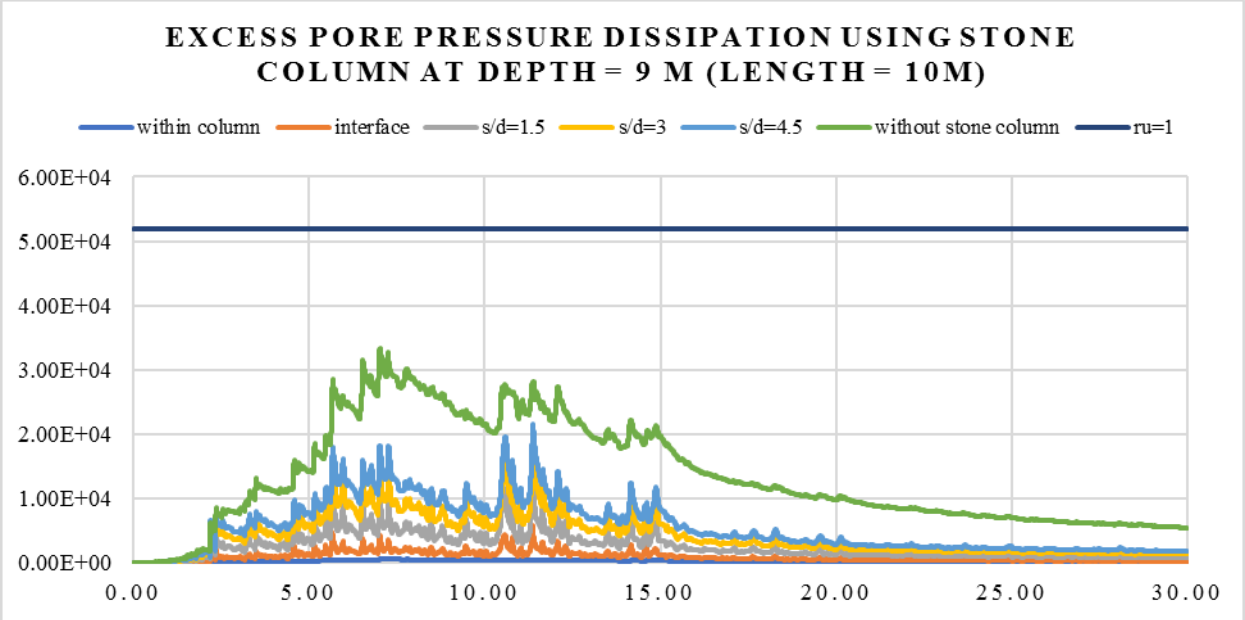

Fig. 4.64 Pore pressure dissipation comparison at lateral distance from center of stone column depth=9 m from G.L (with stone column, L=10m)

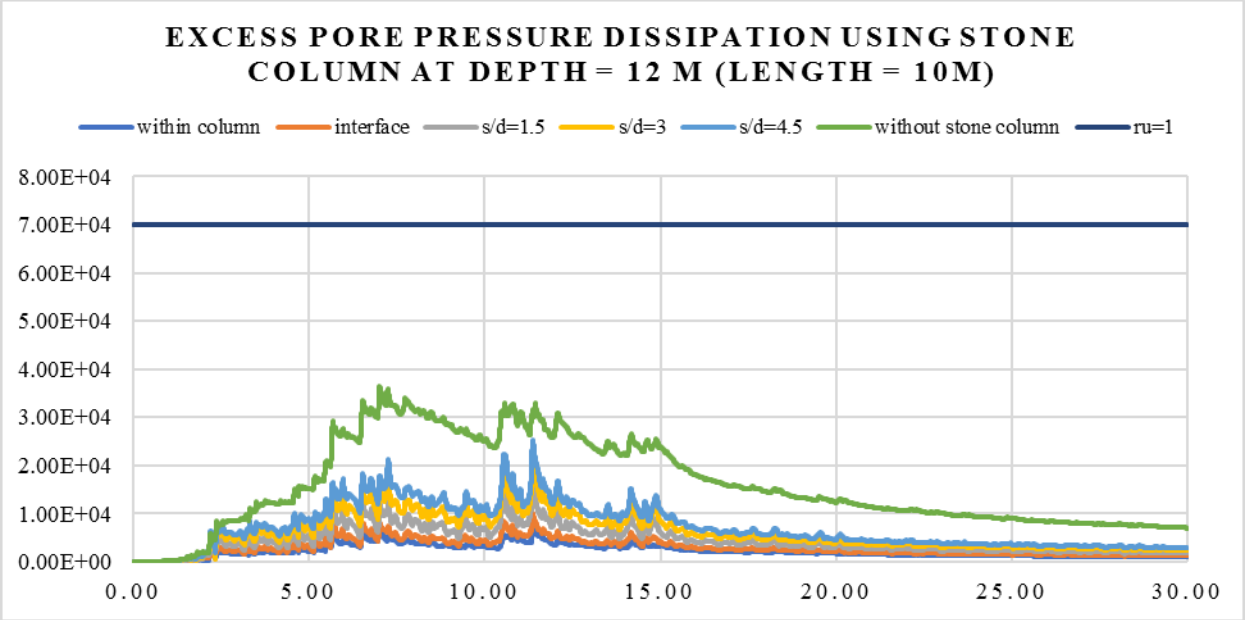

Fig. 4.65 Pore pressure dissipation comparison at lateral distance from center of stone column depth=12 m from G.L (with stone column, L=10m)

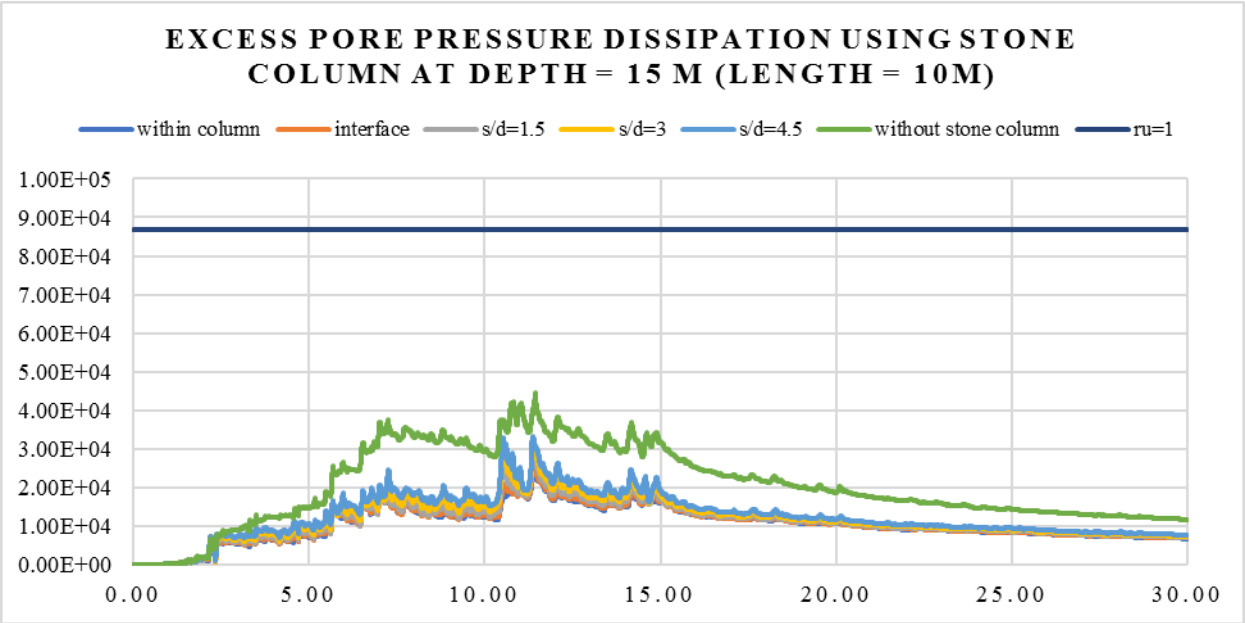

Fig. 4.66 Pore pressure dissipation comparison at lateral distance from center of stone column depth=15 m from G.L (with stone column, L=10m)

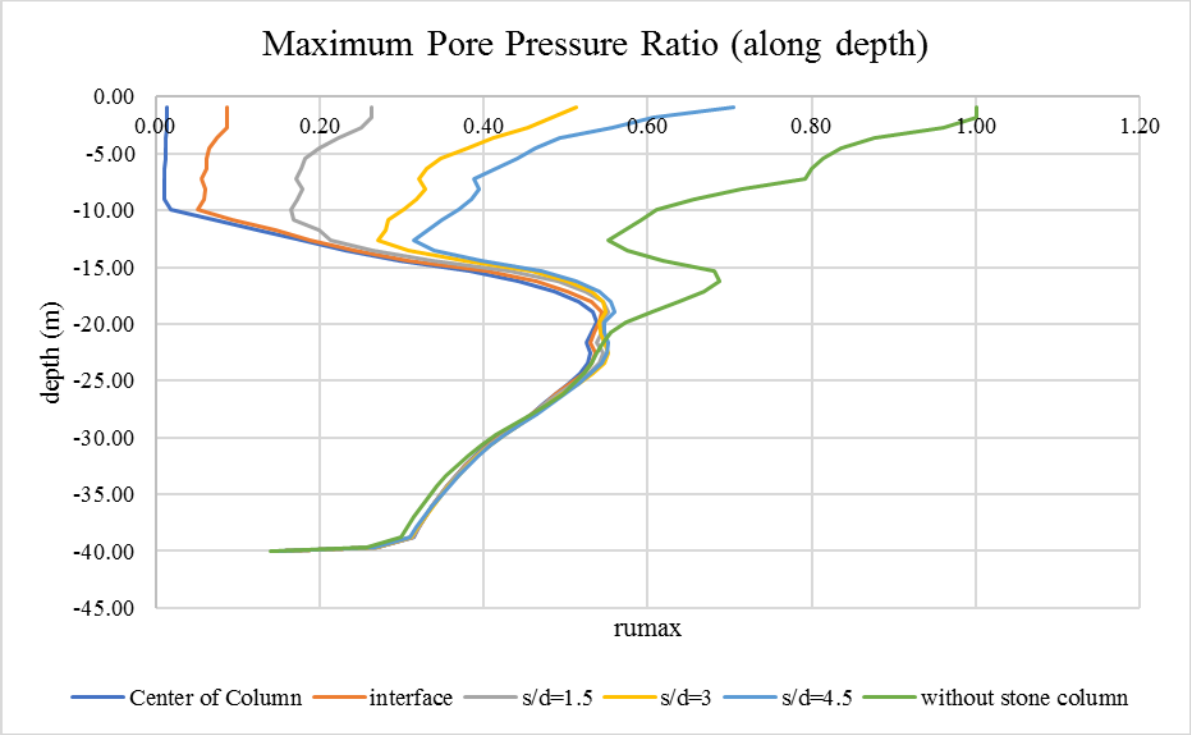

Fig. 4.67 Maximum Excess pore pressure ratio along with depth comparison at different lateral distance (with stone column, L=10m)

4.2.7.1 Discussion on Results of dynamic analysis (MOD-7)

In this case, model have stone column of length 10m shown in the schematic diagram. Mammoth-lake 0.3g PGA Acceleration is used as a seismic excitation at the base of the model. This simulation is done with flow on condition or couple flow condition as the excess pore pressure is dissipate by the stone column on this soil stratification.

Fig. 4.59 showing excess pore pressure contour. The excess pore water pressure (EPWP) is increasing with depth. The EPWP is 70kPa at bottom dense sand. But initially under the sharp acceleration the EPWP is generated at middle layer of depth 9m to 15m depth but latter stage, EPWP is dissipated as flow on condition from top layer but EPWP at bottom layer can't dissipate easily. So, this type of pattern is generated in fig.4.59.

Fig. 4.60 showing the pore pressure ratio is reduce around the column and up to a depth of 10-13 m from ground level. As In this model stone column length used is 10 m.

Fig. 4.62 showing the comparison result of excess pore pressure with stone column of length 10m and without stone column. At depth of 1.5 m, without stone column case EPWP was 5kPa. But when stone column is used, at depth of 1.5 m from ground level, Excess pore water pressure at the center of stone column is negligible (90Pa) because stone column have very high permeability, so when water from the surrounding reach just the column, instantly dissipated. At interface EPWP reached 1.1kPa. And at a distance 1.2 m distance from center indicated as s/d =1.5 or distance of 1.5 times diameter of stone column, EPWP is reach 2.8 kPa. And at s/d=3.0, EPWP is reach 4 kPa. So, we observed, at first three distances stone column worked properly (i.e. with center of column, interface, and s/d=1.5). But after s/d=1.5

m, excess pore pressure is not as dissipated as compare to the other cases, and excess pore pressure reached closed to 1.

Similarly, Fig. 4.61, Fig. 4.62, Fig.4.63, Fig.4.64 and Fig. 4.65 showing similar pattern as Fig. 4.62, stone column of length 10 m dissipates excess pore water pressure up to a distance of 1.5d from the center of column. But in case fig.4.66, at depth 15m stone column not worked as stone column is a length of 10m only. Even liquefaction is not reached at that depth (15m form ground surface).

Fig. 4.67 shows maximum pore pressure ratio along the depth at various lateral distance from the center of stone column. From this figure it is very clearly that up to the distance of 1.5d distance from center of column stone column dissipates EPWP effectively and mitigates liquefaction.

4.2.8 [MOD6] With Stone Column (L=15m)–Mammoth-lake(a_{max}=0.3g)

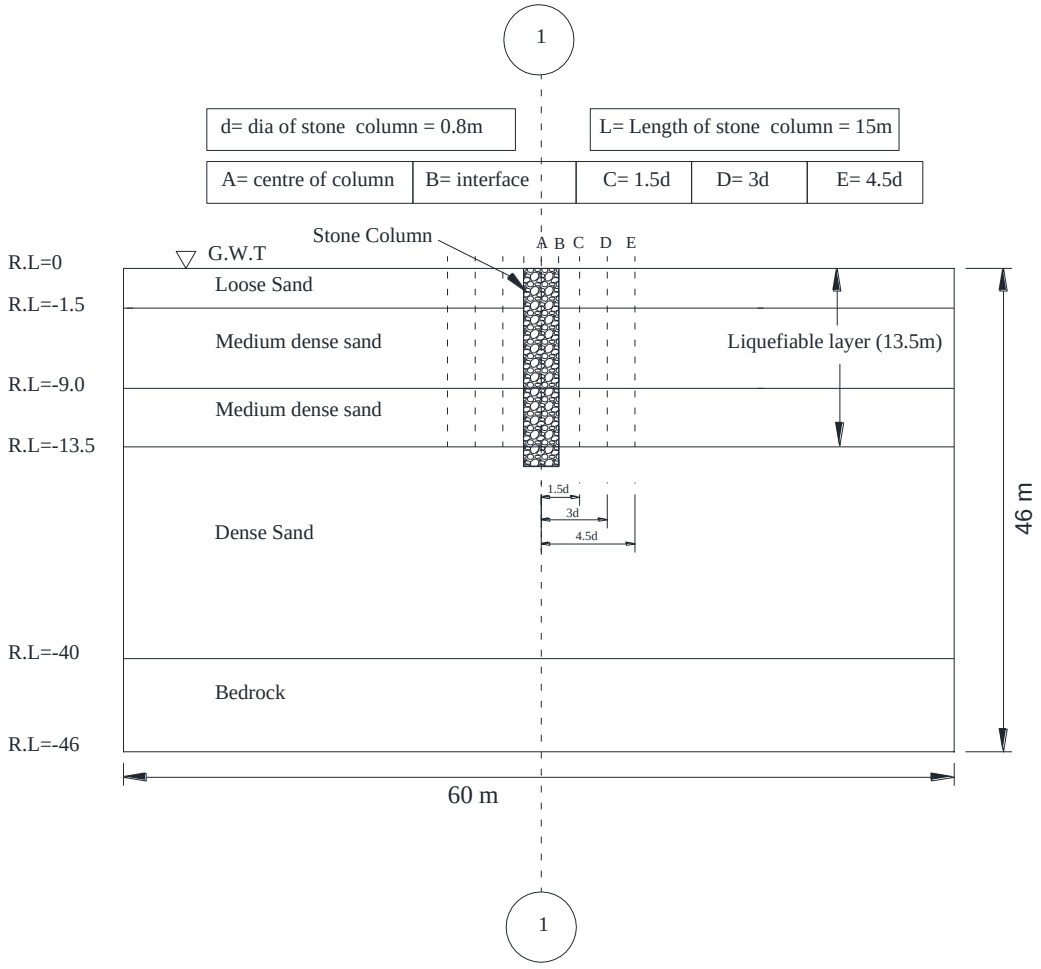

Fig. 4.68 Schematic diagram of MOD8 showing different observation points where excess pore pressure parameter calculated

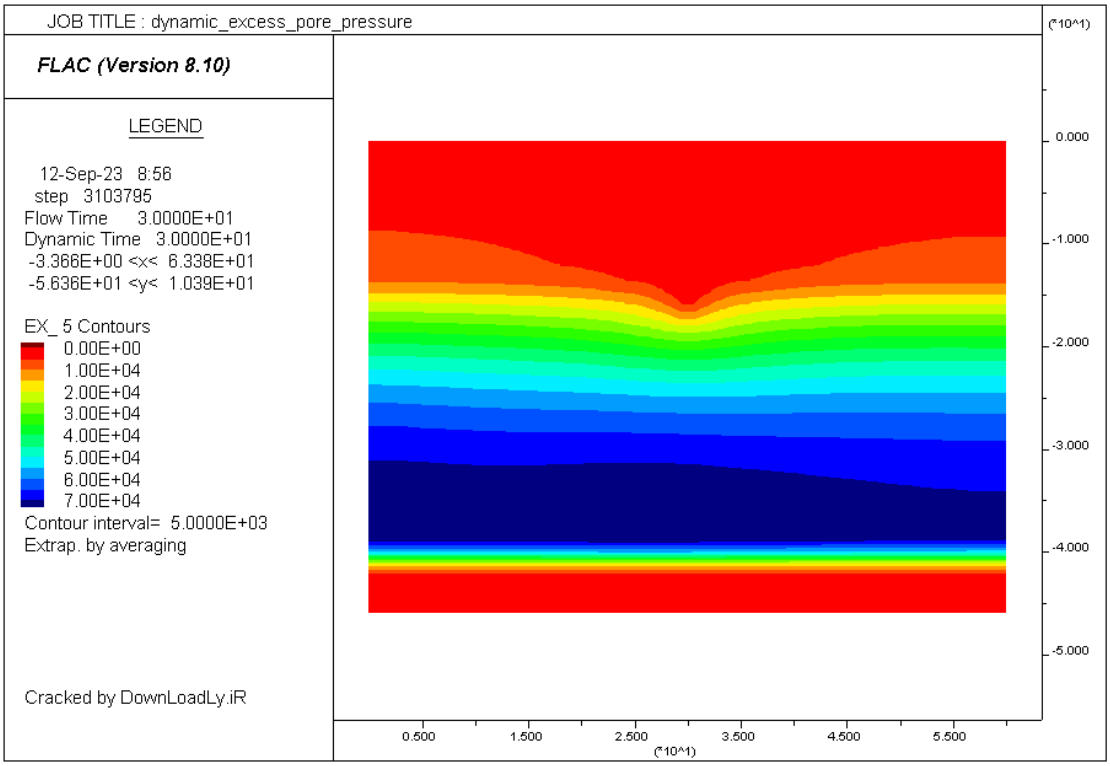

Fig. 4.69 Excess pore water pressure contour (EPWP) at the end of earthquake (with stone column, L=15m)

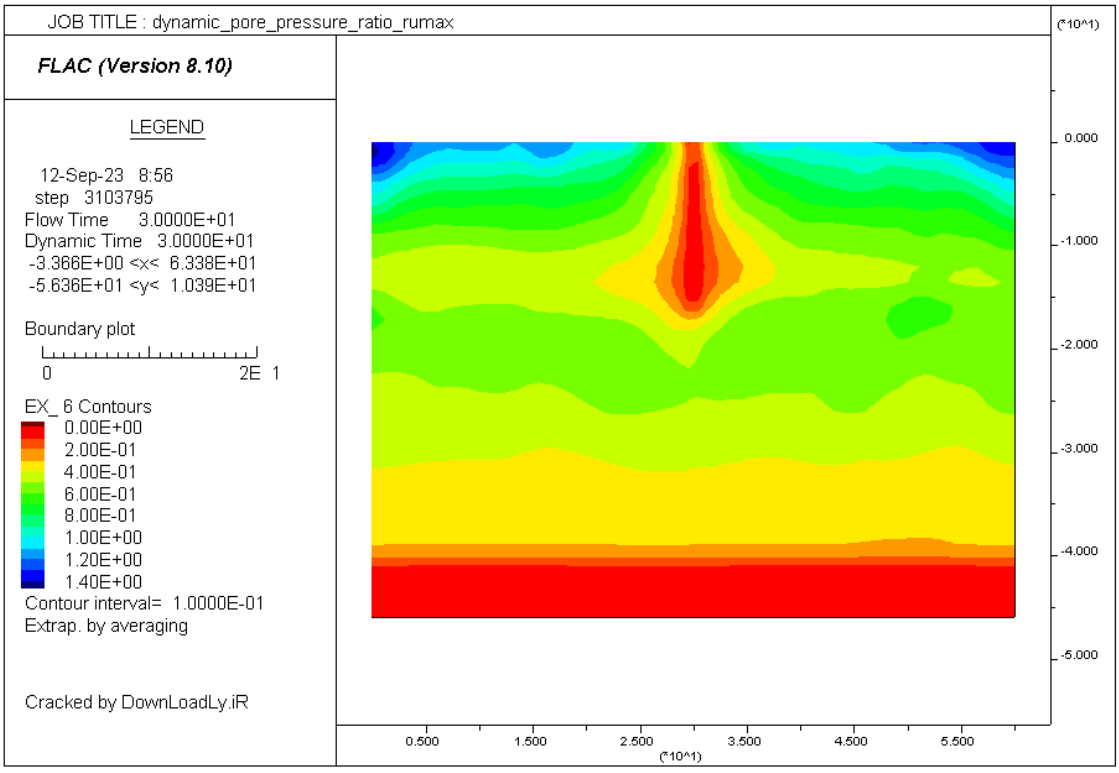

Fig. 4.70 Maximum Excess pore pressure ratio contour (with stone column, L=15m)

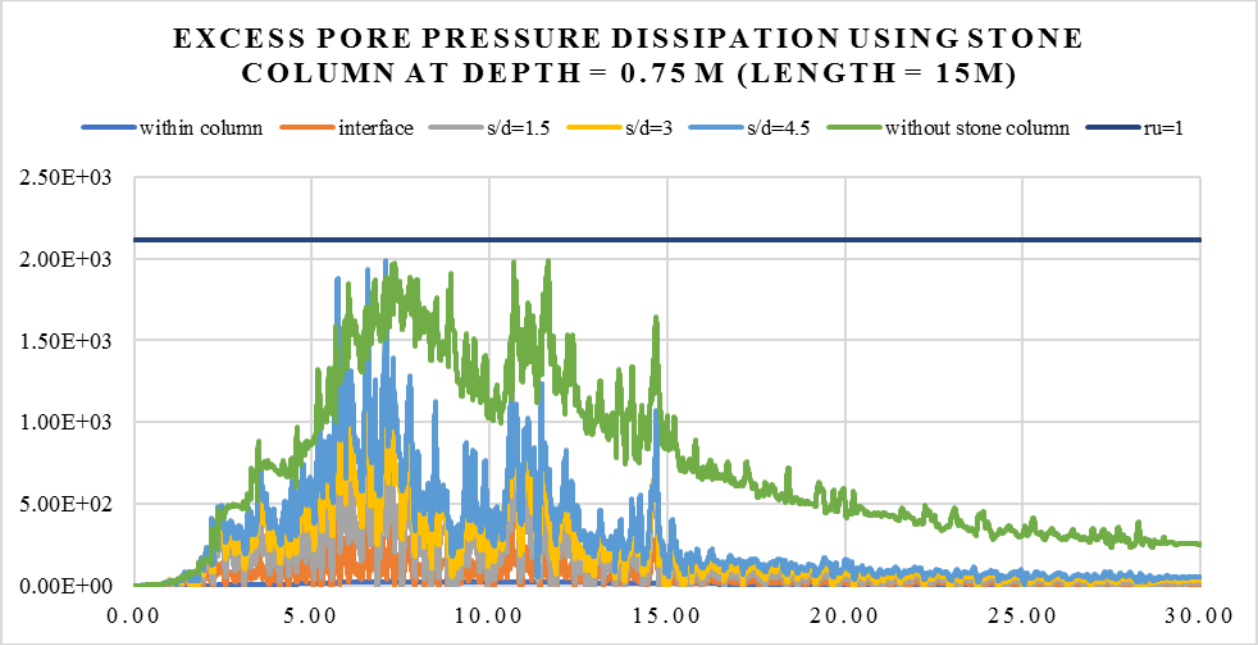

Fig. 4.71 Pore pressure dissipation comparison at lateral distance from center of stone column depth=0.75m from G.L (with stone column, L=15m)

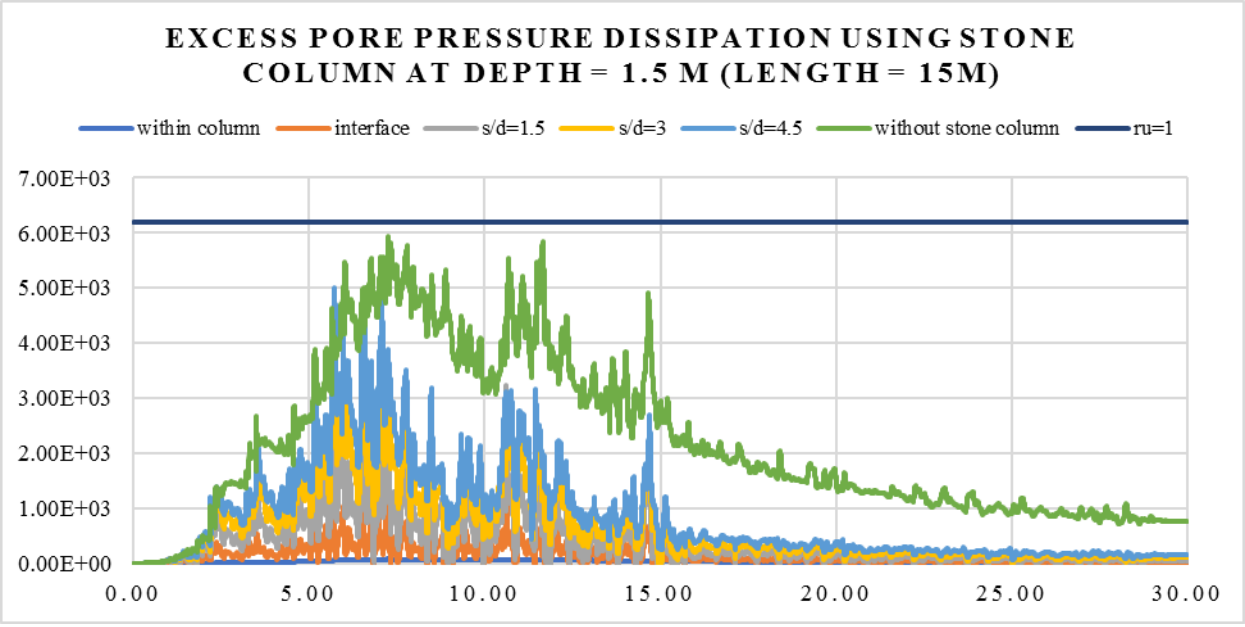

Fig. 4.72 Pore pressure dissipation comparison at lateral distance from center of stone column depth=1.5m from G.L (with stone column, L=15m)

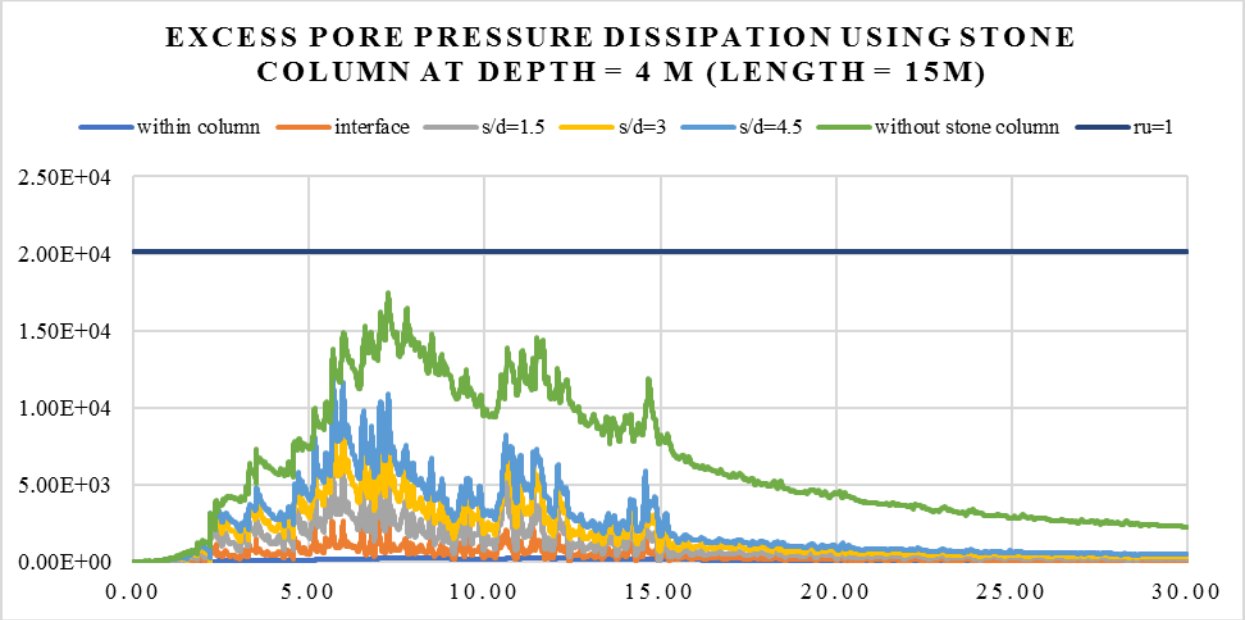

Fig. 4.73 Pore pressure dissipation comparison at lateral distance from center of stone column depth=4m from G.L (with stone column, L=15m)

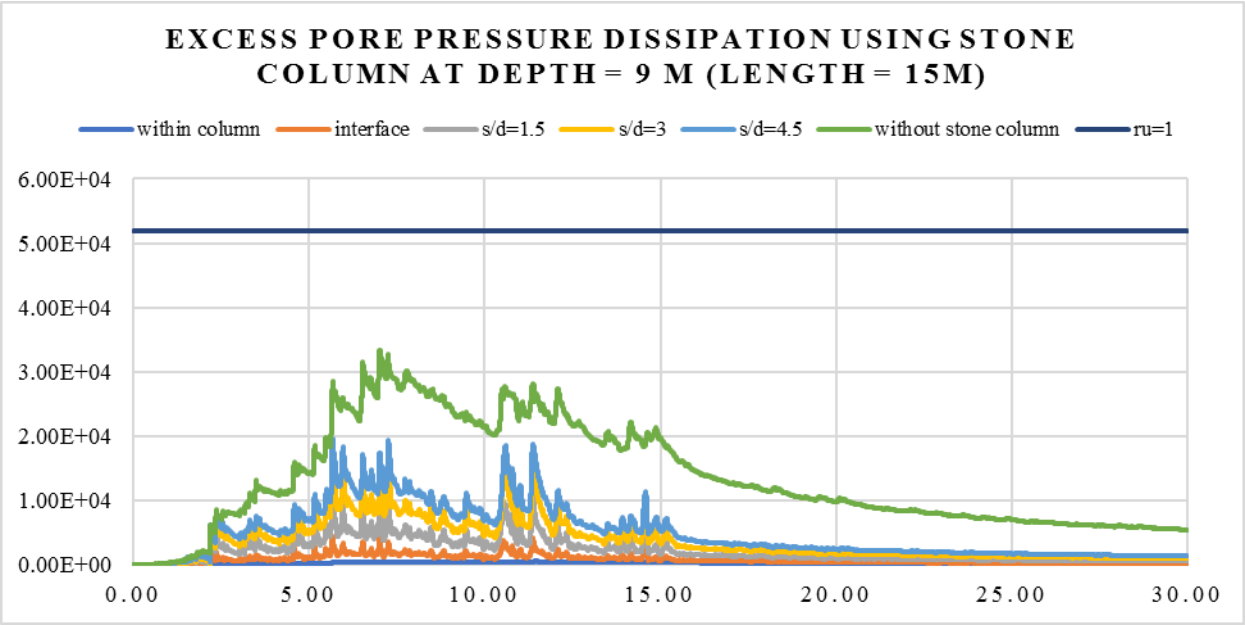

Fig. 4.74 Pore pressure dissipation comparison at lateral distance from center of stone column depth=9m from G.L (with stone column, L=15m)

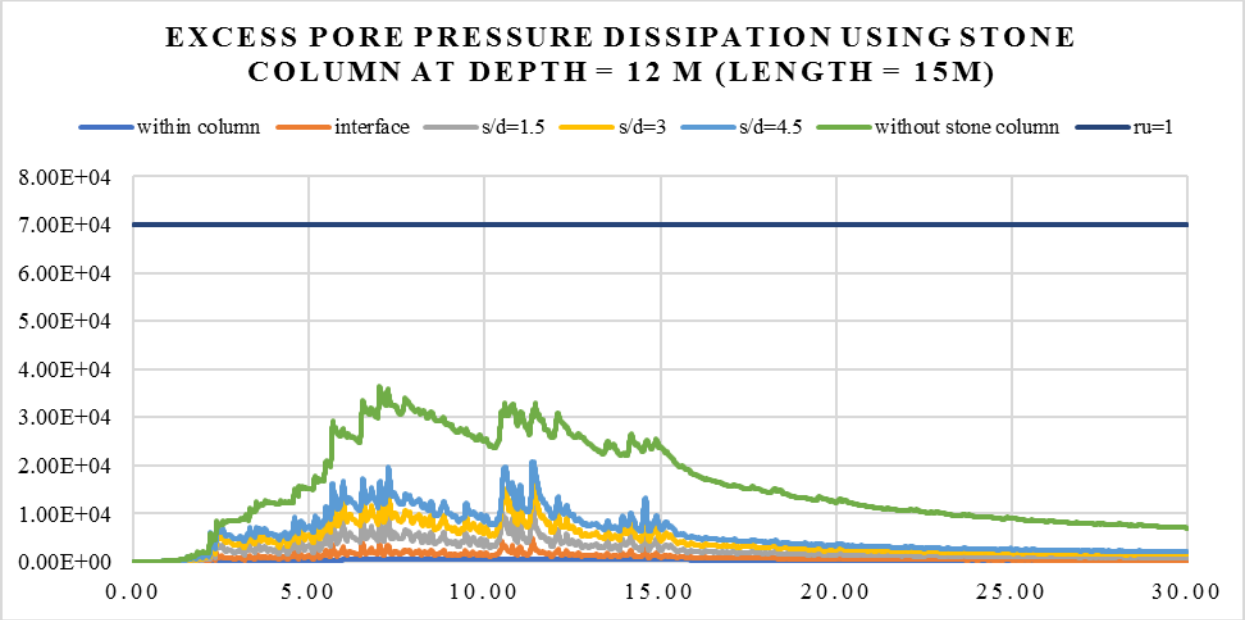

Fig. 4.75 Pore pressure dissipation comparison at lateral distance from center of stone column depth=12m from G.L (with stone column, L=15m)

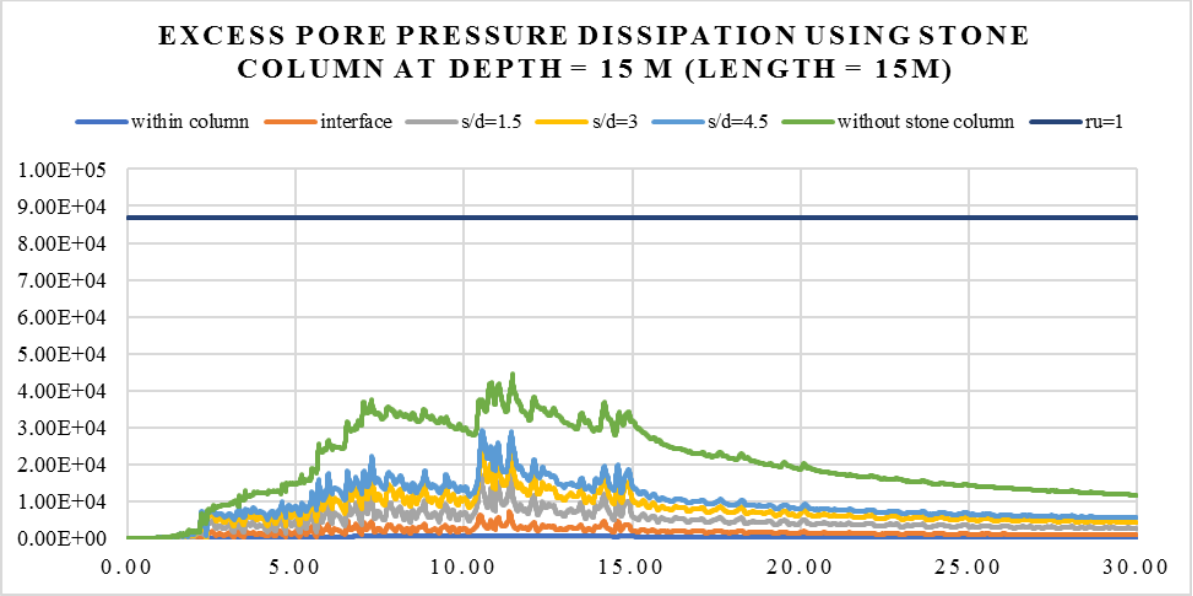

Fig. 4.76 Pore pressure dissipation comparison at lateral distance from center of stone column depth=15m from G.L (with stone column, L=15m)

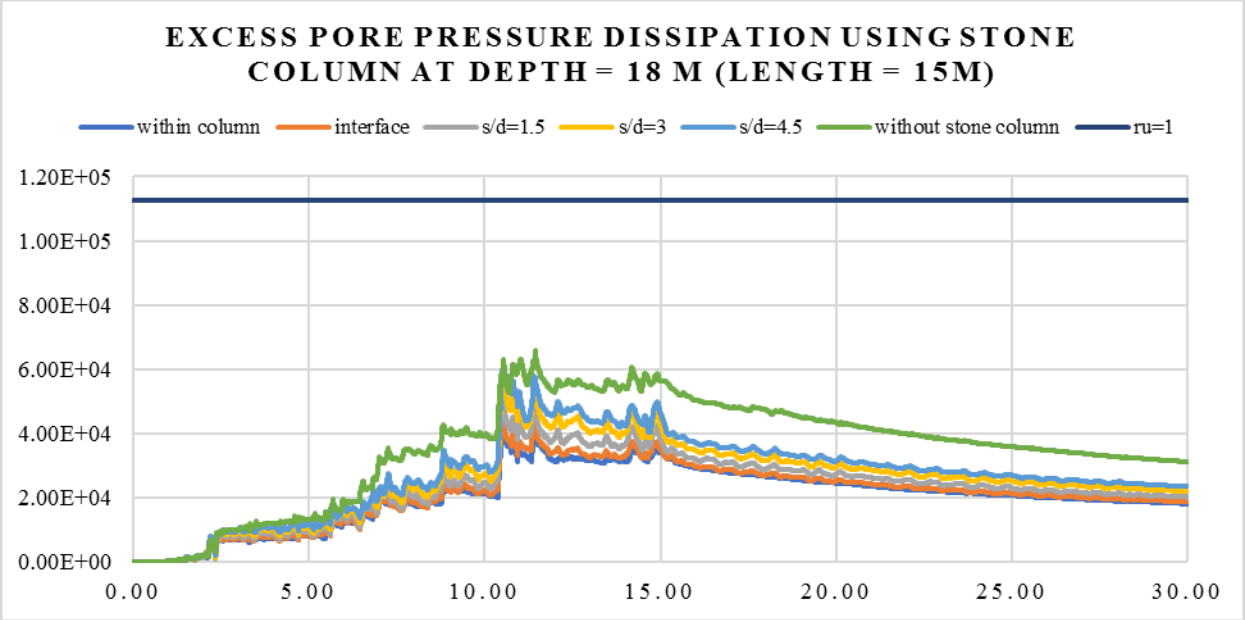

Fig. 4.77 Pore pressure dissipation comparison at lateral distance from center of stone column depth=18m from G.L (with stone column, L=15m)

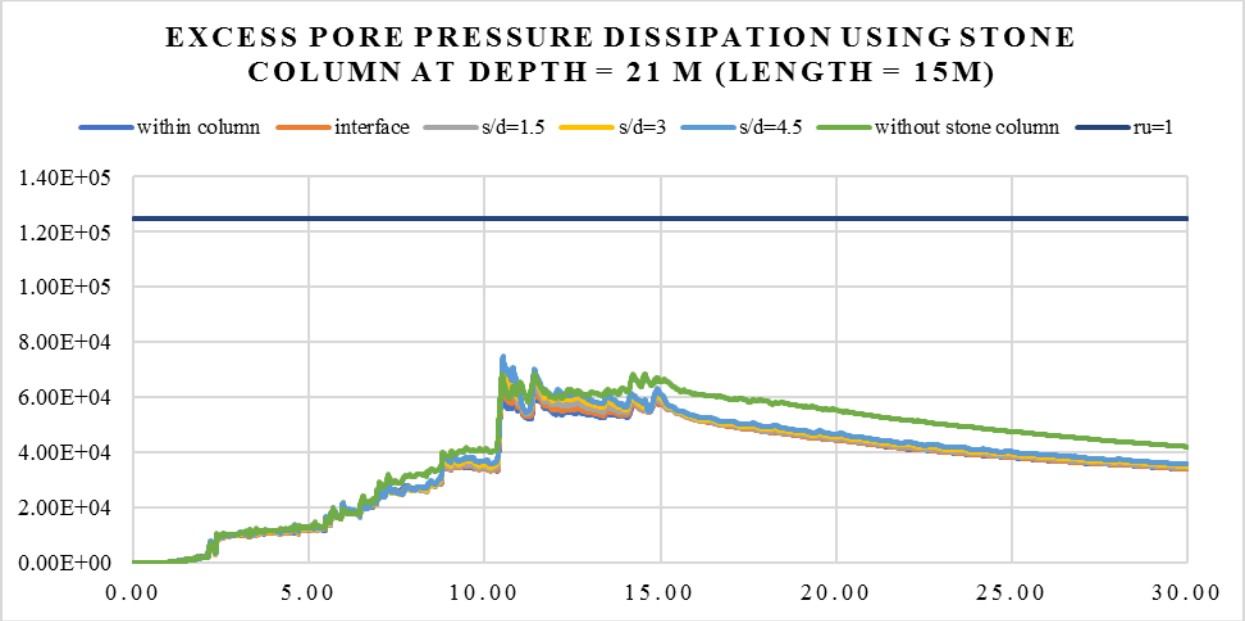

Fig. 4.78 Pore pressure dissipation comparison at lateral distance from center of stone column depth=21m from G.L (with stone column, L=15m)

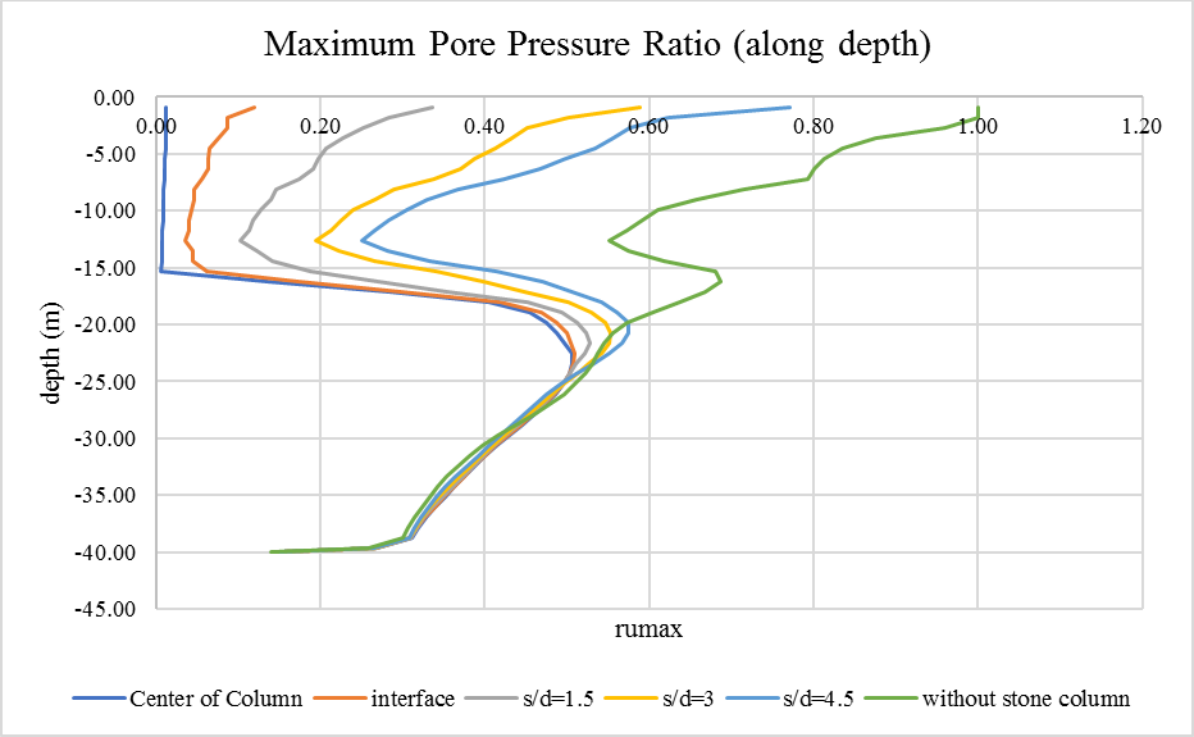

Fig. 4.79 Maximum Excess pore pressure ratio along with depth comparison at different lateral distance (with stone column, L=15m)

4.2.8.1 Discussion on Results of dynamic analysis (MOD-8)

In this case, model have stone column of length 15m shown in the schematic diagram. Mammoth-lake 0.3g PGA Acceleration is used as a seismic excitation at the base of the model. This simulation is done with flow on condition or couple flow condition as the excess pore pressure is dissipate by the stone column on this soil stratification.

Fig. 4.69 showing excess pore pressure contour. The excess pore water pressure (EPWP) is increasing with depth. The EPWP is 70kPa at bottom dense sand. But initially under the sharp acceleration the EPWP is generated at middle layer of depth 9m to 15m depth but latter stage, EPWP is dissipated as flow on condition from top layer but EPWP at bottom layer can't dissipate easily. So, this type of pattern is generated in fig.4.59.

Fig. 4.70 showing the pore pressure ratio is reduce around the column and up to a depth of 15-17 m from ground level. As In this model stone column length used is 15m.

Fig. 4.73 showing the comparison result of excess pore pressure with stone column of length 15m and without stone column. At depth of 4 m, without stone column case EPWP was 17kPa. But when stone column is used, at depth of 4 m from ground level, Excess pore water pressure

at the center of stone column is negligible (0.24kPa) because stone column have very high permeability, so when water from the surrounding reach just the column, instantly dissipated. At interface EPWP reached 3kPa. And at a distance 1.2 m distance from center indicated as s/d =1.5 or distance of 1.5 times diameter of stone column, EPWP is reach 7.3 kPa. And at s/d=3.0, EPWP is reach 10.5 kPa. So, we observed, at first three distances stone column worked properly (i.e. with center of column, interface, and s/d=1.5). But after s/d=1.5 m, excess pore pressure is not as dissipated as compare to the other cases, and excess pore pressure reached closed to 1.

Similarly, Fig. 4.71, Fig. 4.72, Fig.4.73, Fig.4.74 and Fig. 4.75 showing similar pattern as Fig. 4.73, stone column of length 15 m dissipates excess pore water pressure up to a distance of 1.5d from the center of column. But in case of fig.4.76 and fig.4.77 at depth 18m and 21m stone column not worked as stone column is a length of 15m only. Even liquefaction is not reached at that depth (18m form ground surface).

Fig. 4.78 shows maximum pore pressure ratio along the depth at various lateral distance from the center of stone column. From this figure it is very clearly that up to the distance of 1.5d distance from center of column stone column dissipates EPWP effectively and mitigates liquefaction.

4.3 Comparisons of PGA Variation Along the soil depth:

In this study peak ground acceleration are calculated using Finite difference code (FLAC2D) along the various depth of sandy soil layer by a seismic motion applied at the base. Then at various depth PGA are note down. Here Lomaprieta (0.3g) and Mammoth-lake (0.3g) are used as an input motion.

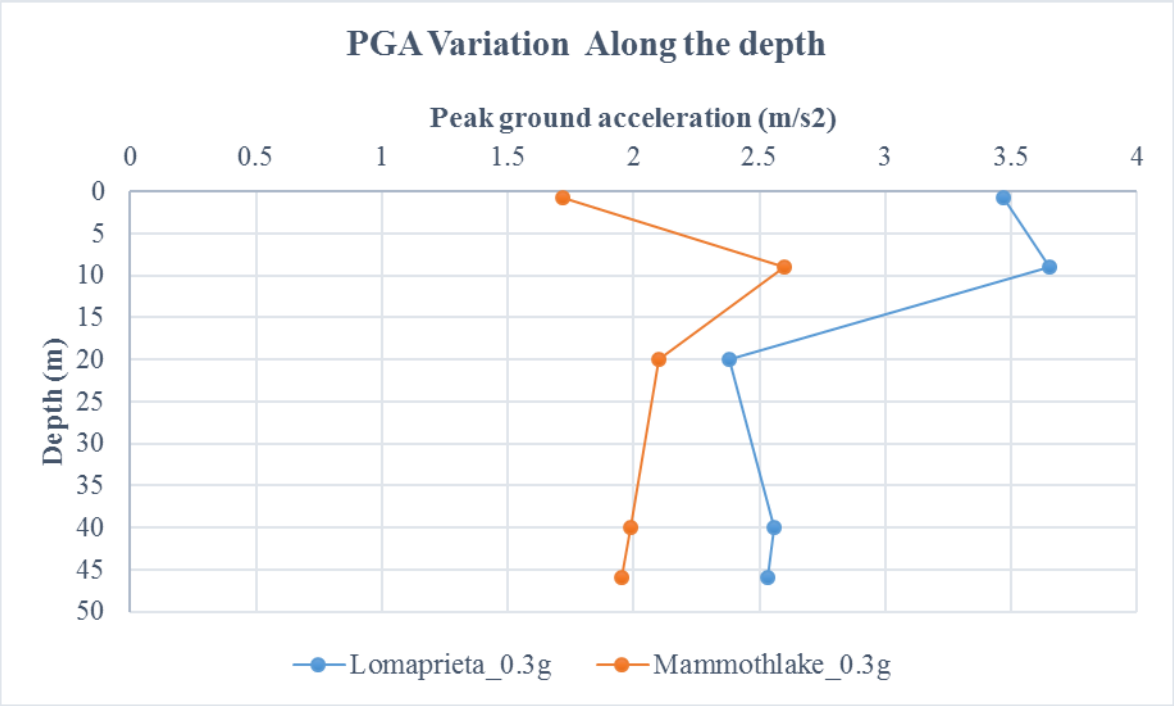

Fig. 4.80: Comparisons of PGA variation along the depth for two different earthquakes

CHAPTER – 5

5.1 CONCLUSIONS

From the current numerical study on the mitigation of soil liquefaction using stone column, analyzing under different type seismic excitation and under different length of stone column conditions are simulated. The study is a basically ground improvement where we trying to reduce the liquefaction of soil using the property of stone column. From the study following conclusions can be made……..

1. We apply a shear stress wave history (after converting from velocity time history) at the bottom of a bedrock for the dynamic simulation. Then the shear wave propagates upwards through different soil layer. And when reached finally at the ground surface it gets modified. PGA amplification between the base of bedrock and ground surface ($a_{max\ surface}/a_{max\ base}$) is 1.67 for the case of Lomaprieta, 0.3g PGA whose actual peak acceleration is 0.357g. PGA amplification for the case of Mammoth-lake, 0.3g PGA is 1.3 whose actual peak acceleration is 0.43g. So, for two different earthquake of same magnitude which one have higher original PGA have less amplified.

2. Excess pore water pressure generation in a stratified soil layer under couple flow condition is at 9m to 15m at initial acceleration time record, when the peak acceleration is reached, maximum excess pore water pressure generation zone shift to bottom depth. This is because of huge pore pressure dissipation is continue from the top layer as top layer have high permeability than bottom layer. And bottom layer have more drainage length.

3. In this study two different earthquake having different original PGA but same peak acceleration is used by scale down the original PGA. For 0.3g lomaprieta depth of liquefaction is reached about 9m to 10m because Lomaprieta acceleration have 40s earthquake and reached the Peak within a shorter time (3sec to 6sec time range) but in case of 0.3g Mammoth-lake earthquake depth of liquefaction reached up to 3-4m, quite low because its acceleration have 30s earthquake and reached the peak slowly, taking longer time.

4. When Stone column install on a stratified soil layer the excess pore pressure ratio is reduce around the column. For 5m length of stone column has reduce excess pore pressure ratio up to a depth of 6m. For 10m length of stone column has reduce excess pore pressure ratio up to a depth of 12m. And lastly for 15m length of stone column has reduce the excess pore pressure ratio up to a depth of 17m.

5. From the center of column in either left or right laterally stone column of diameter 0.8m dissipates excess pore water pressure up to a distance of 1.5d (d = diameter of stone column). After that distance, excess pore water pressure not reduce effectively and reached excess pore pressure ratio=1. So finally, we can conclude, considering both left side and right side, stone column creates a zone of three time of its diameter where excess pore water pressure reduce effectively i.e. liquefaction reduce significantly.

6. For moderate to high earthquake like 0.3g PGA where depth of liquefaction is reached to 9m. Stone column having length of 10m can sufficiently mitigate against liquefaction. So, 15m length of stone column is not required. And for low depth of liquefaction like 3-4m, a stone column having length 5m can successfully mitigate the liquefaction.

5.2 Future Scope of Work

In future this worked can be further extended considering the bedrock level is at different depth, Surcharge effects also can be considered on stone column ground while analysis of stone column for mitigation of earthquake. Also, stone column in a group by varying diameter of stone column and depth of liquefiable layer. The stone column and gravel drain combine effects can also be study. This study is performed under a couple flow condition and upper boundary is open to the world. So, a stone column study may be considered in future for uncouple flow condition.

REFERENCES

[1] Seed, H.B. and Idriss, I.M. (1971) ‘’Simplified Procedure for Evaluating Soil Liquefaction Potential’’. Journal of the Soil Mechanics and Foundations Division, ASCE 97, SM9, 1249-1273.

[2] M. H. T. Rayhani, M. H. El Naggar & S. H. Tabatabaei (2007),” Nonlinear Analysis of Local Site Effects on Seismic Ground Response in the Bam Earthquake”. Geotechnical and Geological Engineering volume 26, pages91–100 (2008)

[3] M. R. MADHAV and A Murali Krishna. (2008) “Liquefaction Mitigation of Sand Deposits by Granular Piles- an Overview”, Proceedings of the 2nd International Conference on Geotechnical Engineering for Disaster Mitigation & Rehabilitation DOI: 10.1007/978-3-540-79846-0_3

[4] G.D. Bouckovalas, A.G. Papadimitriou and D. Niarchos 2009 “Gravel drains for the remediation of liquefiable sites: The Seed & Booker (1977) approach revisited” DOI: 10.1201/NOE0415556149.ch4

[5] T. M. WEBER, M. PLOTZE, J. LAUE, G. PESCHKE and S. M. SPRINGMAN (2010), “Smear zone identification and soil properties around stone columns constructed in-flight in centrifuge model tests” Geotechnique 60, No. 3, 197–206 [doi: 10.1680/geot.8. P .098]

[6] Carlos Omar Vargas Moreno, Ricardo Ortiz Hermosillo, Francisco Alonso Flores (2015) “Liquefaction Analysis Using Pore Pressure Generation Models During Earthquakes” DOI:10.3233/978-1-61499-603-3-1057, Conference: From Fundamentals to Applications in Geotechnics, Proceedings of the 15th Pan-American Conference on Soil Mechanics and Geotechnical Engineering At: Buenos Aires, Argentina.

[7] Liang Tang, Xiaoyu Zhang, and Xianzhang Ling (2015), “Numerical Simulation of Centrifuge Experiments on Liquefaction Mitigation of Silty Soils using Stone Columns” KSCE Journal of Civil Engineering (2016) 20(2):631-638, DOI 10.1007/s12205-015-0363-7

[8] Ahmad Asaadi and Mohammad Sharifipour (2015), “Numerical simulation of liquefaction susceptibility of soil interacting by single pile” Int. J. Min. & Geo-Eng. Vol.49, No.1, June 2015, pp.47-56.

[9] Z. Ben Salem, W. Frikha and M. Bouassida (2015), “Effect of Granular-Column Installation on Excess Pore Pressure Variation during Soil Liquefaction” Conference: 16th African Regional Conference on Soil Mechanics and Geotechnical Engineering, Innovative Geotechnics for Africa at: Hammaet (Tunisia)Volume: 1, DOI: 10.1061/(ASCE)GM.1943-5622.0000516.

[10] Kyle Rollins, Bradford Price, E. Dibb and J. B. Higbee (2015),” Liquefaction Mitigation of Silty Sands in Utah Using Stone Columns with Wick Drains”. Conference: Geo Shanghai International Conference, May 2006, DOI:10.1061/40864(196)46

[11] Chunxia Huang, Zhilong Sui, Lei Wang & Kaifu Liu (2015), "Mitigation of Soil Liquefaction Using Stone Columns: An Experimental Investigation". Marine Geo resources & Geotechnology, 34:3, 244-251, DOI: 10.1080/1064119X.2014.1002872.

[12] Haleh Meshkinghalam, Masoud Hajialilue-Bonab and Ali Khoshravan Azar (2017), "Numerical investigation of stone columns system for liquefaction and settlement diminution potential" International Journal of Geo-Engineering, (2017) 8:11 DOI 10.1186/s40703-017-0047-x.

[13] Raj Banerjee, Sanku Konai, Aniruddha Sengupta and Kousik Deb (2017), "Shake Table Tests and Numerical Modeling of Liquefaction of Kasai River Sand". Geotechnical and Geological Engineering (2017) 35:1327–1340 DOI 10.1007/s10706-017-0178-z

[14] Zeineb Ben Salem, Wissem Frikha, and Mounir Bouassida (2018), "Numerical Analysis of Liquefaction Susceptibility of Reinforced Soil with Stone Columns". Conference: International Congress and Exhibition, July 2018, DOI:10.1007/978-3-319-63543-9_6 .

[15] Suravi Pal and Kousik Deb (2018), "Effect of Stiffness of Stone Column on Drainage Capacity during Soil Liquefaction" International Journal of Geomechanics, doi.org/10.1061/(ASCE)GM.1943-5622.0001108

[16] Suravi Pal and Kousik Deb (2019), "Effect of Smear, Well Resistance, and Stiffness on the Performance of Stone Column during Soil Liquefaction" - Geo congress 2019GSP 308.

[17] Suravi Pal, Kousik Deb (2019), "Effect of clogging of stone column on drainage capacity during soil liquefaction" (2019), Volume 59, Issue 1, February 2019, Pages 196-207, doi.org/10.1016/j.sandf.2018.10.005

[18] Reza BABAEI And Rouzbeh DABIRI (2019), "EFFECTS OF STONE COLUMNS ON IMPROVEMENT OF LIQUEFIABLE SOIL LAYERS" 8TH International Conference on Seismology and earthquake Engineering, Nov 2019, Iran, Tehran.

[19] Amrendra Kumar, Sunita Kumari and V. A. Sawant (2020), "Numerical Investigation of Stone Column Improved Ground for Mitigation of Liquefaction". September, 2020, International Journal of Geomechanics.

[20] Jamal Hleibieh, Ivo Herle (2020), "Numerical Analysis of Stone Columns for the Reduction of the Risk of Soil Liquefaction". December 2020, Transportation Infrastructure Geotechnology 7(3-4) DOI:10.1007/s40515-020-00108-9.

[21] Quimby, Michael James, "Liquefaction Mitigation in Silty Sands Using Stone Columns with Wick Drains" (2009). Thesis and Dissertations. https://scholarsarchive.byu.edu/etd/2228.

[22] Boulanger, R. W and Idriss, I. M. (2004). “Evaluating the potential for liquefaction or cyclic failure of silts and clays.” Report No. UCD/CGM-04/01. Department of Civil & Environmental Engineering, College of Engineering, University of California at Davis.

[23] Chapter-9 Geotechnical Earthquake Engineering By Steven L. Kramer.

[24] FLAC 2D 8.1 Dynamic manual.